Centro de Investigación en Matemáticas, A.C.

Pursuit-Evasion Problems with a Differential Drive Robot and an Omnidirectional Agent

by

Ubaldo Ruiz López

Thesis Advisor

Dr. Rafael Murrieta Cid

A thesis submitted in partial fulfillment for the degree of Doctor of Science

in the

Computer Science Department

January 2013

CENTRO DE INVESTIGACIÓN EN MATEMÁTICAS

Abstract

Computer Science Department

Doctor of Science

by Ubaldo Ruiz López

This thesis focuses in the development of algorithms for mobile robotics. We investigate the interaction between two antagonistic agents in an environment without obstacles. One of the agents wants to track/capture the other despite any opposition. This kind of problems has interesting applications, as for example: stopping a malicious intruder, maintaining connectivity between a mobile user and a base station, or monitoring of children. In particular, we are focused in finding theoretical guarantees for tracking/capturing an omnidirectional agent (evader) using a differential drive robot (pursuer). We are also interested in finding the motion strategies used by the players to accomplish their goals. First, we consider the surveillance problem of tracking an omnidirectional evader at constant distance using a DDR in the plane without obstacles. The players have maximum bounded speeds and the DDR is faster than the evader. We assume that both players have full knowledge of their instantaneous positions and the instantaneous velocity of the evader. We construct a partition of the configuration space that allows to know at the beginning of the game whether or not the DDR is able to maintain tracking at constant distance. We also find optimal motion strategies for both players, in the sense that they require the minimum capabilities of the players for winning. Next, we propose a generalization of the problem described above. We present the conditions that establish whether or not it is possible for a DDR to track an Omnidirectional Agent (OA) at a bounded variable distance. We propose motion strategies for the DDR; these motion strategies can also be used by a DDR to capture an OA. Finally, we address the problem of capturing an omnidirectional evader with a DDR in minimal time. In this case, the players have only knowledge of their instantaneous positions. We obtain the motion primitives and time-optimal motion strategies for the players that are in Nash Equilibrium. We propose a partition of the space where the strategies of the players are well established. Using this partition, we found feedback motion policies for the DDR. We also give the conditions defining the winner of the game.

Acknowledgements

I am grateful to Professor Rafael Murrieta Cid for providing useful advice and support during my research. Without his guidance this work would not have came to light. I want to thank Professor Jose Luis Marroquin and Professor Seth Hutchinson for helpful discussions and suggestions. I am also thankful to my committee members Professor Raúl Monroy, Professor Jean Bernard Hayet and Professor Hector Becerra for helpful discussions.

Moreover, I would like to thank my parents Ubaldo Ruiz and Ma. Guadalupe López, and my sisters Ana Elizabeth and Vianey for encourage me in all my projects.

I would also like to thank Yazmin Vazquez for her love and support during this journey.

I would like to thank all my partners during my studies at CIMAT, Rigo, Luis, Israel, Judith, Nacho, Moncho, David, Gustavo, Hugo, Memo and Emma.

Finally, I want to thank CIMAT and CONACyT for providing me financial support during all my doctoral studies.

Contents

List of Figures

List of Tables

Dedicated to my family

Chapter 1

Introduction

This thesis focuses in the development of algorithms for mobile robotics, and it is related to works proposing motion strategies based on visibility [2–6]. This work, is also connected to the area of Sensor Based Motion Planning for mobile robots. Sensing information is used for different purposes; in some cases, it is employed as a tool to perform a task. For example, sensing is important in navigation problems [7, 8], where the goal is to move a robot from an initial configuration to a final configuration avoiding obstacles.

We are interested in those tasks where a key goal is to sense the environment (perception planning [9–11]). In general, the sensing stages are taken into account in the plan generation as a constraint that must be fulfilled during the execution of the plan. There are a lot of problems that fall in this category, some of them are exploration, coverage and pursuit-evasion.

The exploration problem involves the generation of a motion strategy to efficiently move a robot in order to sense and discover its surroundings and build a representation (map or model) of the environment [11–14]. Usually the construction is done fusing different views of the environment. The representation should be useful to accomplish other robotic tasks.

In the coverage problem [8, 15], the objective is usually to sweep a known environment with a robot or with the viewing region of a sensor (footprint). In this problem, it is often desirable to minimize the sensing overlap to avoid that the same region is covered more than once.

The problems we consider in this thesis are related to pursuit-evasion games. A pursuit-evasion game can be defined in several ways. For example, a problem which has been extensively studied, consists in maintaining visibility of a moving evader in an environment with obstacles [3, 16–19]. In this case, the pursuer must maintain visual contact

with the evader (refer to Fig. 1.1) or a bounded distance between both players. The evader may try to escape the pursuer's field of view or reach a distance from the pursuer outside the range.

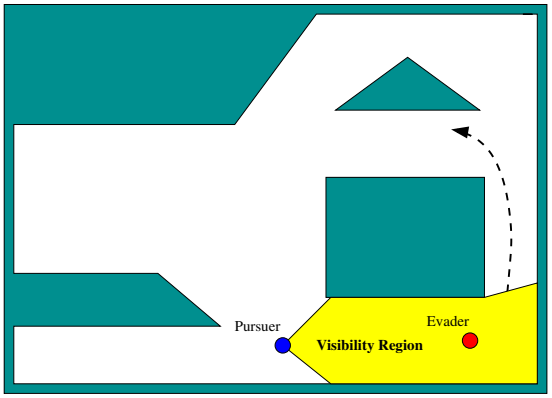

FIGURE 1.1: Target tracking.

Alternatively, the pursuer(s) might have as a goal to actually "capture" the evader(s) [20–22], that is, move to a contact configuration, or closer than a given distance (refer to Fig. 1.2).

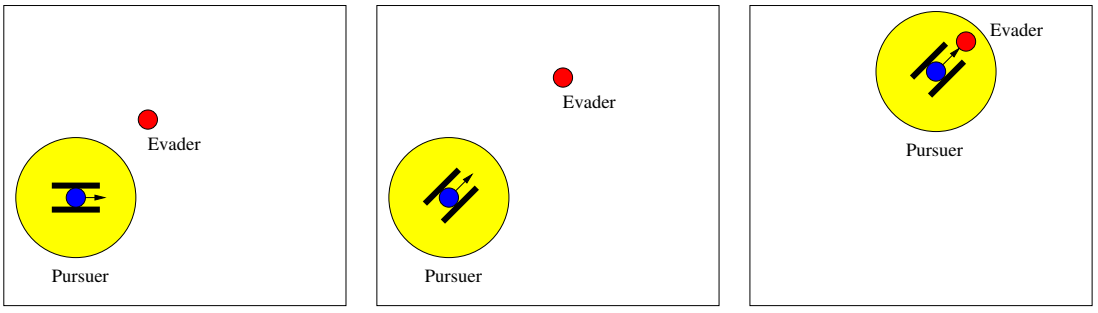

(a) (b) (c)

FIGURE 1.2: Target capturing.

In another problem, one or more pursuers could be given the task of *finding* an evader [5, 6, 18, 23–27]. To solve this problem, the pursuer(s) must sweep the environment so that the evader is not able to eventually sneak into an area that has already been explored (refer to Fig. 1.3).

Some characteristics can be added to the problems described above in order to make them more general, for example, kinematic constraints on the players' motion [28], position uncertainty [29–31], limited sensors [11, 14], etc. The motion strategies considering

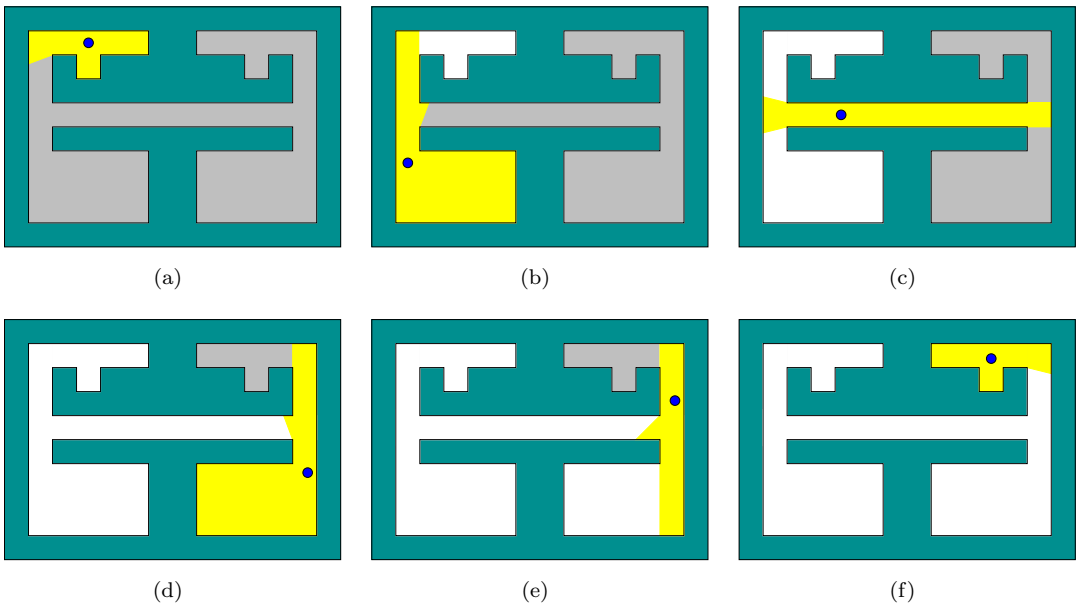

FIGURE 1.3: Target finding.

multiple robots [32–35] are generally hard to construct but usually yield better performance (compared to a single robot). In these kind of problems, it is often challenging but very interesting to develop complete algorithms[1] that find optimal solutions.

This thesis addresses problems where the pursuer must maintain surveillance or capture of a moving evader in an environment without obstacles. The evader aims to avoid these conditions. We are interested in developing motion strategies for the players so that they can achieve their goals. We are also interested in obtaining the conditions determining the winner of the games.

1.1 Problems Addressed in this Work

In this work, we study three pursuit-evasion problems involving a Differential Drive Robot (DDR) and an Omnidirectional Agent. The robot has two wheels that are actuated independently, if they rotate in the same direction and with the same speed the robot moves forward or backward following a straight line. If the wheels rotate in opposite directions with the same speed the robot rotates in place either clockwise or counterclockwise. In our case, the players have bounded speeds, and the pursuer is faster than the evader. We consider purely kinematic problems and any dynamic constraints are neglected (e.g. acceleration bounds). All the problems take place on an environment without obstacles.

[1]Such an algorithm is guaranteed to return a correct solution when one exists, or to report failure in finite time when a solution does not exist

First, we consider the surveillance problem of tracking an omnidirectional evader at constant distance using a DDR.

Second, we address the pursuit-evasion problem in which a DDR (the pursuer) tracks an Omnidirectional Agent (OA) at bounded variable distance, maintaining surveillance of the agent at all times.

Finally, we consider the problem of capturing in minimum time an omnidirectional evader using a DDR. At the beginning of this game the evader is at a distance $L > l$ (the capture distance) from the pursuer. The goal of the evader is to keep the pursuer farther than this capture distance as long as possible. The pursuer wants to capture the evader as fast as possible.

1.2 Thesis Outline and Contributions

In Chapter 2, we present a brief summary of the work that has been done in the area of pursuit-evasion games, particularly, in the robotics community.

In Chapter 3, we consider the surveillance problem of tracking an omnidirectional evader at constant distance using a DDR. The players have maximum bounded speeds and the DDR is faster than the evader. We assume that both players have full knowledge of their instantaneous positions and the instantaneous velocity of the evader. In this chapter, we construct a partition of the configuration space that allows to know at the beginning of the game whether or not the DDR will be able to maintain tracking at constant distance. We also find optimal motion strategies for both players, in the sense that they require the minimum capabilities of the players for winning. This work has appeared in [36].

In Chapter 4, we propose a generalization of the problem in Chapter 3. We present the conditions that establish whether or not it is possible for a DDR to track an Omnidirectional Agent at a bounded variable distance. In this chapter, we also propose motion strategies for the DDR; these motion strategies can also be used by a DDR to capture an OA.

In Chapter 5, we present a brief introduction to optimal control theory and differential games. The objective of the chapter is describe to the reader some basic concepts and techniques that are used in the solution of the problem addressed in Chapter 6.

In Chapter 6, we address the problem of capturing an omnidirectional evader with a DDR in minimum time. As in Chapters 2 and 3, we assume that both players have maximum bounded speeds and that the DDR is faster than the evader. In this case, however, the players have only knowledge of their instantaneous positions. In this chapter, we

obtain the motion primitives and time-optimal motion strategies for the players that are in Nash Equilibrium. We propose a partition of the space where the strategies of the players are well established. We also give the conditions defining the winner of the game. This work has appeared in [37] and it is under review in [38].

Finally, in Chapter 7 we present some general conclusions and future work.

For the problems in Chapters 3, 4 and 6, we present simulation results of the strategies followed by the players.

Chapter 2

Related Work

A lot of work has been done in the area of pursuit-evasion games [20, 39, 40], where the three problems described in last chapter have received a lot of attention. In this chapter, we describe the most representative works in the literature. Usually the tools that are used to deal with them are similar (graph theory, probabilistic tools, optimal control theory, differential games, combinatorics, etc.), below we describe some prior work.

2.1 Target Finding

In the target finding problem [6, 27], the objective is to establish some sort of visibility between the pursuer and the evader. In this case, the pursuer must sweep the environment so that the evader is not able to eventually sneak into an area that has already been explored. Deterministic [25, 41–44] and probabilistic algorithms [26, 45, 46] have been proposed to solve this problem.

Some interesting results have been obtained for the problem of target finding in a graph, in this problem, the pursuers and the evader can move from vertex to vertex until eventually the pursuer guarantees to touch the evader [41, 47]. The *search number of a graph* refers to the minimum number of pursuers needed to solve a target finding problem, and it is closely related to other graph properties such as *cut-width* [48, 49]. It has also been shown that a suitable strategy is to search the graph monotonically (i.e. without revisiting places multiple times) in [50, 51].

The problem of target finding in a graph was introduced by Suzuki and Yamashita [25]. They were interested in the existence and complexity of an algorithm which,

given a simple polygon P with n edges, decides whether P is 1-searchable[1] and if so, outputs a search schedule. Although the problem has been open for a while, no complete characterizations or efficient algorithms have been developed. Some variations have been considered. Icking and Klein [52] defined the two-guard walkability problem, a search problem for two guards whose starting and goal positions are given, and who move on the boundary of a polygon so that they are always mutually visible. Icking and Klein proposed an $O(n \log n)$ solution, which was improved by Heffernan [53] to the $\Theta(n)$ optimal. Tseng et al. [53] extended the two-guard walkability problem relaxing the constraint that the initial and final position are given. They presented an $O(n \log n)$ algorithm that decides if a polygon can be searched by two guards, and a $O(n)$ algorithm that gives as its output all the possible starting and goal positions that allow searchability by those two guards. Lee et al. [54] defined the problem of 1-searchability for a room (i.e. a polygon with one door – a point that must be visible for the observer all time). They proposed an $O(n \log n)$ decision algorithm and a method to compute a solution in $O(n^2)$ time.

Originally, the problem of 1-searchability for a polygon was introduced in [25] together with a more general problem in which the pursuer (a.k.a k-searcher) has k flashlights; when k is not bounded this corresponds to 360° vision. For results involving 360° refer to [5, 25, 54, 55] for search in polygons and to [24] for curved planar environments.

Recently, probabilistic [26] and randomized algorithms [6, 22] have been proposed to address the target finding problem. Other works have focused on minimizing the required information to accomplish the task, see for instance [56].

2.2 Target Tracking

In the tracking problem, the goal is to maintain visibility of the evader at all times, usually in an environment with obstacles [3, 16–19]. This problem has been traditionally addressed with a combination of vision and control techniques [57–59]. Game theory [40] has been extensively used to approach target tracking [20, 39].

A great deal of previous research exists for this problem, particularly in the area of dynamics and control in the free space (without obstacles) [20, 39, 40]. Purely control approaches, usually, do not take into account the complexity of the environment. For the target tracking problem, the basic question that has to be answered is where should the robot observer move in order to maintain visibility of a target moving in a *cluttered environment*. Both visibility and motion obstructions have to be considered. Therefore,

[1] A graph is k-searchable if k is the smallest number of searchers for which a search strategy exists to clean an initially contaminated graph avoiding recontamination.

a pure visual servoing technique can fail because it ignores the global geometry of the workspace.

Previous works have studied the problem of maintaining visibility of a moving evader in an environment with obstacles. In [16], game theory [40] was proposed as a framework to formulate the tracking problem. The case for predictable targets is also presented in [16], which describes an algorithm that computes numerical and optimal solutions for problems of low dimensional configuration spaces. However, the assumption that the motion of the target is known in advance is a very limiting constraint.

In [60] an algorithm was presented that operates by maximizing the probability of future visibility of the evader. This algorithm is also studied more formally in [16].

This technique was tested in a Nomad 200 mobile robot with good results. However, the probabilistic model assumed by the planner was often too simplistic, and accurate models are difficult to obtain in practice.

The work in [61] presents an approach that takes into account the positioning uncertainty of the robot pursuer. Game theory is also proposed as a framework to formulate the tracking problem. One contribution of this work is a technique that periodically commands the observer to move into a region that has no localization uncertainty (a landmark region) in order to re-localize itself and better track the target afterwards.

In [17], a technique is proposed to track an evader without the need for a global map. Instead, a range sensor is used to construct a local map of the environment, and a combinatorial algorithm is then used to compute a motion for the pursuer at each iteration.

In [19], a greedy approach was used for the problem of evading surveillance. To drive the greedy motion planning algorithm [19], a local minimum risk function is applied, called the vantage time.

The approach presented in [62, 63] computes a motion strategy by maximizing the *shortest distance to escape*, i.e., the shortest distance the evader needs to move in order to escape the pursuer's visibility region. In that work the evaders were assumed to move unpredictably, and the distribution of obstacles in the workspace was assumed to be known in advance. This planner has been integrated and tested in a robot system which includes perceptual and control capabilities. The approach has also been extended to maintain visibility of two evaders using two pursuers.

In [64], a method has been proposed for dealing with the problem of computing the motions of a robot observer in order to maintain a moving target within the sensing range of an observer reacting with delay. The target moves unpredictably, and the distribution of obstacles in the workspace is known in advance. The algorithm computes a motion

strategy based on partitioning the configuration space and the workspace in non-critical regions separated by critical curves. In this work it is determined the existence of a solution for a given polygon and delay.

[65] proposes a method for dealing specifically with the situation in which the observer has bounded velocity and has as his objective to maintain a constant distance from the evader. Necessary conditions for the existence of a surveillance strategy have been provided as well as an algorithm that generates them. This motion strategy consists of three types of motions: reactive, compliant and rotational.

In [66], the work proposed in [65] has been extended for dealing with the surveillance problem of maintaining visibility at a fixed distance of an unconstrained mobile evader (the target) by a nonholonomic mobile robot equipped with sensors. Only sufficient conditions for the evader's escape are given.

In [67], an approach has been proposed for addressing the pursuit-evasion problem of maintaining surveillance by a pursuer, of an evader in a world populated by polygonal obstacles. This requires the pursuer to plan collision-free motions that honor distance constraints imposed by sensor capabilities, while avoiding occlusion of the evader by any obstacle. The three-dimensional cellular decomposition of Schwartz and Sharir has been extended to represent the four-dimensional configuration space of the pursuer-evader system. Necessary conditions for surveillance (equivalently, sufficient conditions for escape) in terms of this new representation have been provided. That work also gave a game theoretic formulation of the problem, and used this formulation to characterize optimal escape trajectories for the evader. A shooting algorithm that finds these trajectories, using the Pontryagin's Maximum Principle (PMP), has been proposed. Finally, noting the similarities between this surveillance problem and the problem of cooperative manipulation by two robots, several cooperation strategies that maximize system performance for cooperative motions have been proposed.

[3] addresses the problem of maintaining visibility of the evader in an environment containing obstacles. The pursuer and the evader are omnidirectional (holonomic) systems. That work proves the existence of strategies that are in Nash equilibrium: the pursuer wants to maintain visibility of the evader for the maximum possible amount of time, and, the evader wants to escape the pursuer's sight as soon as possible. This work presents necessary and sufficient conditions for the visibility-based target tracking game in conjunction with the equilibrium strategies for the players.

An extended version of the target tracking problem, where multiple evaders and pursuers are involved, has attracted increasing attention. In [34] a method that accomplishes this task but restricted to uncluttered environments is proposed. The method works

by minimizing the total time in which targets escape surveillance from a robot team member. In [18] an approach that maintains visibility of several evaders using mobile and static sensors is proposed. It applies a metric for measuring the degree of occlusion, based on the average mean free path of a random line segment.

In [68], a method shows how to efficiently (low-polynomial time) compute an optimal reply path for the pursuer that counteracts a given evader movement. However, that work does not deal with the problem of deciding whether or not there is an evader path that escapes surveillance, not even for the special case where the evader follows a fixed policy.

Almost all existing work focuses on the 2-D version of the problem of maintaining visibility of an evader, but there are few works that deal with the 3-D version of it, mainly because of the complexity of the visibility relationships in 3-D. One work that deals with the 3-D version of this problem was presented in [69]. Here the authors present an online algorithm for 3-D target tracking among obstacles, using only local geometric information available to a robot's visual sensors. To prevent the target's escape from the robot's visibility region both in short and long terms, a risk function is efficiently computed. The robot motions are calculated minimizing the risk function locally also in a greedy fashion.

In [70], a robot has to track an unpredictable target with bounded speed. The robot's sensors are manipulated to record general information about the target's movements and avoid that detailed information about the target's position be available if the robot's sensors are accessed by other agent that can damage the target.

Pursuit-evasion has been found to be useful in a variety of interesting applications. For example, in [71], the authors noticed the similarity between pursuit-evasion games and mobile-routing for networking. Applying this similarity, they proposed motion planning algorithms for robotic routers to maintain connectivity between a mobile user and a base station.

With some similarities with the problem introduced in [71], in [72] a non-cooperative game is presented where the author proposes a control strategy for a team of robots so that they can localize and track a non-cooperative agent while maintaining a continuously optimized line-of-sight communication chain to a fixed base station. Focusing on these two aspects of the problem (localization of the agent and tracking while maintaining the line-of-sight chain), the author presents feedback control laws that can realize this plan and ensure proper navigation and collision avoidance.

2.3 Target Capturing

In the capturing problem, the pursuer tries to get closer than a given distance l from the evader. The goal of the evader is to keep the pursuer at all times farther from him than this capture distance. This kind of problems are usually solved using techniques from Optimal Control [91] and Differential Game Theory [20, 40].

A classical problem in that direction, is the homicidal chauffeur problem [20, 21]. In that game a faster pursuer (w.r.t. the evader) has as its objective to get closer than a given distance (the capture condition) from a slower but more agile evader, in order to run him over. The pursuer is a vehicle with a minimal turning radius. The game takes place in the Euclidean plane without obstacles, and the evader aims to avoid the capture condition. Several versions of this problem have been studied [73–78], for example, in [74], the evader minimizes time of escaping from inside a detection set which is a two-dimensional semi infinite cone, a multi-agent cooperative variant is addressed in [78] and in [75] it is assumed that the motion of players is subject to random disturbances. A slightly different version where the evader is also a vehicle with a minimal turning radius has been studied in [79–83].

A similar problem to the homicidal chauffeur is called the lady in the lake [40]. A lady is swimming in a circular lake with maximum speed v_l. A man who wishes to intercept the lady, and who has not mastered swimming, is on the side of the lake and can run along the shore with maximum speed v_m. The lady does not want to stay in the lake forever and wants eventually scape. If, at the moment she reaches the shore, the man cannot intercept her, she "wins" the game since on land she can run faster than the man. For this problem, it is assumed that both players can change their motion directions instantaneously and that $v_l < v_m$.

Another closely related problem is known as the lion and the man [84–88]. A lion and a man with the same motion capabilities are confined to move on a circular arena. The lion tries to capture the man and the man wants to avoid to be captured. A revisit of the problem and a solution using the method of Isaacs [20] is presented in [86]. A discrete version of the problem is studied in [6, 87]. In [88], the authors studied a new version of the game which takes place in an Euclidean environment with a circular obstacle.

Chapter 3

Tracking an Omnidirectional Evader with a Differential Drive Robot

In this chapter we consider the surveillance problem of tracking a moving evader by a nonholonomic mobile pursuer. We deal specifically with the situation in which the only constraint on the evader's velocity is a bound on speed (i.e., the evader is able to move omnidirectionally), and the pursuer is a nonholonomic, differential drive system having bounded speed.

We assume that both the pursuer and evader have full knowledge of the other's state, and that the speeds of the pursuer and evader are bounded (though they do not necessarily have the same bound). We consider here a purely kinematic problem, and neglect any effects due to dynamic constraints (e.g., acceleration bounds).

We formulate our problem as a game. Given the evader's maximum speed, we determine a lower bound for the required pursuer speed to track the evader. This bound allows us to determine at the beginning of the game whether or not the pursuer can follow the evader based on the initial system configuration. We then develop the system model, and obtain optimal motion strategies for both players, which allow us to establish the long term solution for the game. We present an implementation of the system model, and motion strategies, and also present simulation results of the pursuit-evasion game.

Our tracking problem consists of determining a pursuer motion strategy to always maintain surveillance of the evader by the pursuer (assuming surveillance in the initial state). The evader is under pursuer surveillance whenever the evader is at a constant distance L from the pursuer (L can be considered as the upper limit of the physical sensor used

by the pursuer). It is pertinent to analyse this specific case for the following reasons: First, commercially available sensors (laser and cameras) have upper range limits. In particular, even in the *absence of obstacles*, if the evader is farther from the pursuer than the sensor range then its location is unknown, and the surveillance is broken. Second, our results are applicable to a variety of non-surveillance problems. For example, shared manipulation by a human and a nonholonomic robot imposes similar constraints on the two agents (maintaining a fixed relative distance between the agents).

In this chapter, we begin in Section 3.1 by developing the system equations for the pursuer-evader system. Using these equations together with the bound on evader speed, in Section 3.1.1, we deduce a lower bound for the pursuer speed that is required to maintain a constant distance from the evader in an environment without obstacles. In Section 3.2, we present the main contribution of this work, namely, (a) the determination of the conditions that permit each of the players to win, and (b) the corresponding motion strategies. These strategies are demonstrated in various scenarios in Section 3.3.

In what follows, we will refer to the line segment that connects the pursuer and evader as the *rod* due to an analogy with the motion planning problem studied in [89]. The evader controls the position of the rod's origin (x, y) and the control of the rod's orientation ϕ is shared by both players. We consider an antagonistic evader that moves continuously, and that full state feedback is available for both players.

3.1 System Model

Figure 3.1 shows the geometric description of the system. The variables x_e, y_e, x_p, y_p denote the evader and pursuer positions with respect to the global reference frame. The variable θ is the angle of the pursuer's wheels with respect to the global x axis, and ϕ represents the angle between the rod and the global x axis. One can also interpret ϕ as the angular coordinate of the pursuer position relative to the evader in polar coordinates and therefore it may be considered to correspond to the sensor angle. Likewise, we can express the orientation of the evader relative to the pursuer as $\phi_p = \phi + \pi$. Note that $\dot{\phi}_p = \dot{\phi}$. The angle of the evader velocity vector with respect to the global x axis is denoted by ψ. Although all these quantities are time dependent, in what follows the explicit time dependence will be omitted, in order to simplify the notation.

For the evader state, the equations are simple, since the evader velocity is taken as an independent input to the system, under full control of the evader. Hence, we have

$$\dot{x}_e = V_e \cos\psi \tag{3.1}$$

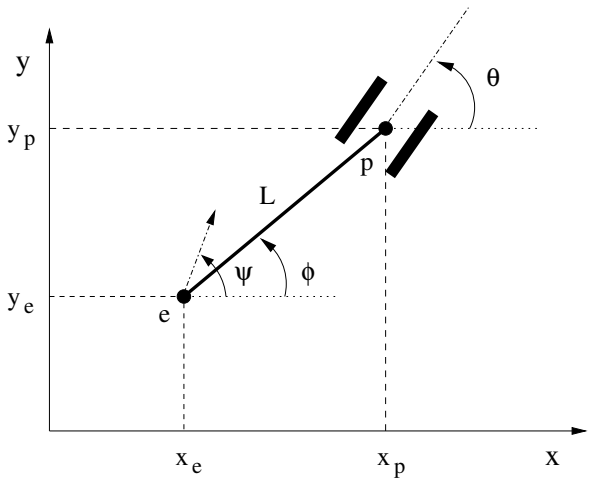

FIGURE 3.1: The geometric model of the pursuer-evader system

$$\dot{y}_e = V_e \sin\psi \tag{3.2}$$

in which V_e is the linear velocity of the evader, and we use

$$\begin{aligned} u_1 &= V_e \\ u_2 &= \psi \end{aligned} \tag{3.3}$$

under the constraint $|V_e| \leq {V_e}^{\max}$. The control u_2 appears as the argument to cos and sin functions in the state equations, and thus the state equations cannot be factored nicely into the form $A(q)u(q)$.

For the pursuer velocity, we have the usual parametrization using unicycle kinematics

$$\dot{x}_p = V_p \cos\theta \tag{3.4}$$

$$\dot{y}_p = V_p \sin\theta \tag{3.5}$$

with the constraint that $|V_p| \leq V_p^{\max}$. Since the pursuer is a differential drive robot, we use the usual assignment of control inputs [90]. For a robot with wheels of unit radius, the control inputs are therefore given by

$$u_3 = V_p = \frac{w_r(t) + w_l(t)}{2} \tag{3.6}$$

$$u_4 = \dot{\theta} = \frac{w_r(t) - w_l(t)}{2b} \tag{3.7}$$

in which b is the distance between the center of the robot and the wheel location. When $u_3 = 0$ and $u_4 \neq 0$, the robot rotates without translation, and when $u_3 \neq 0$ and $u_4 = 0$ the robot translates without rotation.

The bounds on the pursuer's speed derive from bounds on the rate at which the wheels can spin, and are thus naturally expressed as bounds on u_3 and u_4. In this chapter, we will assume symmetric and equal bounds for the two wheels, $-w^{\max} \leq w_r, w_l \leq w^{\max}$. We denote these bounds by (considering the radius of the wheels equal to 1):

$$\begin{aligned} V_p^{\max} = u_3^{\max} = \max u_3 = \frac{1}{2} \max\{w_r(t) + w_l(t)\} = w^{\max} \\ u_4^{\max} = \max u_4 = \frac{1}{2b} \max\{w_r(t) - w_l(t)\} = \frac{1}{b} w^{\max} \end{aligned} \tag{3.8}$$

so that $u_3^{\max}$ is the maximum forward linear speed of the pursuer and $u_4^{\max}$ is the maximum counterclockwise rate of rotation of the pursuer.

When the surveillance constraints are satisfied, the relationship between evader and pursuer positions is given by:

$$\begin{pmatrix} x_p \\ y_p \end{pmatrix} = \begin{pmatrix} x_e \\ y_e \end{pmatrix} + L \begin{pmatrix} \cos\phi \\ \sin\phi \end{pmatrix} \tag{3.9}$$

All pursuer velocities that maintain a constant distance L between the evader and the pursuer must therefore satisfy:

$$\begin{pmatrix} \dot{x}_p \\ \dot{y}_p \end{pmatrix} = \begin{pmatrix} \dot{x}_e \\ \dot{y}_e \end{pmatrix} + L\dot{\phi} \begin{pmatrix} -\sin\phi \\ \cos\phi \end{pmatrix} \tag{3.10}$$

From equations 3.4, 3.5 and 3.10 we obtain the following expression for the evader velocity:

$$\begin{pmatrix} \dot{x}_e \\ \dot{y}_e \end{pmatrix} = V_p \begin{pmatrix} \cos\theta \\ \sin\theta \end{pmatrix} + L\dot{\phi} \begin{pmatrix} \sin\phi \\ -\cos\phi \end{pmatrix} \tag{3.11}$$

which can be re-written as

$$\begin{pmatrix} \dot{x}_e \\ \dot{y}_e \end{pmatrix} = \begin{pmatrix} \cos\theta & L\sin\phi \\ \sin\theta & -L\cos\phi \end{pmatrix} \begin{pmatrix} u_3 \\ \dot{\phi} \end{pmatrix} \tag{3.12}$$

If we define the matrix A as

$$A = \begin{pmatrix} \cos\theta & L\sin\phi \\ \sin\theta & -L\cos\phi \end{pmatrix} \tag{3.13}$$

we find

$$\det A = -L\cos(\theta - \phi) \tag{3.14}$$

which implies that the pursuer can follow the evader only when $(\theta - \phi) \neq \pm\frac{\pi}{2}$. In other words, the rod cannot have a relative angle to the pursuer wheels equal to $\pm\frac{\pi}{2}$ because this would require unbounded pursuer speed to maintain surveillance.

Using equations 3.12 and 3.13, the relationship between the speed of the evader and the linear velocity of the pursuer can be expressed as

$$\begin{aligned} \dot{x_e}^2 + \dot{y_e}^2 &= (u_3 \quad \dot{\phi}) A^T A \begin{pmatrix} u_3 \\ \dot{\phi} \end{pmatrix} && (3.15) \\ &= {u_3}^2 - 2u_3\dot{\phi}L\sin(\theta - \phi) + L^2\dot{\phi}^2 && (3.16) \end{aligned}$$

The pursuer must be able to track the evader for any evader velocity that satisfies $\sqrt{\dot{x_e}^2 + \dot{y_e}^2} \leq {V_e}^{\max}$, and in particular, when the evader moves at maximum speed, the pursuer velocity must satisfy

$$f(u_3, \dot{\phi}) = {u_3}^2 - 2u_3\dot{\phi}L\sin(\theta - \phi) + L^2\dot{\phi}^2 \leq ({V_e}^{\max})^2 \tag{3.17}$$

which defines the interior of an ellipse in the u_3-$\dot{\phi}$ plane (see Figure 3.2).

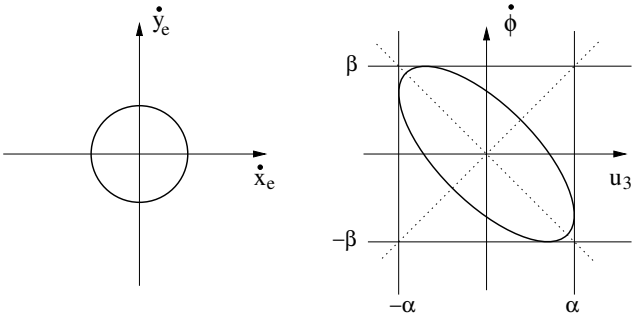

FIGURE 3.2: Velocity bounds in $\dot{x}_e$-$\dot{y}_e$ plane and in the $u_3 - \dot{\phi}$ plane

3.1.1 Bounds for u_3 and $\dot{\phi}$ to maintain surveillance

To track the evader, the robot must be able to attain all the values inside the projection of the ellipse onto the u_3 axis. Let α denote the maximal value for this projection of the ellipse (see figure 3.2). Then we have that $\alpha \leq \max|u_3| = V_p^{max}$.

To determine α we first solve for the value of $\dot{\phi}$ that corresponds to the value of f in equation 3.16 for the extremal of u_3

$$\frac{\partial f}{\partial \dot{\phi}} = 0 \rightarrow \dot{\phi} = \frac{u_3 \sin(\theta - \phi)}{L} \tag{3.18}$$

We now substitute this value into $f(u_3, \dot{\phi}) = ({V_e}^{\max})^2$, and solve for $u_3 = \alpha$ as follows

$$\begin{aligned} ({V_e}^{\max})^2 &= {u_3}^2 - 2u_3^2\sin^2(\theta - \phi) + {u_3}^2\sin^2(\theta - \phi) && (3.19) \\ &= u_3^2(1 - \sin^2(\theta - \phi)) && (3.20) \end{aligned}$$

which implies that

$$\alpha = \frac{{V_e}^{\max}}{|\cos(\theta - \phi)|} = u_3 \leq V_p^{max} \tag{3.21}$$

Using a similar analysis, we derive β as a bound on $\dot{\phi}$. In particular, we project the ellipse $f(u_3, \dot{\phi}) = ({V_e}^{\max})^2$ onto the $\dot{\phi}$ axis (see Figure 3.2), and after manipulations similar to those above we obtain

$$\beta = \frac{{V_e}^{\max}}{|L\cos(\theta - \phi)|} \leq \max|\dot{\phi}| \tag{3.22}$$

This implies that the pursuer must be able to choose its angular velocity to satisfy this constraint in order to track the evader.

From this analysis it follows that when the inequalities given in 3.21 and 3.22 hold, there is a control such that the pursuer can follow the evader moving at maximal velocity, whatever direction the evader chooses. In the next sections we present a detailed analysis that will allow us to determine, for each initial configuration of the system, which player may win the game, along with the corresponding winning strategies.

3.1.2 Determining u_3 and $\dot{\phi}$ to track the evader

If the evader's controls u_1, u_2 and the values of θ and ϕ are given, then the linear speed u_3^* of the pursuer required to maintain a constant distance L from the evader is in fact fixed. In Appendix A.1 we derive an expression for this value of u_3^*, which is given by:

$$u_3^*(\phi, \theta, u_1, u_2) = \frac{u_1\cos(u_2 - \phi)}{\cos(\theta - \phi)} \tag{3.23}$$

Notice that this expression takes its maximum value, which corresponds to the bound presented in 3.21, when $u_1 = {V_e}^{\max}$ and $u_2 = \psi = \phi$ or $u_2 = \psi = \phi + \pi$

In Appendix A.2 we show that when the pursuer successfully tracks the evader (i.e., when $u_3 = u_3^*$), $\dot{\phi}$ is given by:

$$\dot{\phi}(\phi, \theta, u_1, u_2) = \frac{u_1\sin(\theta - u_2)}{L\cos(\theta - \phi)} \tag{3.24}$$

Note that the bound presented in 3.22 is reached when $u_1 = {V_e}^{\max}$ and $u_2 = \psi = \theta \pm \frac{\pi}{2}$. In Section 3.2, we describe a relation between $\dot{\phi}$ and u_4.

If we parametrize the configuration of the pursuer-evader system by the evader position, x_e, y_e, the angle of the rod with respect to the world coordinate frame, ϕ, and the

orientation of the pursuer's wheels (heading) with respect to the world coordinate frame, θ, an alternative system model in state-space form is given by

$$\begin{pmatrix} \dot{x}_e \\ \dot{y}_e \\ \dot{\phi} \\ \dot{\theta} \end{pmatrix} = \begin{pmatrix} u_1 \cos u_2 \\ u_1 \sin u_2 \\ \dfrac{u_1 \sin(\theta - u_2)}{L \cos(\theta - \phi)} \\ u_4 \end{pmatrix} \tag{3.25}$$

It is important to stress the fact that to maintain a constant distance between the evader and the pursuer, equations 3.23 and 3.24 in terms of the evader controls must be satisfied.

3.1.3 Bounds on u_4 when tracking the evader

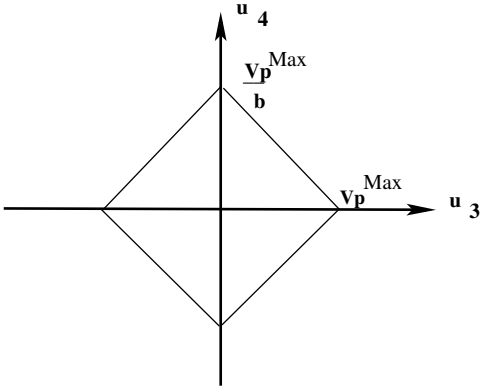

FIGURE 3.3: Control space (u_3, u_4)

For a given choice of u_3, there is a finite range of values that can be taken by u_4, since the differential drive robot wheel speeds are bounded (as described in Section 3.1). As the linear speed of the pursuer $|u_3|$ attains its maximum, the rate of rotation of the pursuer $|u_4|$ attains its minimum. For example, when $|u_3| = V_p^{\max}$, we necessarily have $\dot{\theta} = 0$. Using equations 3.6 and 3.7, the bounds on u_4 are most easily deduced by considering individually the case $u_3 < 0$ and $0 \leq u_3$. For $0 \leq u_3$ we have

$$-\frac{1}{b}(V_p^{\max} - u_3) \leq u_4 \leq \frac{1}{b}(V_p^{\max} - u_3) \tag{3.26}$$

and for $u_3 < 0$ we have

$$-\frac{1}{b}(V_p^{\max} + u_3) \leq u_4 \leq \frac{1}{b}(V_p^{\max} + u_3) \tag{3.27}$$

These four constraints are illustrated in Figure 3.3. They can be combined into the single expression

$$|\dot{\theta}| = |u_4(u_3)| \leq \frac{1}{b}\left(V_p^{max} - |u_3|\right) \tag{3.28}$$

This expression gives the maximum rate of rotation for the pursuer, given a specified linear speed u_3.

3.2 Evader and Pursuer Strategies

From the analysis presented in Section 3.1.1 we can establish that if at any time inequality 3.21 does not hold then the evader wins. But this analysis does not directly address the issue of determining which player wins the game for a given configuration of the system, nor does it determine winning strategies for the pursuer and evader. In this section, we consider these issues. We begin with an intuitive motivation for the pursuer and evader strategies, and then give a more formal treatment.

The result of the pursuit-evasion game depends critically on the rotation speeds for the rod ($\dot{\phi}$) and for the pursuers heading ($\dot{\theta}$). This may be seen in equation 3.23, which gives the linear velocity u_3^* for the pursuer, so that a constant value for L is maintained. As $|\cos(\theta-\phi)|$ increases, the required value for u_3 decreases, and reaches its minimum when $|\cos(\theta-\phi)| = 1$. On the other hand, when $|\cos(\theta-\phi)| = 0$ there is no pursuer with bounded maximum speed that can maintain surveillance, since $u_3^* \to \infty$. For this reason, a good strategy for the pursuer is to move θ (using $u_4 = \dot{\theta}$), so that $|(\theta-\phi)|$ decreases, while for the evader, a good strategy is to increase this value using $\dot{\phi}$, which depends only on its controls u_1, u_2 (equation 3.24). In particular, if $\max|\dot{\theta}| = \frac{1}{b}(V_p^{max} - |u_3|)$ is equal to $|\dot{\phi}|$, the pursuer will be able to compensate exactly the rotation that the evader tries to impose on the rod, keeping $|(\theta-\phi)|$ constant. In this case, the strategy for the pursuer is uniquely determined, and consists in setting $u_3 = u_3^*$, and $u_4 = u_4^*$, with $|u_4^*| = \max|\dot{\theta}| = \frac{1}{b}(V_p^{max} - |u_3^*|)$. The sign for u_4^* must be chosen in such a way that the angle between the rod and the pursuer's wheels $(\theta-\phi)$ moves away from $\pm\frac{\pi}{2}$. Specifically:

$$\begin{aligned} u_4^*(\theta,\phi) &= s(\theta,\phi)\max|\dot{\theta}| \\ &= s(\theta,\phi)\frac{1}{b}(V_p^{max} - |u_3^*(\theta,\phi)|) \end{aligned} \tag{3.29}$$

in which

$$s(\theta,\phi) = \begin{cases} -1: & (\theta-\phi) \in (0,\frac{\pi}{2}) \bigcup (\pi,\frac{3\pi}{2}) \\ +1: & (\theta-\phi) \in (\frac{\pi}{2},\pi) \bigcup (\frac{3\pi}{2},2\pi) \end{cases} \tag{3.30}$$

and the value -1 corresponds to clockwise rotation while the value $+1$ corresponds to counterclockwise rotation.

In the case of the evader, the situation is more complex, since it can control $\dot{\phi}$ directly (equation 3.24), but also $\max|\dot{\theta}|$ indirectly, since it can maximize the required linear speed of the pursuer u_3^* (see equation (3.28)). In particular, one can establish the following lemma.

Lemma 3.1. *Let* $g(\phi, \theta, u_2) = (|\cos(\phi - u_2)| + \gamma|\sin(\theta - u_2)|)$ *with* $\gamma = b/L$. *Then the following two converse conditions hold.*

(i) $\max|\dot{\theta}| < |\dot{\phi}|$ *if and only if* $V_p^{\max}(|\cos(\theta - \phi)|) < |u_1| g(\phi, \theta, u_2)$

(ii) $\max|\dot{\theta}| \geq |\dot{\phi}|$ *if and only if* $V_p^{\max}(|\cos(\theta - \phi)|) \geq |u_1| g(\phi, \theta, u_2)$

Note that since b is the radius of the robot pursuer then $L \geq b$ otherwise the evader is in collision with the pursuer, hence $\gamma \in (0, 1]$.

Proof. The inequality $\max|\dot{\theta}| < |\dot{\phi}|$ can be expanded as follows

$$\max|\dot{\theta}| < |\dot{\phi}| \tag{3.31}$$

$$\frac{1}{b}\left(V_p^{\max} - |u_3^*|\right) < \left|\frac{u_1 \sin(\theta - u_2)}{L\cos(\theta - \phi)}\right| \tag{3.32}$$

$$\frac{1}{b}\left(V_p^{\max} - \left|\frac{u_1\cos(u_2 - \phi)}{\cos(\theta - \phi)}\right|\right) < \frac{|u_1 \sin(\theta - u_2)|}{|L\cos(\theta - \phi)|} \tag{3.33}$$

$$V_p^{\max}(|\cos(\theta - \phi)|) < |u_1|(|\cos(\phi - u_2)| + \gamma|\sin(\theta - u_2)|) \tag{3.34}$$

in which inequality 3.32 follows from equation 3.28 (assuming the maximum value of $|\dot{\theta}|$) and from equation 3.24; inequality 3.33 follows from equation 3.23; and inequality 3.34 follows from straightforward manipulation.

The second part of the proof corresponding to $\max|\dot{\theta}| \geq |\dot{\phi}|$ is analogous to the one presented above, yielding

$$V_p^{\max}(|\cos(\theta - \phi)|) \geq |u_1|(|\cos(\phi - u_2)| + \gamma|\sin(\theta - u_2)|) \tag{3.35}$$

□

From this result, we can infer that a good strategy for the evader is to choose $(u_1, u_2) = (u_1^*, u_2^*)$ at every time instant, such that

$$(u_1^*, u_2^*) = \arg\max_{u_1,u_2} |u_1| g(\phi, \theta, u_2) \tag{3.36}$$

If $V_p^{\max}(|\cos(\theta - \phi)|) = u_1^* g(\phi, \theta, u_2^*) - \epsilon$ at any time, for an arbitrarily small $\epsilon > 0$, then this choice will be the only one that will allow the evader to move $\cos(\theta - \phi)$ towards 0. As we will now show, these choices, i.e., (u_1^*, u_2^*) and (u_3^*, u_4^*), actually represent winning strategies for the evader and pursuer respectively, and in some sense they may be considered as equilibrium strategies for the game [20].

We now proceed with a formal development of the conditions that determine the winner of the game and the players' strategies. The following lemma gives conditions on the value of u_2 that maximizes $g(\phi, \theta, u_2)$.

Lemma 3.2. *Consider the following functions:*

$$\psi_1 = \arctan\left(\frac{\sin\phi - \gamma\cos\theta}{\cos\phi + \gamma\sin\theta}\right) \tag{3.37}$$

$$\psi_2 = \arctan\left(\frac{\sin\phi + \gamma\cos\theta}{\cos\phi - \gamma\sin\theta}\right) \tag{3.38}$$

$$\psi_3 = \arctan\left(\frac{-\sin\phi - \gamma\cos\theta}{-\cos\phi + \gamma\sin\theta}\right) \tag{3.39}$$

$$\psi_4 = \arctan\left(\frac{-\sin\phi + \gamma\cos\theta}{-\cos\phi - \gamma\sin\theta}\right) \tag{3.40}$$

The evader control u_2 that maximizes $g(\phi, \theta, u_2)$ for given values of ϕ and θ is given by

$$u_2 = \begin{cases} \psi_1 \text{ or} \psi_4 = \psi_1 + \pi : & (\theta - \phi) \in [0, \pi] \\ \psi_2 \text{ or } \psi_3 = \psi_2 + \pi : & (\theta - \phi) \in [\pi, 2\pi] \end{cases} \tag{3.41}$$

The proof of this lemma is given in Appendix A.3.

Next, we give some monotonicity properties of some functions that will be used later to establish our main result:

Lemma 3.3. *Define the following functions:*

$$K(\theta, \phi) = \begin{cases} \psi_4(\theta, \phi), \text{If } (\theta - \phi) \in [0, \pi] \\ \psi_3(\theta, \phi), \text{If } (\theta - \phi) \in [\pi, 2\pi] \end{cases} \tag{3.42}$$

$$u_3^{**}(\theta, \phi) = u_3^*(\theta, \phi, V_e^{max}, K(\theta, \phi)) \tag{3.43}$$

$$u_4^{**}(\theta, \phi) = s(\theta, \phi) \max|\dot{\theta}| = s(\theta, \phi)\frac{1}{b}(V_p^{max} - |u_3^{**}(\theta, \phi)|) \tag{3.44}$$

with $s(\theta, \phi)$ *given by equation 3.30.*

If $(\theta - \phi) \in (0, \frac{\pi}{2}) \bigcup (\pi, \frac{3\pi}{2})$ *then* $g(\phi, \theta, K)$ *and* $|\dot{\phi}(V_p^{max}, K, \theta, \phi)|$ *increase monotonically (w.r.t* $(\theta - \phi)$*), and* $|u_4^{**}(\theta, \phi)| = \max|\dot{\theta}|$ *decreases monotonically (w.r.t* $(\theta - \phi)$*).*

Symmetrically, if $(\theta - \phi) \in (\frac{\pi}{2}, \pi) \bigcup (\frac{3\pi}{2}, 2\pi)$*then* $g(\phi, \theta, K)$ *and* $|\dot{\phi}(V_p^{max}, K, \theta, \phi)|$ *decrease monotonically (w.r.t* $(\theta - \phi)$*), and* $|u_4^{**}(\theta, \phi)| = \max|\dot{\theta}|$ *increases monotonically (w.r.t* $(\theta - \phi)$*).*

We note here the two main properties of the proof of this lemma.

- The possible admissible values of the ratio $\gamma \in (0, 1]$ do not affect the monotonicity of $g(\phi, \theta, K)$.
- All the possible values of $(\theta - \phi)$ are considered, i.e., all four quadrants are covered.

The proof of Lemma 3.3 appears in Appendix A.4.

As it was mentioned above, the selected evader control must produce a rod rotation that brings the rod perpendicular to the pursuer wheels (pursuer heading) without bringing the rod and the pursuer heading (pursuer wheels) closer to parallelism. Let's call this direction of rotation Desirable Evader Direction of Rotation (DEDR). Conversely, the selected pursuer control must produce a pursuer heading rotation that brings the pursuer wheels (pursuer heading) closer to parallelism with the rod, without bringing the pursuer heading (pursuer wheels) and the rod closer to perpendicularity. Let's call this direction of rotation Desirable Pursuer Direction of Rotation (DPDR). Refer to figure 3.4, which shows (DPDR) w.r.t the rod's orientation.

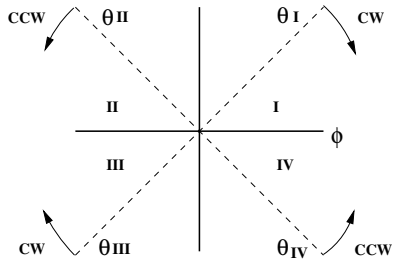

FIGURE 3.4: Direction of rotation

Thus, it is necessary to analyse the direction of rotation (clockwise or counterclockwise) of both the pursuer heading (directly controlled by the pursuer with u_4) and the rod (controlled by the evader by virtue of u_2). The desirable direction of rotation of both u_4^{**} and $\dot{\phi}(V_p^{max}, K, \theta, \phi)$ is provided in the following corollary.

Corollary 3.4 (Lemma 3.3)**.** *If* $(\theta-\phi)\in(0,\frac{\pi}{2})\cup(\pi,\frac{3\pi}{2})$ *then the DPDR is clockwise (cw), i.e.* $sgn(u_4^{**})=s(\theta,\phi)=-1$ *(as given by Eq. 3.30), and the DEDR is also clockwise (cw), i.e.* $sgn(\dot{\phi}(\psi_i))=-1$*. Conversely, if* $(\theta-\phi)\in(\frac{\pi}{2},\pi)\cup(\frac{3\pi}{2},2\pi)$ *then the DPDR is counterclockwise (ccw)* $sgn(u_4^{**})=s(\theta,\phi)=+1$ *(as given by Eq. 3.30), and the DEDR is also counterclockwise (ccw)* $sgn(\dot{\phi}(\psi_i))=+1$*. Thus, the following controls must be applied by the players according to the value of* $(\theta-\phi)$*, to obtain the required direction of rotation of both* u_4^{**} *and* $\dot{\phi}(V_p^{max},K,\theta,\phi)$*.*

The evader control u_2^**, is given in table 3.1.*

$(\theta-\phi)$	$sgn(\dot{\phi}(V_p^{max},K,\theta,\phi))$	$u_2^*=\psi_i$
$(\theta-\phi)\in[0,\frac{\pi}{2}]$	$sgn(\dot{\phi}(V_p^{max},K,\theta,\phi))=-1$	$u_2^*=\psi_4$
$(\theta-\phi)\in[\frac{\pi}{2},\pi]$	$sgn(\dot{\phi}(V_p^{max},K,\theta,\phi))=+1$	$u_2^*=\psi_4$
$(\theta-\phi)\in[\pi,\frac{3\pi}{2}]$	$sgn(\dot{\phi}(V_p^{max},K,\theta,\phi))=-1$	$u_2^*=\psi_3$
$(\theta-\phi)\in[\frac{3\pi}{2},2\pi]$	$sgn(\dot{\phi}(V_p^{max},K,\theta,\phi))=+1$	$u_2^*=\psi_3$

TABLE 3.1: Evader control u_2 and rod's direction of rotation

The sign (direction of rotation) of $u_4^{**}=\max|\dot{\theta}|=\frac{1}{b}(V_p^{max}-|u_3^{**}|)$ *is defined by equation 3.30.*

The proof of this Corollary appears in Appendix A.5.

Remark 3.5. Note that with this definition for $u_2^*=\psi_i$ one gets precisely $u_2^*=K(\theta,\phi)$.

Remark 3.6. The DPDR for u_4^{**} also holds for u_4^*.

Remark 3.7. The control u_1 that maximizes $|u_1|*g$ is $u_1^*=V_e^{max}$.

The next theorem represents our main result.

Theorem 3.8. *Let*

$$u_1^*=V_e^{max} \tag{3.45}$$

$$u_2^*=K(\theta,\phi) \tag{3.46}$$

and let u_3^* *be as given by equation 3.23, and* u_4^* *as given by equation 3.29. Now define*

$$M(V_e^{max},V_p^{max},\theta,\phi)=|\dot{\phi}(u_1^*,u_2^*)|-\frac{1}{b}(V_p^{max}-|u_3^{**}|) \tag{3.47}$$

The manifold $M(V_e^{max},V_p^{max},\theta,\phi)=0$ *partitions the space spanned by* $V_e^{max},V_p^{max},\theta,\phi$ *into 2 regions, one in which the pursuer can maintain surveillance indefinitely, and another in which the evader can eventually escape.*

If $M(V_e^{max},V_p^{max},\theta,\phi)>0$ *at the beginning of the game, then the evader eventually wins at some time* $t>t_0$ *if the strategy* $(u_1,u_2)=(u_1^*,u_2^*)$ *is applied at all times,*

regardless of the strategy applied by the pursuer. Otherwise, if at the beginning of the game $M(V_e^{max}, V_p^{max}, \theta, \phi) \leq 0$*, the pursuer wins, if the strategy* $(u_3, u_4) = (u_3^*, u_4^*)$ *is applied at all times, regardless of the strategy applied by the evader.*

Proof. The theorem can be proved based on the maximization of g and the monotonicity of $\max\{g\}$, $|\dot{\phi}|$, $\max|\dot{\theta}|$ and $|\cos(\theta - \phi)|$. Because $|\cos(\theta - \phi)|$ behaves differently depending on which quadrant contains $\theta - \phi$, we consider individually the four quadrants. Here, we consider the case for which $\theta - \phi \in [0, \frac{\pi}{2}]$. The proofs of the other cases are analogous and are included in Appendix A.6.

The proof proceeds as follows. We first consider the case when the pursuer applies the strategy $(u_3, u_4) = (u_3^{**}, u_4^{**})$ and the evader applies the strategy $(u_1, u_2) = (u_1^*, u_2^*)$. We show that under these strategies the pursuer wins if $\max|\dot{\theta}(t_0)| \geq |\dot{\phi}(t_0)|$ (i.e., if at the beginning of the game $M(V_e^{max}, V_p^{max}, \theta, \phi) \leq 0$), otherwise the evader wins. Second, we show that if the pursuer applies the strategy $(u_3, u_4) = (u_3^*, u_4^*)$ and $|\dot{\phi}(t_0)| \leq \max|\dot{\theta}(t_0)|$, then the pursuer wins regardless of the strategy applied by the evader. Symmetrically, if the evader applies the strategy $(u_1, u_2) = (u_1^*, u_2^*)$ and $|\dot{\phi}(t_0)| > \max|\dot{\theta}(t_0)|$ then the evader wins regardless of the pursuer strategy. We now develop the details.

Assume that $M(V_e^{max}, V_p^{max}, \theta, \phi) \leq 0$ at the beginning of the game. We analyse this inequality first considering $M(V_e^{max}, V_p^{max}, \theta, \phi) < 0$. For this case, we have that $\max|\dot{\theta}(t_0)| > |\dot{\phi}(t_0)|$, and from Lemma 3.1, $V_p^{max}|\cos(\theta - \phi)| > |u_1^*| \cdot g(\phi, \theta, u_2^*)$. By Lemmas 3.2 and 3.3, $g(\phi, \theta, u_2^*)$ is maximal and varies monotonically by applying the optimal $u_2^* = \psi_4$. By Lemma 3.3, $g(\phi, \theta, u_2^*)$ monotonically decreases and $|\cos(\theta - \phi)|$ monotonically increases as $(\theta - \phi)$ varies from $\frac{\pi}{2}$ to 0.

If $\max|\dot{\theta}(t_0)| > |\dot{\phi}(t_0)|$ then for $\epsilon \to 0$ we have $(\theta(t_0) - \phi(t_0)) > (\theta(t_0 + \epsilon) - \phi(t_0 + \epsilon))$, and by Lemma 3.3, $\max|\dot{\theta}|$ monotonically increases and $|\dot{\phi}|$ monotonically decreases as $(\theta - \phi)$ varies from $\frac{\pi}{2}$ to 0. Hence $\forall t > t_0$, $\max|\dot{\theta}(t)| > |\dot{\phi}(t)|$, and therefore $\forall t > t_0, (\theta(t_0) - \phi(t_0)) > (\theta(t) - \phi(t))$, and $(\theta(t) - \phi(t))$ decreases monotonically until it reaches 0 and the pursuer wins.

Now assume that $M(V_e^{max}, V_p^{max}, \theta, \phi) > 0$ at the beginning of the game. Then $\max|\dot{\theta}(t_0)| < |\dot{\phi}(t_0)|$ and $V_p^{max}|\cos(\theta - \phi)| < |u_1^*| \cdot g(\phi, \theta, u_2^*)$. Then by Lemma 3.3, $g(\phi, \theta, u_2^*)$ monotonically increases and $|\cos(\theta - \phi)|$ monotonically decreases as $(\theta - \phi)$ varies from 0 to $\frac{\pi}{2}$.

If $\max|\dot{\theta}(t_0)| < |\dot{\phi}(t_0)|$ then for $\epsilon \to 0$ we have $(\theta(t_0) - \phi(t_0)) < (\theta(t_0 + \epsilon) - \phi(t_0 + \epsilon))$, and by Lemma 3.3, $\max|\dot{\theta}|$ monotonically decreases and $|\dot{\phi}|$ monotonically increases as $(\theta - \phi)$ varies from 0 to $\frac{\pi}{2}$. Hence $\forall t > t_0$, $\max|\dot{\theta}(t)| < |\dot{\phi}(t)|$, and therefore $(\theta(t_0) - \phi(t_0)) <$

$(\theta(t) - \phi(t))$ and $(\theta(t) - \phi(t))$ increases monotonically until it reaches $\frac{\pi}{2}$ and the evader wins.

In the case of equality, i.e., $\max|\dot{\theta}(t_0))| = |\dot{\phi}(t_0)|$ (equivalently, $V_p^{max}|\cos(\theta - \phi)| = |u_1^*| \cdot g(\phi, \theta, u_2^*)$), for $\epsilon \to 0$ we will have $(\theta(t_0) - \phi(t_0)) = (\theta(t_0 + \epsilon) - \phi(t_0 + \epsilon))$. By Lemma 3.3, $\max|\dot{\theta}|$ and $|\dot{\phi}|$ remain constant for a given value of $(\theta - \phi)$. Hence $\forall t > t_0$, $\max|\dot{\theta}(t)| = |\dot{\phi}(t)|$ and $(\theta(t) - \phi(t)) = (\theta(t_0) - \phi(t_0))$. Therefore, the values of both $g(\phi, \theta, u_2 = K)$ and $|\cos(\theta - \phi)|$ remain constant and the pursuer wins. Note that this result is obtained regardless of the quadrant in which $(\theta - \phi)$ lies.

We now show that, if $\max|\dot{\theta}(t_0)| < |\dot{\phi}(t_0)|$ then the evader wins regardless of the pursuer strategy, whenever the evader applies $(u_1, u_2) = (u_1^*, u_2^*)$.

If $u_3 \neq u_3^*$, the pursuer immediately loses, it cannot maintain the constant distance.

If $u_3 = u_3^*$ but $u_4 \neq u_4^*$ then for all time t we will have $|u_4| = |\dot{\theta}(t)| < |u_4^*| = \max|\dot{\theta}(t)| < |\dot{\phi}(t)|$. Hence, $(\theta(t) - \phi(t))$ under $(u_1^*, u_2^*, u_3^*, u_4)$ is closer to $\pm\frac{\pi}{2}$ than $(\theta(t) - \phi(t))$ under $(u_1^*, u_2^*, u_3^*, u_4^*)$. Therefore, if $\max|\dot{\theta}(t_0)| < |\dot{\phi}(t_0)|$, the evader wins regardless the pursuer strategy.

Symmetrically, if $|\dot{\phi}(t_0)| \leq \max|\dot{\theta}(t_0)|$ then the pursuer wins regardless the evader strategy. By Lemma 3.1, the condition $|\dot{\phi}(t_0)| \leq \max|\dot{\theta}(t_0)|$ is equivalent to

$$g(\phi(t_0), \theta(t_0), u_2(t_0))|u_1(t_0))| \leq V_p^{max}|\cos(\theta(t_0) - \phi(t_0))| \tag{3.48}$$

Let us assume that the evader uses (u_1^*, u_2^*). These evader controls maximize

$g(\phi(t), \theta(t), u_2(t))|u_1(t)|$. The inequality

$$g(\phi(t), \theta(t), u_2^*(t))|u_1^*(t)| \leq V_p^{max}|\cos(\theta(t) - \phi(t))| \tag{3.49}$$

is also equivalent to (again by Lemma 3.1):

$$\begin{array}{ccccc} \underbrace{\dfrac{|u_1^* \sin(\theta - u_2^*)|}{|L\cos(\theta - \phi)|}} & - & \underbrace{\dfrac{1}{b}\left(V_p^{\max} - \overbrace{\left|\dfrac{u_1^*\cos(u_2^* - \phi)}{\cos(\theta - \phi)}\right|}^{u_3^{**}(u_1^*, u_2^*)}\right)} & \leq & 0 \\ |\dot{\phi}(t)| & - & |u_4^{**}| = \max|\dot{\theta}(t)| & \leq & 0 \end{array} \tag{3.50}$$

Thus, the evader's controls (u_1^*, u_2^*) maximize the difference $|\dot{\phi}(u_1^*(t), u_2^*(t))| - \max|u_4(u_1^*(t), u_2^*(t))|$.

If the evader uses $(u_1, u_2) \neq (u_1^*, u_2^*)$ then

$$\forall t: \; g(\phi(t), \theta(t), u_2(t))|u_1(t)| < g(\phi(t), \theta(t), u_2^*(t))|u_1^*(t)| \tag{3.51}$$

and

$$|\dot{\phi}(u_1(t), u_2(t))| - \max|u_4^*(u_1(t), u_2(t))| < |\dot{\phi}(u_1^*(t), u_2^*(t))| - \max|u_4^{**}(u_1^*(t), u_2^*(t))| \leq 0 \tag{3.52}$$

If the evader uses at all times the controls that maximize the difference $|\dot{\phi}(t)| - \max|\dot{\theta}(t)|$, and this difference is still negative or equal to zero, then no evader control will make the difference greater than zero. Therefore

$$\forall t: \; g(\phi(t), \theta(t), u_2(t))|u_1(t)| < V_p^{max}|\cos(\theta(t) - \phi(t))| \tag{3.53}$$

and

$$|\dot{\phi}(u_1(t_0), u_2(t_0))| < |u_4^*(u_3^*(t_0))| = \max|\theta(t_0)| \tag{3.54}$$

The result follows.

□

Corollary 3.9 (Theorem 3.8)**.** *For $|M(V_e^{max}, V_p^{max}, \theta, \phi)| < \epsilon$, i.e., in a neighborhood of the manifold described above, for $\epsilon \to 0$, the strategies: $(u_3, u_4) = (u_3^*, u_4^*)$ for the pursuer and $(u_1, u_2) = (u_1^*, u_2^*)$ for the evader are the only equilibrium strategies for the game. The application of these strategies are necessary and sufficient conditions for guaranteeing that the corresponding player wins.*

Note that when both players follow these strategies we have $(u_3^*, u_4^*) = (u_3^{**}, u_4^{**})$.

Proof. If each of V_e^{max}, V_p^{max}, and $(\theta - \phi)$ are given, and $\max|\dot{\theta}(t_0)| = |\dot{\phi}(t_0)|$ then there is no valid control, other than $|u_4^*| = \max|\dot{\theta}|$, which guarantees that the pursuer will win. Any other value of u_4 makes $|\dot{\theta}|$ smaller, yielding $|\dot{\theta}(t_0)| < |\dot{\phi}(t_0)|$, which corresponds to the evader winning. Hence, that the pursuer use strategy $u_4^* = \max|\dot{\theta}(t_0)|$ is both a necessary and sufficient condition for the pursuer to win.

Suppose now that $\max|\dot{\theta}(t_0)| < |\dot{\phi}(t_0)|$. By Lemma 3.1, this is equivalent to:

$$V_p^{max}|\cos(\theta(t_0) - \phi(t_0))| < |u_1(t_0)| \cdot g(\phi(t_0), \theta(t_0), u_2(t_0)) \tag{3.55}$$

If V_p^{max}, $(\theta - \phi)$ are given, and $u_1 = u_1^*$, $u_2 = u_2^*$ are such that $|u_1^*| \cdot g(\phi, \theta, u_2^*)$ has the minimum value for the inequality to hold, then there are not controls other than

(u_1^*, u_2^*) that maintain the condition. Any other controls make $|u_1| \cdot g(\phi, \theta, u_2)$ smaller, and consequently the inequality will change to:

$$V_p^{max} |\cos(\theta(t_0) - \phi(t_0))| \geq |u_1| \cdot g(\phi, \theta, u_2) \tag{3.56}$$

and the pursuer will win. Hence, that the evader apply the strategy (u_1^*, u_2^*) that maximizes $|u_1| \cdot g(\phi, \theta, u_2)$ is both a necessary and sufficient condition for the evader to win.

□

Remark 3.10. By Corollary 3.9, the players' strategies may be considered Local Equilibrium Strategies (LES). As the system moves away from the manifold, the winning player's choice of controls is constrained (so that the system remains in the corresponding region), but is not unique. The constraints are: for the pursuer $u_3 = u_3^*$ and $|u_4| \geq |\dot{\phi}|$, for the evader $|u_1| g(\phi, \theta, u_2) > V_p^{max} |\cos(\theta - \phi)|$. If the LES are followed, however, there are some interesting properties that are obtained. If the pursuer wins, the LES eventually leads to an alignment of its wheels with the rod (i.e., $\theta = \phi$ or $\theta = \phi + \pi$), which allows it to maintain surveillance with the minimal effort (i.e., minimal $|V_p|$). Notice that at the moment the pursuer heading reaches parallelism with the rod, it is possible for the pursuer to keep this parallelism by applying $u_4 = \dot{\theta} = \dot{\phi}$, thus avoiding oscillations. If the evader wins, the LES progressively increases the required value of u_3 up to ∞, so that it allows it to escape from any pursuer with bounded speed.

Remark 3.11. If V_p^{max} and V_e^{max} are given as inputs to the problem, the LES create a partition over the value of $(\theta - \phi)$ into two sets which define the winner of the game. On the other hand, for a given initial $(\theta - \phi)$ and if either V_p^{max} or V_e^{max} is given, these motion strategies allow the calculation of the remaining minimum value of V_e^{max} or V_p^{max} respectively, which correspond to the minimal capabilities for the players to win.

Remark 3.12. It is interesting to note that, when the evader wins g converges to 2 (for $\gamma = 1$) and $|\cos(\theta - \phi)|$ converges to 0, and when the pursuer wins g converges to $\sqrt{2}$ (for $\gamma = 1$) and $|\cos(\theta - \phi)|$ converges to 1.

3.3 Simulations

In this section, we present numerical simulations to illustrate the pursuer's and the evader's motion strategies. Since the pursuer is a nonholonomic system, we use numerical integration to compute the approximate paths for the pursuer.

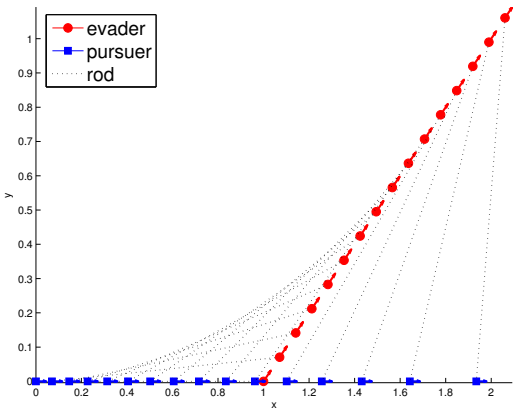

FIGURE 3.5: Evader wins, pursuer follows a straight line trajectory $u_4 = 0$

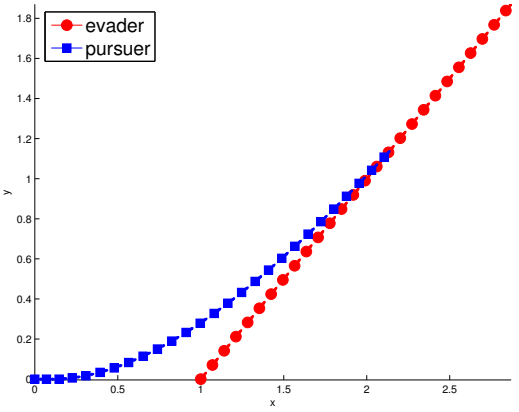

FIGURE 3.6: Pursuer wins by making $\theta = \phi$

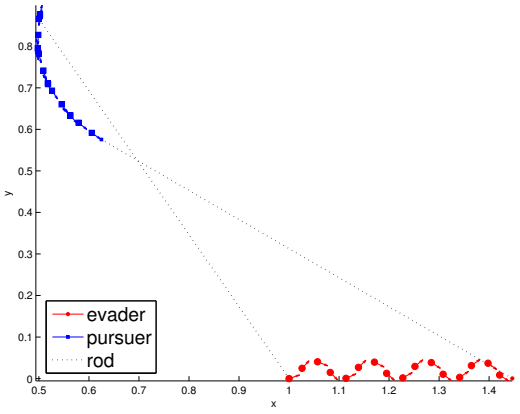

FIGURE 3.7: Evader moves tracing a sinusoidal path, pursuer wins by pointing its heading parallel to the rod

In all figures, the evader is shown with a (red) circle and the pursuer with a (blue) square, the rod is represented with a dotted line segment. The (blue) arrows emerging from the pursuer show the heading of the pursuer (heading of the wheels of the differential drive

robot pursuer), and the (red) arrows emerging from the evader show the direction of the evader velocity vector.

In Figure 3.5, the initial system configuration is $\theta = 0$ and $\phi = \pi$. The evader chooses its velocity vector at a constant orientation ($u_2 = \psi = \frac{\pi}{4}$). The pursuer does not change its heading ($u_4 = 0$), but it uses the required u_3^* and $\dot{\phi}$ to follow the evader. The pursuer is able to follow the evader for a short period of time until the rod orientation gets close to being perpendicular to the pursuer heading.

In Figure 3.6, again the initial system configuration is $\theta = 0$ and $\phi = \pi$ and the evader chooses at all time its velocity vector at a constant orientation ($u_2 = \psi = \frac{\pi}{4}$). But this time the pursuer changes u_4 to point its heading to be parallel to the rod, yielding a pursuer win. Note that for the simulations in Figures 3.5 and 3.6 the evader has followed a sub-optimal strategy.

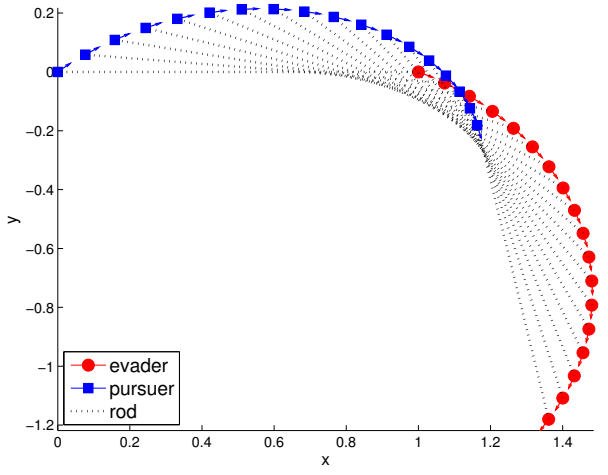

FIGURE 3.8: Pursuer wins by making $\theta = \phi + \pi$, evader uses optimal $u_2 = \psi$ but its maximal velocity ${V_e}^{\max}$ is insufficient for winning

In Figure 3.7 the evader moves tracing a sinusoidal path, the pursuer wins by making $\theta = \phi$. Again the evader has followed a sub-optimal strategy.

Figures 3.8 and 3.9 show optimal pursuer and evader motion strategies. In the two simulations presented in these figures, at the beginning of the game $\gamma = 1$, $\theta = 40$ degrees and $\phi = 180$ degrees. In both of these simulations, the evader uses the optimal $u_2^* = \psi_i$. The pursuer uses $u_4^{**} = s(\theta, \phi) \max |\dot{\theta}|$ trying to make it parallel to the rod orientation.

In figure 3.8, the pursuer wins since $\max |\dot{\theta}(t_0)| > |\dot{\phi}(t_0)|$, hence at the end the pursuer is able to point its heading parallel to the rod orientation $(\theta - \phi) = \pi$.

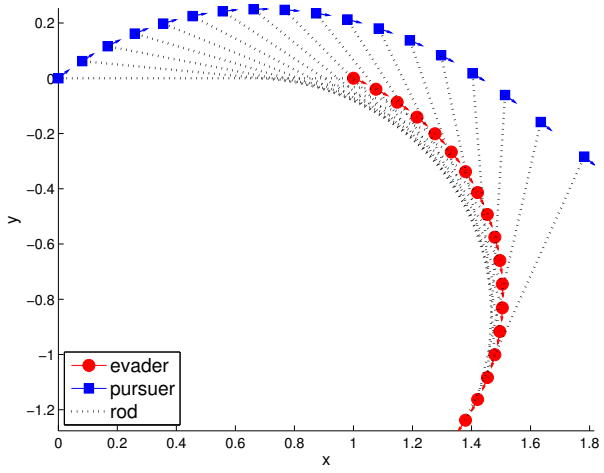

FIGURE 3.9: Evader wins using optimal $u_2 = \phi$ yielding $(\theta - \phi) = \frac{\pi}{2}$

In figure 3.9, the evader wins since $|\dot{\phi}(t_0)| > \max|\dot{\theta}(t_0)|$, hence at the end the evader is able to get the rod orientation perpendicular to the pursuer heading $(\theta - \phi) = \frac{\pi}{2}$.

From inequality 3.33, it is possible to compute a smallest critical value of the evader velocity V_e^{max} or even a ratio of the pursuer and evader velocities, which determines either the evader or pursuer winning, the critical ratio is defined by $\rho = \frac{V_e{}^{max}}{V_p{}^{max}} = \frac{|\cos(\theta-\phi)|}{g}$.

For the simulations shown in figures 3.8 and 3.9, $V_p{}^{\max} = 1$. Then the critical evader velocity determining the winner of the game is $V_e^{max} = 0.4226$. When the evader wins $V_e^{max} = 0.43$, and when the evader loses $V_e^{max} = 0.41$.

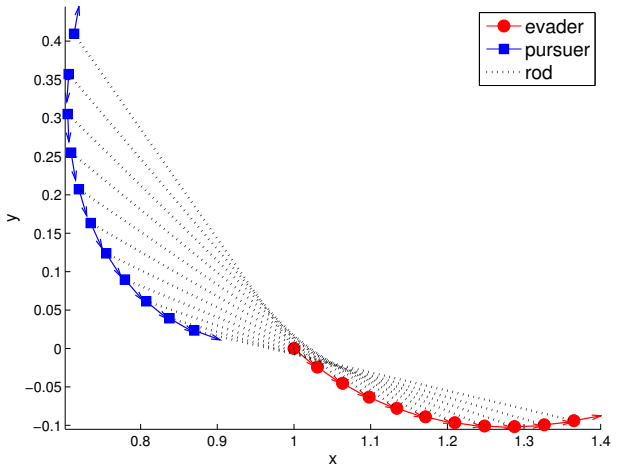

FIGURE 3.10: The initial conditions are identical to those for the example of figure 3.11. Here, the pursuer wins since $\rho \leq 0.5054$ (see text).

Figures 3.10 and 3.11 show additional two simulations in which both players use optimal motion strategies. In these simulations $b = 0.25$ and $L = 0.5$, thus $\gamma = 0.5$. At the

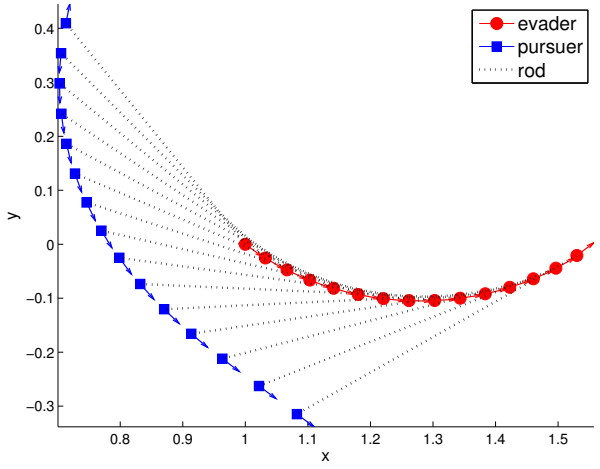

FIGURE 3.11: The initial conditions are identical to those for the example of figure 3.10. Here, the evader wins since $\rho > 0.5054$ (see text).

beginning of the game $\theta = 80$ degrees, and $\phi = 125$ degrees. In figure 3.10 the pursuer wins, in figure 3.11 the evader wins. For the initial system configuration corresponding to this simulations, the critical value for the ratio ρ is given by $\rho = \frac{V_e{}^{max}}{V_p{}^{max}} = \frac{|\cos(\theta-\phi)|}{g} = 0.5054$. If $\rho > 0.5054$ then evader wins, else when $\rho \leq 0.5054$ the pursuer wins. Note that this ratio can be computed based only on θ, ϕ and the optimal $u_2^* = \psi_i$.

Finally, figures 3.12 and 3.13 show a simulation in which the evader moves randomly, the pursuer wins aligning its wheels parallel to the rod ($\overrightarrow{V_P} \parallel \overrightarrow{L}$), figure 3.13 shows the initial and final orientations of the pursuer wheels w.r.t the rod. Figures 3.12 and 3.13 exemplify that whenever Theorem I is satisfied for the pursuer, the pursuer can track the evader even if the evader follows a random motion. If the pursuer is able to track an evader following the optimal policy, it shall be able to track an evader following any other policy. Hence, it is not needed to know the policy chosen by the evader at every instant of time.

3.4 Conclusions and Future Work

In this chapter, we have considered the surveillance problem of tracking of a moving evader by a differential drive pursuer (nonholonomic robot).

We have analysed the case in which the pursuer and the evader move in an environment without obstacles. We have shown that in order to maintain a constant distance to the evader, the linear speed of the pursuer is totally determined for every configuration of the system, so that its only degree of freedom is its rotation angle. We have derived a lower bound for the pursuer speed to follow the evader. We have obtained optimal motion

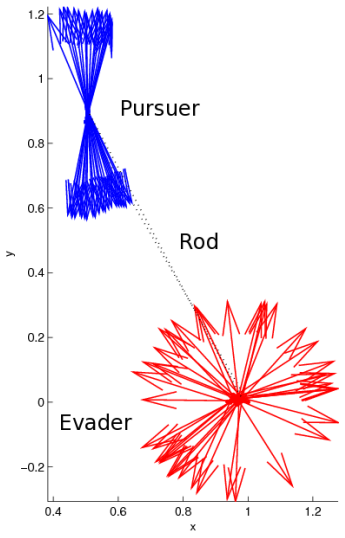

FIGURE 3.12: Evader moves randomly, pursuer wins aligning its wheels parallel to the rod

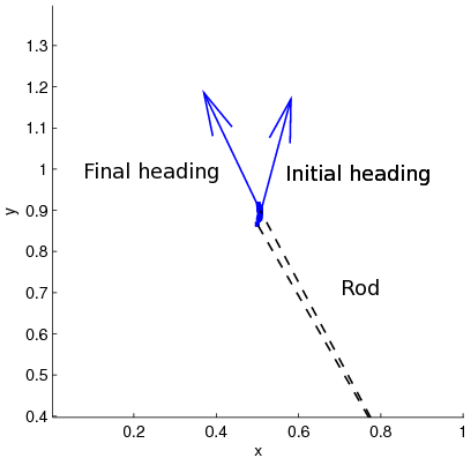

FIGURE 3.13: Initial and final pursuer heading, at the end the pursuer wheels are aligned with the rod

strategies for both players, in the sense that they require the minimal capabilities of the players for winning. We have also obtained the long term solution for the game, and we have presented simulation results of the game of pursuit. The methodology proposed in this chapter basically has two main components: 1) Find the optimal policies for each player for a given criterion. 2) Show that these policies induce a monotonic evolution under the condition defining the winner. This methodology might be used to solve other related problems (e.g., tracking and omnidirectional evader with a car-like robot).

Chapter 4

Tracking an Omnidirectional Evader with a Differential Drive Robot at Bounded Variable Distance

In this chapter, we address the pursuit-evasion problem for a differential drive robot (DDR) and an omnidirectional agent (OA) in the plane without obstacles. Specifically, we provide a criterion for partitioning the configuration space of the problem into 2 regions, so that in one of them the DDR is able to control the system, in the sense that, by applying a specific strategy (also provided), the DDR can achieve any feasible inter-agent distance, regardless of the actions taken by the other agent. Particular applications of these results include the capture of the OA by the DDR. Simulations that illustrates the trajectories of the system are also included.

In this study we assume that both agents have maximum bounded speeds. The differential drive robot is faster that the OA, but it can only change its motion direction up to a rate that is inversely proportional to its translational speed. In this work, only a purely kinematic problem is considered, and any effect due to dynamic constraints (e.g., acceleration bounds) is neglected.

In the previous chapter, we have presented a solution for the problem of tracking an omnidirectional mobile evader at *constant* distance with a differential drive robot. In that work we have obtained optimal motion strategies for both players and the long term solution for the game. This current work represents a generalization of the work presented in [36]. In this chapter, we present conditions that establish whether or not it

is possible for a DDR to track an OA at a bounded variable distance. We also present motion strategies for the DDR. Defining the capture condition as moving the pursuer closer than a given distance from the evader, then the motion strategies proposed in this work can be used by a DDR to capture an OA.

In this work, we define a manifold over the space of parameters for this game, such that it induces a partition of this space into two disjoint regions. The DDR will be able to control the system whenever the system is in one of these regions. By controlling, we mean that the DDR can vary the inter-player distance freely. When the system is exactly on the manifold, no player controls the system and it can be interpreted as a tied game.

The motion strategies presented in this paper are applicable to several problems related to surveillance or capture:

- They allow a DDR to maintain an omnidirectional evader within a limited sensing range defined by a maximal $L_{\max}$ and a minimal $L_{\min}$ sensing distances.
- They allow a DDR to reduce the distance from the evader.

In the remaining of this chapter, we describe the conditions that make possible the tasks listed above.

4.1 Pursuit-evasion at a bounded variable distance

In the last chapter, we established that $M(V_e^{\max}, V_p^{\max}, L, \theta, \phi) = 0$ defines a partition of the space $(V_e^{\max}, V_p^{\max}, \theta, \phi)$ into two regions, one in which the DDR can maintain tracking at a constant distance indefinitely, and another in which the OA can eventually escape. Therefore, as long as the evolution in time of the system configuration remains in the same region, it will be possible for the DDR to maintain tracking at a constant distance or for the OA to avoid it. In this section, we present the conditions and motion strategies for both players that allow one to relax the constant distance constraint as long as the configuration of the system remains in the initial region.

For simplicity, instead of working with the variables $(V_e^{\max}, V_p^{\max}, L, \theta, \phi)$ we will use the space (L, δ) with $\delta = \theta - \phi$, where $V_e^{\max}$ and $V_p^{\max}$ are fixed. In this case,

$M(V_e^{\max}, V_p^{\max}, L, \theta, \phi) = 0$ may be written as $M(L, \delta) = 0$. We have that

$$M(V_e^{\max}, V_p^{\max}, L, \theta, \phi) = |\dot{\phi}(u_1^*, u_2^*)| - \frac{1}{b}(V_p^{\max} - |u_3^{**}|) \tag{4.1}$$

the last equation can be rewritten in the form

$$M(V_e^{\max}, V_p^{\max}, L, \theta, \phi) = V_e^{\max}[|\cos(\phi - u_2^*)| + \frac{b}{L}|\sin(\theta - u_2^*)|] - V_p^{\max}|\cos(\theta - \phi)| \quad (4.2)$$

We previously defined

$$g(\phi, \theta, u_2) = |\cos(\phi - u_2)| + \frac{b}{L}|\sin(\theta - u_2)| \quad (4.3)$$

thus (4.2) can be rewritten as

$$M(V_e^{\max}, V_p^{\max}, L, \theta, \phi) = V_e^{\max} g(\phi, \theta, u_2^*) - V_p^{\max}|\cos(\theta - \phi)| \quad (4.4)$$

For $\theta - \phi \in [0, \frac{\pi}{2}]$, we have from the previous chapter that (4.3) takes the form

$$g(\phi, \theta, u_2) = -\cos(\phi - u_2) - \frac{b}{L}\sin(\theta - u_2) \quad (4.5)$$

Evaluating $g(\phi, \theta, u_2)$ with the optimal u_2^* as in the previous chapter, we get

$$g(\phi, \theta) = \sqrt{1 + \frac{2b}{L}\sin(\theta - \phi) + \left(\frac{b}{L}\right)^2} \quad (4.6)$$

Recalling that $\delta = \theta - \phi$, we have for fixed $V_e^{\max}, V_p^{\max}$,

$$M(L, \delta) = V_e^{\max}\sqrt{1 + \frac{2b}{L}\sin(\delta) + \left(\frac{b}{L}\right)^2} - V_p^{\max}\cos(\delta) \quad (4.7)$$

Figure 4.1 shows the regions in the (L, δ) space where $M(L, \delta) > 0$ or $M(L, \delta) < 0$, and the curves (bold lines) where $M(L, \delta) = 0$ for $\delta \in [-\pi, \pi]$.

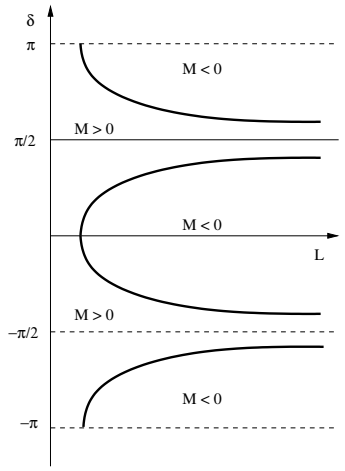

FIGURE 4.1: Representation of $M(L, \delta)$ in (L, δ) space.

In Figure 4.1, we can observe that the value of $M(L,\delta)$ has some symmetry properties as the value of δ varies in $[-\pi,\pi]$. Using these properties, we have that the problem can always be reduced to the interval $[0,\frac{\pi}{2}]$. Figure B.1 (refer to Appendix B.1) shows the curve representing $M(L,\delta)=0$ in this interval. In the upper region of the figure are the configurations (L,δ) where the OA avoids constant distance tracking and $M(L,\delta)>0$. In the bottom region are those where the DDR maintains tracking and $M(L,\delta)<0$.

As our analysis will be based on the two regions composing the space (L,δ), it is important to prove some useful properties of the curve separating those regions.

Lemma 4.1. *Let $\delta^*(L)$ be the curve separating the regions where $M(L,\delta)<0$ and $M(L,\delta)>0$.*

1. *There is a critical value $L=L_o^*$ such that $\delta^*(L_o)=0$.*
2. *For $L>L_o^*$, $\delta^*(L)$ is a strictly increasing function.*
3. *If $L\to\infty$ then $\delta^*(L)\to\cos^{-1}\left(\frac{V_e^{\max}}{V_p^{\max}}\right)\leq\frac{\pi}{2}$.*
4. *For $L<\infty$, $\delta^*(L)<\cos^{-1}\left(\frac{V_e^{\max}}{V_p^{\max}}\right)\leq\frac{\pi}{2}$.*

This lemma implies that $\delta^*(L)$ is a bounded strictly increasing function with respect to the inter-player distance L. These properties allow one to define the regions in which each player controls the system. The proof of this lemma is given in Appendix B.1.

Remark 4.2. From Lemma 4.1, we have that there is a critical value $L=L_o^*$ bounding $\delta^*(L)$ by the left. From the proof of that lemma, see Appendix B.1, we have that $L_o^*=\frac{\rho b}{\sqrt{1-\rho^2}}$ where $\rho=\frac{V_e^{\max}}{V_p^{\max}}$. In some cases $L_o^*<b$, the critical value corresponds to a inter-player distance located inside of the robot radius. In those cases, we must assume that the curve $\delta^*(L)$ is bounded by the critical value $L_o^*=b$, corresponding to configurations where the robot is in collision with the OA.

In what follows, we will show that from a given initial configuration L_I,δ_I, the DDR —depending on the sign of $M(L_I,\delta_I)$ — will be able to move in such a way that any desired inter-player distance L_G (with certain restrictions) may be obtained in finite time.

4.1.1 DDR strategy

First, consider the case where $M(L_I,\delta_I)<0$. The following theorem establishes a strategy with which, the DDR can reach a distance $L\in[L_G-\epsilon,L_G+\epsilon]$ (assuming $L_G-\epsilon\geq 0$) in finite time for any $\epsilon>0$, independently of the strategy followed by the OA.

Theorem 4.3. *Assume that for the initial configuration $M(L_I, \delta_I) < 0$. Given $\epsilon > 0$, define $L_B^* = L_o^* + \epsilon > 0$. Let $(L_I, L_G, L) > L_B^* + \epsilon$, be the initial, the goal and the current distance between the DDR and the OA. The DDR can reach a distance $L \in [L_G - \epsilon, L_G + \epsilon]$ in finite time, repeating the following strategy:*

1. *If $\delta(L) > 0$, move at constant L, changing the DDR's heading until it is parallel to the orientation of the rod, i.e., make $\delta(L) = 0$.*
2. *If $\delta(L) = 0$, move during a time $\widehat{T} = \min(T^*, \frac{|L - L_G|}{2V_p^{\max}})$ directly towards or away from the position of the OA at time t, depending on the sign of $L - L_G$, with a velocity $V = sgn(L - L_G) \cdot V_p^{\max}$ where*

$$T^* = \min\left(\frac{\epsilon}{2V_p^{\max}}, \frac{L_B^* \sin(\delta^*(L_B^*))}{V_e^{\max}}\right) \tag{4.8}$$

This theorem is proved by cases finding upper bounds on the OA motions. The proof is provided in Appendix B.2. Note that the theorem gives a constructive analysis which yields feasible motions for the DDR to win. In the theorem, ϵ is a parameter, which represents the tolerance of reaching the desired inter-player distance. It allows one to determine a safety margin for not crossing the manifold defining the space partition (recall that the regions of the partition define the winner of the game). Note that as ϵ decreases, the time required to execute each DDR sub-motion also decreases (see Equation 4.8), and hence the number of sub-motions necessary to reach a given configuration increases.

4.2 Simulations

In this section, we present some simulations of the players' strategies described before. The first simulation corresponds to the case when the DDR wants to reduce the inter-player distance. The initial parameters of the system are $V_p^{\max} = 1$, $V_e^{\max} = 0.5$, $b = 1$, $x_e = 1$, $y_e = 0$, $L = 2$, $\theta = 40°$, $\phi = 0°$, $\epsilon = 0.20$, $L_o = 1$, and $L_G = 1.25$.

Figure 4.2 shows the system trajectory in the space (L, δ). The trajectories followed by the players in the Euclidean plane are shown in Figure 4.3. Note that in this case, the DDR first aligns its heading with the rod's orientation, and then it moves directly towards the OA. The OA tries to move directly away from the DDR.

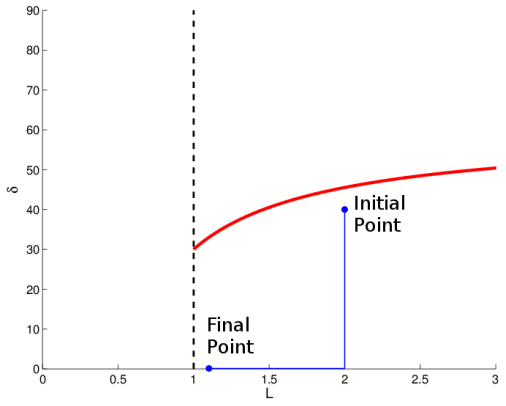

FIGURE 4.2: Representation in (L, δ) of the case when the DDR decreases the inter-player distance. The red bold curve corresponds to $M(L, \delta) = 0$, and the bold dashed line to the value of L_B. The system is initially at the point $(2, 40°)$. The blue lines show the trajectory followed by the system. At the end, the system is at the point $(1.1, 0°)$.

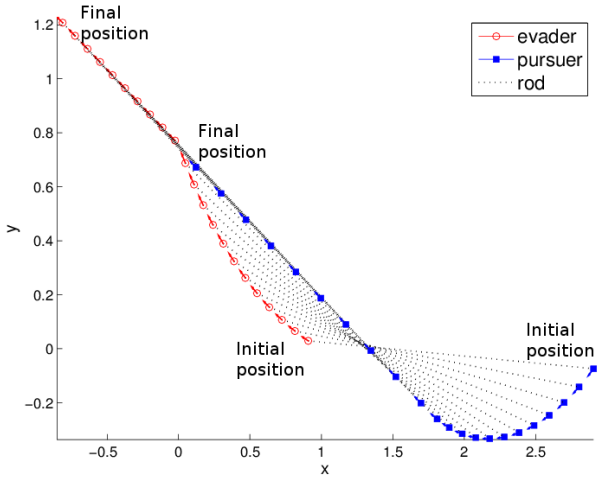

FIGURE 4.3: Representation of the trajectories of the players corresponding to the system of Fig 4.2. The DDR decreases the inter-player distance. The trajectories of the players were sub-sampled to show the motion direction of the players.

In Fig. 4.4, we can observe the variation of the inter-player distance L with respect to time, when the DDR wants to get closer to the OA. Initially, the DDR is aligning its heading with the rod orientation. During this time interval, the distance between both players remains constant. Once the DDR has aligned its heading, it starts moving toward the OA, while this player moves away from the DDR. Both players move in the same direction, but as the DDR is faster than the OA, the inter-player distance decreases.

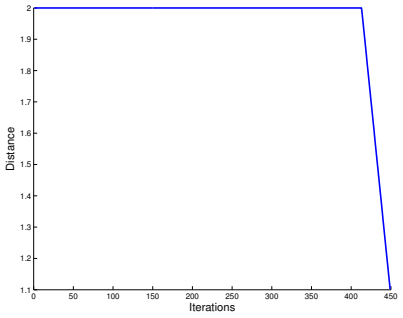

FIGURE 4.4: Variation of L as time elapses, corresponding to the system trajectory of Fig 4.2. The DDR decreases the inter-player distance.

4.3 Discussion and Conclusions

This chapter proposes a generalization of the work presented in [36]. The motion strategies presented in this chapter are applicable to several problems related to surveillance or capture.

1. They allow a DDR to maintain an omnidirectional evader within a limited sensing range defined by a maximal $L_{\max}$ and a minimal $L_{\min}$ sensing distances, provided that the limited sensing range satisfies the restriction imposed by $L_{\min} > L_o^* + 2\epsilon$.

2. They allow a DDR to reduce the distance from the omnidirectional evader, again provided that the desired inter-player distance satisfies the restriction $L_G > L_o^* + 2\epsilon$. Indeed, the problem of capturing an evader can be established in terms of this inter-player distance. That is, the capture condition is defined as moving the DDR closer than a given distance from the omnidirectional evader.

To our knowledge this is the first time that a solution is proposed for the problems of tracking and capturing an omnidirectional evader with a differential drive robot or vice versa in free space.

It is important to stress that if $M(L, \delta) < 0$ then the DDR can obtain in finite time an inter-player distance $L \in [L_G - \epsilon, L_G + \epsilon]$, which satisfies $M(L, \delta) < 0$, and such that $L_G > L_o^* + 2\epsilon$. In order to obtain the desired inter-player distance L_G (within a tolerance ϵ), the DDR performs the motion strategy described in Theorem 4.3.

The main drawback of the motion strategies presented in this paper is that they are not necessarily optimal in time. However, note that the analysis presented gives constructive proofs which yield feasible motions for the players to obtain their goals in finite time.

As future work, we will analyze the simultaneous variation of δ and L to obtain smoother trajectories in $L - t$ space. We shall also consider acceleration bounds on the pursuer and the evader.

Chapter 5

Optimal Control Theory and Differential Games

In this chapter, we describe some basic concepts from optimal control theory and differential games that will be used in the solution of the problem in Chapter 6.

5.1 Definitions

A differential game consists of the following elements:

5.1.1 Space

The space in which the action takes place, X, a connected subset of an n-dimensional Euclidean space. The state of the game is given by $\mathbf{x} = (x_1, x_2, \ldots, x_n)$, where x_1, x_2, ..., x_n are called the state variables, it is a position in X.

5.1.2 Control Variables

u, v where u is controlled by the first player and v by the second player, are called the control variables. The two players strive against one another to accomplish their desired outcome through the choice of their control variables. The control variables may be bounded, typically in the form $a \leq u \leq b$. Within those bounds the players must be able to chose any value at each instant.

5.1.3 Kinematics Equations

During the course of the game, the state $\mathbf{x}$ will change according to the decisions made by each player, this change is specified by the kinematics equations which takes the form

$$\dot{x}_i = f_i(\mathbf{x}, u, v) \tag{5.1}$$

We require that each f_i be smooth with respect to the state variables, and continuous with respect to the control variables.

5.1.4 Payoff

The numerical quantity which the players strive to maximize and minimize respectively can assume a variety of forms. However, a common representation of the payoff is

$$J(\mathbf{x}(t_s), u, v) = \int_{t_s}^{t_f} L(\mathbf{x}(\bar{t}), u(\bar{t}), v(\bar{t}))d\bar{t} + G(\mathbf{x}(t_f)) \tag{5.2}$$

The time integral extends over the path traversed by $\mathbf{x}(\bar{t})$ during the game; its lower limit (we could call it t_s) refers to the starting point $\mathbf{x}(t_s)$; its upper limit is the time t_f to reach the final point $\mathbf{x}(t_f)$. $L(\mathbf{x}(t), u(t), v(t))$ is called the *running cost function* and it is the cost incurred while the game is being played. The term $G(\mathbf{x}(t_f))$ is called the *terminal cost function* and it is the cost incurred for reaching a particular terminal state.

5.1.5 Value of the Game

For a given state of the system $\mathbf{x}(t_s)$, $V(\mathbf{x}(t_s))$ represents the outcome if the players implement their optimal strategies starting at the point $\mathbf{x}(t_s)$, and it is called the *value of the game* at $\mathbf{x}(t_s)$

$$V(\mathbf{x}(t_s)) = \min_{u(t)\in\widehat{U},\forall t} \max_{v(t)\in\widehat{V},\forall t} J(\mathbf{x}(t_s), u, v) \tag{5.3}$$

where $\widehat{U}$ and $\widehat{V}$ are the set of valid values for the controls at all time t. $V(\mathbf{x}(t))$ is defined over the entire state space.

5.1.6 Open and Closed-loop Strategies

A strategy γ is a rule that tells the player the control it has to apply at each time instant. If the strategy only depends on time $\gamma(t)$ is called an open-loop strategy [40], and if it depends on the state of the system $\gamma(\mathbf{x}(t))$ is called a closed-loop strategy [40].

5.1.7 Open and Closed-loop Equilibrium Strategies

Let $\gamma_p(\mathbf{x}(t))$ and $\gamma_e(\mathbf{x}(t))$ denote a pair of closed-loop strategies of the pursuer and the evader, respectively, therefore $u(t) = \gamma_p(\mathbf{x}(t))$ and $v(t) = \gamma_e(\mathbf{x}(t))$. A strategy pair $(\gamma_p^*(\mathbf{x}(t)), \gamma_e^*(\mathbf{x}(t)))$ is in closed-loop (saddle-point) equilibrium if

$$\begin{aligned} J(\gamma_p^*(\mathbf{x}(t)), \gamma_e(\mathbf{x}(t))) &\leq J(\gamma_p^*(\mathbf{x}(t)), \gamma_e^*(\mathbf{x}(t))) \\ &\leq J(\gamma_p(\mathbf{x}(t)), \gamma_e^*(\mathbf{x}(t))),\ \forall \gamma_p(\mathbf{x}(t)), \gamma_e(\mathbf{x}(t)) \end{aligned} \tag{5.4}$$

where J is the payoff of the game in terms of the strategies. An analogous relation exists for open-loop strategies.

5.1.8 Terminal Surface

Let ζ be the subset of X on which the game terminates, i.e., a subset where the state variables take a desired value or property. ζ defines a boundary of X, which consists of piecewise smooth surfaces, i.e. $n-1$ dimensional manifolds in the underlying n-dimensional space.

5.1.9 Usable Part

The portion of the terminal surface where one player can guarantee termination regardless of the choice of controls of the other player is called the *usable part* (UP) [20]. From [20], we have that the UP is given by

$$\text{UP} = \left\{ \mathbf{x}(t) \in \zeta : \min_{u(t)\in\widehat{U}} \max_{v(t)\in\widehat{V}} \mathbf{n} \cdot f(\mathbf{x}(t), u(t), v(t)) < 0 \right\} \tag{5.5}$$

where $\widehat{U}$ and $\widehat{V}$ are the sets of valid values for the controls, and $\mathbf{n}$ is the normal vector to ζ from point $\mathbf{x}(t)$ on ζ and extending into the playing space. $\mathbf{n} \cdot f(\mathbf{x}(t), u(t), v(t))$ is a projection of the motion directions of both players along the best direction for penetrating ζ and tells us if the strategies of both players will allow crossing the terminal surface or not. Those points of ζ where the expression in (5.5) holds with the inequality

reversed are called the *non-usable* part (NUP) and the game will never terminate on the NUP. The set of points that separates these parts is called the *boundary of the usable part* (BUP). The BUP can be computed replacing the inequality in (5.5) by an equality.

5.2 Necessary and Sufficient Conditions for Saddle-Point Equilibrium Strategies

This section describes the necessary and sufficient conditions for existence of saddle-point equilibrium strategies in pursuit-evasion games [40]. The sufficient condition is provided by an extension of the Hamilton-Jacobi-Bellman (HJB) equation [40] to a non-cooperative game with two players. This extension is called the Isaacs equation (Eq. (5.6)) [20]. An analogous extension of the Pontryagin's Maximum Principle (PMP) [91] to a two-players non-cooperative game provides a necessary condition [40]. This extension of the PMP may provide a constructive manner of computing saddle-point strategies. The necessary conditions are valid for the open-loop representation of the closed-loop strategies, and in order to obtain the closed-loop strategies these open-loop solutions have to be synthesised. This means that a partition of the complete playing space has to be constructed using the open-loop strategies. In each region of the partition a precise combination of the players' controls is used. This information can be employed to derive the closed-loop strategies, i.e., a policy that maps regions of the state space partition to the corresponding optimal controls for the players.

5.2.1 Isaacs Equation

Eq. (5.6) is known as the *Isaacs equation* [40]:

$$-\frac{\partial V(t,\mathbf{x}(t))}{\partial t} = \min_{u(t)\in\widehat{U}} \max_{v(t)\in\widehat{V}} [\frac{\partial V(t,\mathbf{x}(t))}{\partial x} \cdot f(t,\mathbf{x}(t),u(t),v(t)) + L(t,\mathbf{x}(t),u(t),v(t))] \tag{5.6}$$

where $\widehat{U}$ and $\widehat{V}$ are the sets of valid values for the controls.

Usually, $V(\mathbf{x}(t))$, $f(\mathbf{x}(t),u(t),v(t))$ and $L(\mathbf{x}(t),u(t),v(t))$ do not explicitly depend on time, therefore Eq. (5.6) takes the form

$$\min_{u(t)\in\widehat{U}} \max_{v(t)\in\widehat{V}} [\frac{\partial V(\mathbf{x}(t))}{\partial x} \cdot f(\mathbf{x}(t),u(t),v(t)) + L(\mathbf{x}(t),u(t),v(t))] = 0 \tag{5.7}$$

Eq. (5.7) is known as the main equation in [20]. Solving the HJB is a functional optimization problem. This equation provides a sufficient condition for saddle-point strategies, which is stated in the following theorem from [40]:

Theorem 5.1. *If*

1. *a continuously differentiable function $V(\mathbf{x}(t))$ exists that satisfies the Isaacs equation (5.7),*
2. *$V(\mathbf{x}(t)) = 0$ on the boundary of the terminal surface ζ,*
3. *either $u^*(t) = \gamma_p^*(\mathbf{x}(t))$ or $v^*(t) = \gamma_e^*(\mathbf{x}(t))$, as derived from Eq. (5.7), generates trajectories that terminate in finite time (whatever γ_e, respectively γ_p, is),*

then $V(\mathbf{x}(t))$ is the value of the game and $(\gamma_p^*(\mathbf{x}(t)), \gamma_e^*(\mathbf{x}(t)))$ constitutes a saddle point.

The assumption of interchangeability of the min and max operations in the Isaacs equation is referred as the *Isaacs condition*. The Isaacs condition holds if both $L(\mathbf{x}(t), u(t), v(t))$ and $f(\mathbf{x}(t), u(t), v(t))$ are separable in $u(t)$ and $v(t)$, i.e., they can be written as

$$\begin{aligned} L(\mathbf{x}(t), u(t), v(t)) &= L_1(\mathbf{x}(t), u(t)) + L_2(\mathbf{x}(t), v(t)) \\ f(\mathbf{x}(t), u(t), v(t)) &= f_1(\mathbf{x}(t), u(t)) + f_2(\mathbf{x}(t), v(t)) \end{aligned} \tag{5.8}$$

5.2.2 Pontryagin's Principle

$V(\mathbf{x}(t))$ is not known at the beginning of the game therefore Eq. (5.7) cannot directly be used in the derivation of saddle-point strategies. A possibility is to use Theorem 5.2 from [40], given below, which provides a set of necessary conditions for an *open-loop representation* of the *closed-loop saddle-point solution*. Regardless of the fact that it does not deal with closed-loop solutions directly, Theorem 5.2 is very useful in their computation.

Theorem 5.2 (PMP)**.** *Suppose that the pair $\{\gamma_p^*, \gamma_e^*\}$ provides a saddle-point solution in closed-loop strategies, with $\mathbf{x}^*(t)$ denoting the corresponding state trajectory. Furthermore, let its open-loop representation $\{u^*(t) = \gamma_p(\mathbf{x}^*(t)), v^*(t) = \gamma_e(\mathbf{x}^*(t))\}$ also provide a saddle-point solution (in open-loop polices). Then there exists a costate function $p(\cdot) : [0, t_f] \to R^n$ such that the following relations are satisfied:*

$$\dot{\mathbf{x}}^*(t) = f(\mathbf{x}^*(t), u^*(t), v^*(t)),\ \mathbf{x}^*(0) = \mathbf{x}(t_s) \tag{5.9}$$

$$H(p(t), \mathbf{x}^*(t), u^*(t), v(t)) \leq H(p(t), \mathbf{x}^*(t), u^*(t), v^*(t)) \leq H(p(t), \mathbf{x}^*(t), u(t), v^*(t)) \tag{5.10}$$

$$\dot{p}^T(t) = -\frac{\partial}{\partial x} H(p(t), \mathbf{x}^*(t), u^*(t), v^*(t)) \tag{5.11}$$

$$p^T(t_f) = \frac{\partial}{\partial x} G(\mathbf{x}^*(t_f)) \; along \, \zeta(\mathbf{x}^*(t)) = 0 \tag{5.12}$$

where

$$H(p(t), \mathbf{x}(t), u(t), v(t)) = p^T(t) \cdot f(\mathbf{x}(t), u(t), v(t)) + L(\mathbf{x}, u(t), v(t)) \tag{5.13}$$

$G(\mathbf{x}^*(t_f))$ *is the terminal cost function and* T *denotes the transpose operator.*

Equation (5.11) is known as the *adjoint equation*, and Eq. (5.13) as the *Hamiltonian function*. Using Eq. (5.13) with $p(t) = \nabla V(\mathbf{x}(t))$ for the case of vector-valued functions, and assuming that the Hamiltonian is separable in $u(t)$ and $v(t)$ (refer to Lemma 6.2), we can rewrite Eq. (5.7) as

$$\begin{aligned} &\min_{u(t)\in\widehat{U}} \max_{v(t)\in\widehat{V}} H(\mathbf{x}(t), \nabla V(\mathbf{x}(t)), u(t), v(t)) = 0 \\ &u^*(t) = \arg\min_{u(t)\in\widehat{U}} H(\mathbf{x}(t), \nabla V(\mathbf{x}(t)), u(t), v(t)) \\ &v^*(t) = \arg\max_{v(t)\in\widehat{V}} H(\mathbf{x}(t), \nabla V(\mathbf{x}(t)), u(t), v(t)) \end{aligned} \tag{5.14}$$

where $u^*(t)$ and $v^*(t)$ are the optimal controls . The vector $\nabla V(\mathbf{x}(t))$ can be interpreted as the Lagrange multipliers used in constrained optimization or optimal control theory.

The maximum principle, in particular Eqs. (5.10) and (5.11), can be considered as a specialization of the HJB equation which corresponds to the application of the optimal actions $u^*(t)$ and $v^*(t)$. This causes the min max to disappear, but along with it the global properties of the HJB equation also vanish. The PMP expresses conditions along the optimal trajectory, as opposed to the value of the game $V(\mathbf{x}(t))$ over the whole state space. Therefore, it can at best assure local optimality in the space of possible trajectories [92].

In the PMP methodology, the optimal controls for the players are functions of $p(t) = \nabla V(\mathbf{x}(t))$, it is important to note that once $u^*(t)$ and $v^*(t)$ are chosen the relation with the state $\mathbf{x}(t)$ is lost. That is the reason why we use the notation $p(t)$ and not $p(\mathbf{x}(t))$. Later, the optimal motion trajectories of the players are constructed using $u^*(t)$ and $v^*(t)$. Therefore, the resulting optimal trajectories are not directly related with the state. This means that a partition of the complete playing space has to be constructed using the open-loop strategies. In each region of the partition a precise combination of the players' controls is used. This information can be employed to derive the closed-loop strategies, i.e., a policy that maps regions of the state space partition to the corresponding optimal controls for the players.

5.3 Decision problem

A game of kind is a game in which we are interested in what conditions lead to a winning for each one of the players, rather than seeking the best procedures in terms of optimizing some continuous payoff. For the game of capturing in pursuit-evasion games, this corresponds to finding the conditions that make capture possible for the pursuer or escape for the evader.

5.3.1 The barrier

There is a surface called the *barrier* [20], which separates the set of starting positions in those that result in capture and those that result in escape for the evader. From starting points on the barrier, optimal behaviour leads to a contact of the terminal surface without crossing it. The outcome of following the barrier is called neutral, and it can be understood as intermediate between capture and escape. The techniques we have used in the calculation of the optimal strategies and their corresponding trajectories, are also applied in the construction of the barrier, which can be interpreted as a *neutral trajectory of the system*. The answer to the capture-escape question relies on whether or not the barrier divides the playing space into two parts.

5.3.2 Construction of the barrier

Let $\mathbf{x}$ be a point initially on ζ, the terminal surface. As we previously mentioned, the portion of the terminal surface where the pursuer can guarantee termination regardless of the choice of controls of the evader is called the usable part (UP), and its boundary (BUP) is characterized by

$$\text{BUP} = \left\{ \mathbf{x}(t) \in \zeta : \min_{u(t)\in\widehat{U}} \max_{v(t)\in\widehat{V}} \mathbf{n} \cdot f(\mathbf{x}(t), u(t), v(t)) = 0 \right\} \tag{5.15}$$

where $\mathbf{n}$ is the normal vector to ζ from point $\mathbf{x}(t)$ on ζ and extending into the playing space.

For such points, when each player applies its optimal strategies $\mathbf{x}$ moves tangentially to ζ. As the BUP separates the points on ζ where immediate capture occurs from those where it does not, it is used as initial condition for the barrier. The barrier is constructed integrating the adjoint equation (6.19) and the equations of motion (6.27), starting at the BUP. The resulting surface may or may not divide the playing space into two parts,

one of them contiguous to the UP. Note that the construction of the barrier depends on the ratio ρ_v of the players' velocities.

Suppose the barrier separates the playing space into two parts. If $\mathbf{x}$ is in the outer side, the one that is not contiguous to the UP, then the pursuer cannot force the capture because the UP is not accessible. If the barrier fails to separate the playing space, then capture can always be attained by the pursuer. However, from starting points in each side of the barrier (in local sense) the pursuer must adopt different strategies.

5.4 Singular surfaces

A fundamental requirement of the Isaacs methodology is that $V(\mathbf{x})$ is a continuously differentiable function. To obtain the optimal controls generating trajectories for the players in the entire state space it is sufficient to split this space into a set of mutually disjoint regions where this condition is met. In each region, the value function $V(\mathbf{x})$ is continuously differentiable, and its behaviour and construction is well established.

The boundaries of these regions are called *singular surfaces* [20, 21, 40], and the value function is not continuously differentiable across them. In some cases, we identify these regions and their boundaries by a switch in the players' controls or the intersection of two distinct families of trajectories in the reduced space. Inside each region, a new integration of the motion equations is done based on the controls obtained through the adjoint equation of the PMP. The adjoint equation is solved backwards using as initial conditions the values of $\nabla V(\mathbf{x})$ on the corresponding singular surface. Note that the controls' form in each region continues being based on the Hamiltonian of the system and satisfying the Isaacs equation (5.6).

The singular surfaces and their construction will be described in the next paragraphs giving a solution of the game for the complete playing space.

5.4.1 Definition of a singular surface

Following the definition given in [40], a singular surface is a manifold on which

1. The equilibrium strategies are not uniquely determined by the necessary conditions of Theorem 5.2, or
2. The value function is not continuously differentiable, or
3. The value function is discontinuous.

From [1], we get the following definition for a singular surface based on the regularity of the Hamiltonian $H(\mathbf{x}, \nabla V(\mathbf{x}))$ and the value function $V(\mathbf{x})$.

A regular point of a differential game is an internal point $\mathbf{x}^*$ *of the domain of definition of the game value* $V(\mathbf{x})$ *such that the function* $V(\mathbf{x})$ *is twice differentiable in the neighbourhood* D *of* $\mathbf{x}^*$, $V(\mathbf{x}) \in C^2(D)$, and the Hamiltonian $H(\mathbf{x}, \nabla V(\mathbf{x}))$ is also twice differentiable in its arguments; i.e., $H(\mathbf{x}, \nabla V(\mathbf{x}) \in C^2(N)$ where N is a neighbourhood of the point $(\mathbf{x}^*, \nabla V(\mathbf{x}^*))$. A singular point is any point in the phase space which is not regular. Singular curve, surface or manifold consist of singular points.

The above definition meets the geometrical definitions of [20, 40, 93]. Fig. 5.1 shows the qualitative behaviour of the regular and singular paths for different types of singular surfaces. Some of the surfaces contain singular paths, while others, like dispersal or switching surfaces, do not. Several surfaces are associated with a jump of $\nabla V(\mathbf{x})$, while others, like the switching or universal ones, are not. The classification presented in Figure 5.1 is not complete; it is a list of singularities met so far and more or less fully investigated [1].

Below, we give a geometrical description of the singular surfaces that will appear in the problem addressed in Chapter 6. For information about the remaining singular surfaces in Fig. 5.1 or a identification based on the regularity of the $H(\mathbf{x}, \nabla(\mathbf{x}))$ and $\nabla(\mathbf{x})$, we encourage the reader to consult [1, 20, 40, 93].

5.4.1.1 Transition surface (TS)

The place where a control variable abruptly changes in value, is known as a transition surface (see Fig. 5.1). The procedure for locating a transition surface is fairly straightforward, since it follows from the adjoint and motion equations (see Subsection 6.3.8 and Lemma 6.23 for its construction and description in the problem described in Chapter 6).

5.4.1.2 Universal surface (US)

A surface to which optimal trajectories enter from both sides –called the tributary trajectories– and then stay on, is called a universal surface (see Fig. 5.1). In differential games, one can think of such a surface as a union of especially advantageous paths. Optimal play will demand that the state of the system $\mathbf{x}$ be brought to the universal surface and thereafter remain on it (see Lemma 6.25 for its construction in the problem described in Chapter 6).

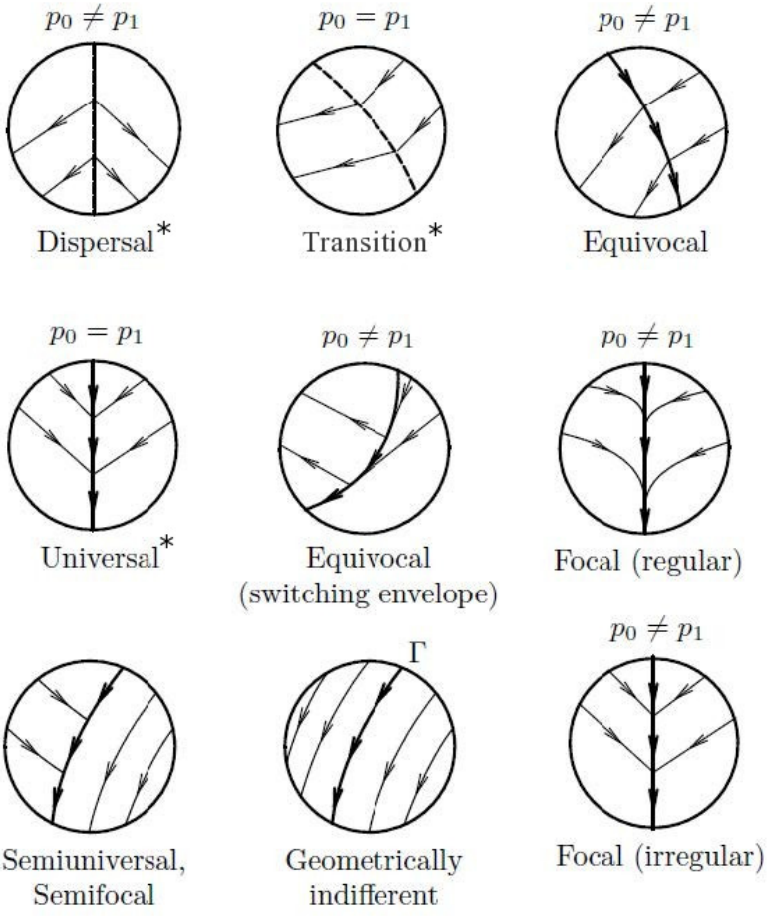

FIGURE 5.1: Singular surfaces (in bold), taken from [1]. p_o and p_1 represents the values of $\nabla V(\mathbf{x})$ at each side of the surface. The symbol * indicates the surfaces that appear in the problem described in Chapter 6.

5.4.1.3 Dispersal surface (DS)

A dispersal surface is defined in [20, 40] as the locus of initial conditions along which the optimal strategy of one player or the optimal strategies of both players are not unique (see Fig. 5.1). They are often found as the retro-time intersection of two distinct families of optimal paths, for each of which the Isaacs equation is satisfied. At the intersection, the optimal time-to-go is the same for either pair of strategies. In Chapter 6, they appear due to symmetries in the reduced space, see subsection 6.6.3 and Fig. 6.7.

The partition of the playing space using the singular surfaces tell us the regions in the space where a particular combination of the players' controls was used. Therefore, it is possible to compute a closed-loop solution of the problem using this information. Additionally, following the corresponding trajectories through the regions in the partition,

will lead us to a continuous $V(\mathbf{x})$ and a global trajectory ending at the UP in finite time that satisfies the Isaacs equation (5.6).

Chapter 6

Time-Optimal Motion Strategies for Capturing an Omnidirectional Evader using a Differential Drive Robot

In this chapter, we address the problem of capturing in minimum time an omnidirectional evader using a Differential Drive Robot (DDR) in an environment without obstacles.

6.1 Problem formulation

A Differential Drive Robot (DDR), the pursuer, and a omnidirectional evader move on a plane without obstacles. The DDR tries to capture the evader in *minimum time*. The game is over when the distance between the DDR and the evader is smaller than a critical value l. Both players have maximum bounded speeds $V_p^{\max}$ and $V_e^{\max}$, respectively. The DDR is faster than the evader, $V_p^{\max} > V_e^{\max}$, but it can only change its direction of motion at a rate that is inversely proportional to its translational speed [90]. We consider here a purely kinematic problem, and neglect any effects due to dynamic constraints (e.g., acceleration bounds). *The DDR wants to minimize the capture time t_f while the evader wants to maximize it. The goal is to find optimal strategies that are in Nash Equilibrium and may be used by both players to achieve their goals.*

6.2 Model

The system model is the same as the one presented in Chapter 2. Here, we summarize it again to make this chapter self contained.

6.2.1 Realistic space

The kinematics of the game can be described in a global coordinate system (see Fig. 6.1) usually called realistic space in the literature [20]. $(x_p(t), y_p(t), \theta_p(t))$ represents the pose of the DDR and $(x_e(t), y_e(t))$ is the position of the omnidirectional evader, both at time t. The state of the system can be expressed as $(x_p(t), y_p(t), \theta_p(t), x_e(t), y_e(t)) \in \mathbb{R}^2 \times S^1 \times \mathbb{R}^2$.

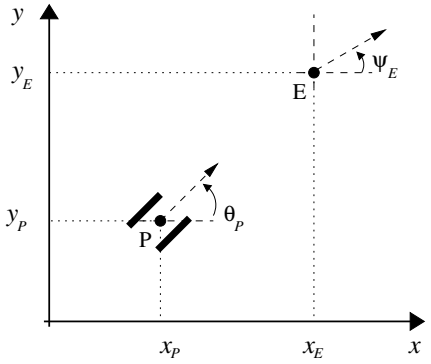

FIGURE 6.1: Realistic space

The evolution of the system is described by the following equations of motion

$$\begin{aligned}
\dot{x}_p(t) &= \left(\frac{u_1(t) + u_2(t)}{2}\right) \cos\theta_p(t) \\
\dot{y}_p(t) &= \left(\frac{u_1(t) + u_2(t)}{2}\right) \sin\theta_p(t) \\
\dot{\theta}_p(t) &= \left(\frac{u_2(t) - u_1(t)}{2b}\right) \\
\dot{x}_e(t) &= v_1(t)\cos\psi_e(t), \quad \dot{y}_e(t) = v_1(t)\sin\psi_e(t)
\end{aligned} \tag{6.1}$$

where $u_1, u_2 \in [-V_p^{\max}/r, V_p^{\max}/r]$ are the controls of the DDR, and they correspond to the angular velocities of its wheels. r is the radius of the wheels, in this problem we assume $r = 1$. Let u_1 be the angular velocity of the left wheel and u_2 of the right wheel. If both controls have the same magnitude and are either positive or negative, respectively, the robot moves forward or backward in a straight line, and with a suitable choice of units [90], the traslational speed is equal to $V_p = \frac{1}{2}(u_1 + u_2)$. If u_1 and u_2 have the same magnitude but opposite signs the robot rotates in place either clockwise or counter-clockwise [90]. The evader controls its speed $v_1 \in [0, V_e^{\max}]$ and its direction

of motion $\psi_e \in [0, 2\pi)$. We present two useful definitions for the rest of the chapter, $\rho_v = V_e^{\max}/V_p^{\max}$ is the ratio between the maximum translational speed of both players, and $\rho_d = b/l$ is the ratio of the distance between the center of the robot and the wheel location b and the capture distance l. We must have that $l \geq b$, otherwise the capture distance would be located inside the robot.

6.2.2 Reduced space

Usually it is more convenient to analyse the problem and perform all the computations in a space of reduced dimension. In our case, the problem can be stated in a coordinate system that is fixed to the body of the DDR (see Fig. 6.2). The state of the system now can be expressed as $\mathbf{x}(t) = (x, y) \in \mathbb{R}^2$ where x and y are now the (relative) coordinates of the evader in the intrinsic frame related to the pursuer. All the orientations in this system are measured with respect to the positive y-axis, in particular, the direction of motion of the evader v_2. Using the coordinate transformation given by

$$\begin{aligned} x(t) &= (x_e(t) - x_p(t)) \sin\theta_p(t) - (y_e(t) - y_p(t)) \cos\theta_p(t) \\ y(t) &= (x_e(t) - x_p(t)) \cos\theta_p(t) + (y_e(t) - y_p(t)) \sin\theta_p(t) \\ v_2(t) &= \theta_p(t) - \psi_e(t) \end{aligned} \tag{6.2}$$

and computing the time-derivative of x and y in Eq. (6.2) we get

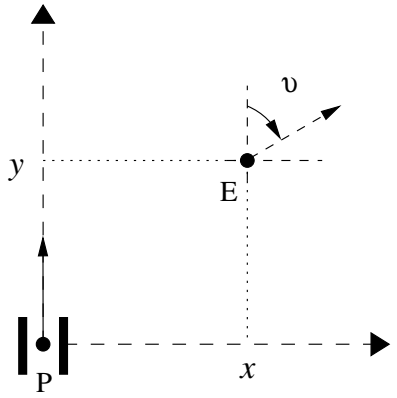

FIGURE 6.2: Reduced space

$$\begin{aligned} \dot{x}(t) =& (\dot{x}_e(t) - \dot{x}_p(t)) \sin\theta_p(t) + (x_e(t) - x_p(t))\dot{\theta}_p(t) \cos\theta_p(t) \\ & - (\dot{y}_e(t) - \dot{y}_p(t)) \cos\theta_p(t) + (y_e(t) - y_p(t))\dot{\theta}_p(t) \sin\theta_p(t) \\ \dot{y}(t) =& (\dot{x}_e(t) - \dot{x}_p(t)) \cos\theta_p(t) - (x_e(t) - x_p(t))\dot{\theta}_p(t) \sin\theta_p(t) \\ & + (\dot{y}_e(t) - \dot{y}_p(t)) \sin\theta_p(t) + (y_e(t) - y_p(t))\dot{\theta}_p(t) \cos\theta_p(t) \end{aligned} \tag{6.3}$$

Substituting into Eq. (6.3) the expressions for $\dot{x}_p(t)$, $\dot{y}_p(t)$, $\dot{\theta}_p(t)$, $\dot{x}_e(t)$ and $\dot{y}_e(t)$ in Eq. (6.1), and the expressions for $x(t)$ and $y(t)$ in Eq. (6.2), the following model of the kinematics in the DDR-fixed coordinate system is obtained

$$\begin{aligned}\dot{x}(t) &= \left(\frac{u_2(t)-u_1(t)}{2b}\right) y(t) + v_1(t)\sin v_2(t) \\ \dot{y}(t) &= -\left(\frac{u_2(t)-u_1(t)}{2b}\right) x(t) - \left(\frac{u_1(t)+u_2(t)}{2}\right) + v_1(t)\cos v_2(t)\end{aligned} \tag{6.4}$$

where $u_1(t), u_2(t) \in [-V_p^{\max}, V_p^{\max}]$ are again the controls of the DDR, $v_1(t) \in [0, V_e^{\max}]$ is the control associated to the speed of the evader and $v_2(t) \in [0, 2\pi)$ is the control associated to the direction of motion of the evader in the new coordinate system. This set of equations can be expressed in the form $\dot{\mathbf{x}} = f(t, \mathbf{x}(t), u(t), v(t))$, where $u(t) = (u_1(t), u_2(t)) \in \widehat{U} = [-V_p^{\max}, V_p^{\max}] \times [-V_p^{\max}, V_p^{\max}]$ and $v(t) = (v_1(t), v_2(t)) \in \widehat{V} = [0, V_e^{\max}] \times [0, 2\pi)$.

6.3 Optimal Motion Primitives and Trajectories

In this section, we will derive the saddle-point equilibrium strategies for both players. The goal of the DDR is to capture the evader as soon as possible, and the goal of the evader is to delay the capture as long as possible. For this, we will refer to trajectories in the reduced and realistic spaces. In the realistic space, we will describe trajectories for both the pursuer and the evader over a global reference frame in a Cartesian plane. We will show that time-optimal trajectories in the realistic space correspond to straight lines and rotations in place for the DDR and straight lines for the evader. In the reduced space, we will refer to trajectories of the system, i.e., relative motions of the evader with respect to the pursuer in a local reference frame defined by the pursuer.

6.3.1 Overview of the methodology applied on our problem

We use the Isaacs' methodology [20] to find the solution of our problem. The Isaacs' methodology [20] is based on an extension of the Hamilton-Jacobi-Bellman (HJB) equation [40] to a non-cooperative game with two players (see Subsection 5.2.1). The HJB equation is a partial differential equation having the value function $V(\mathbf{x})$ as the unknown function. This equation provides sufficient conditions for the existence of saddle point equilibrium strategies [40]. Solving the HJB allows one to know the value function $V(\mathbf{x})$ over the entire space; however, obtaining a closed-form solution is a difficult task. An alternative, is to use an extension of the Pontryagin's Maximum Principle (PMP) [91]

to a two-players non-cooperative game which provides a necessary condition for saddle-point equilibrium strategies. This extension of the PMP provides a constructive manner of computing saddle-point strategies (refer to Subsection 5.2.2).

The necessary conditions are valid for the open-loop representation of the closed-loop strategies, and in order to obtain the closed-loop strategies these open-loop solutions have to be synthesized. This means that a partition of the complete playing space has to be constructed using the open-loop strategies. In each region of the partition, a precise combination of the players' controls is used. This information is employed to derive the closed-loop strategies, i.e., a policy that maps regions of the state space partition to the corresponding optimal controls for the players (refer to Section 6.6).

In summary, the methodology consists of the following steps:

1. Compute the usable part (Subsection 6.3.2). This allows one to find the initial conditions needed to solve the differential equation, so-called adjoint equation.
2. Construct the Hamiltonian of the system (Subsection 6.3.3) and obtain the *expressions* of the optimal controls satisfying it (Subsection 6.3.4).
3. Find $\nabla V(\mathbf{x})$ solving the adjoint equation backwards in time (retro-time, see Eq. (6.17)) using the values of $V(\mathbf{x})$ and $\nabla V(\mathbf{x})$ on the UP as initial conditions (Subsections 6.3.5 and 6.3.6). $V(\mathbf{x})$ is used to find the controls used by the players.
4. Find the switches in the controls of the players (Subsection 6.3.8)
5. Use the pair of controls found in the backward integration of the motion equations to find the trajectory followed by the players at each stage (Subsections 6.3.7 and 6.3.9).
6. Find the region of the playing space where capture is possible for the DDR (Section 6.4).
7. Obtain the optimal controls and the trajectories for the players in the entire reduced space (Section 6.6). This is known as the partition of the space.

Steps 1 to 5 corresponds to use the Pontryagin's principle. In step 6, we solve the decision problem corresponding to determining the winner of the game. Finally in step 7, we find the trajectories of the players for the entire space, which is known as the synthesis.

6.3.2 Computing the usable part and its boundary

In this section, we compute the portion of the space where the pursuer guarantees termination regardless of the choice of controls by the evader. For this problem, the terminal surface ζ is characterized by the distance l between both players. In the reduced space, ζ is a circle of radius l centred at the origin, hence we can parametrise it by the angle s (see Fig. 6.3), which is the angle between the evader's position and the pursuer's heading *at the end of the game*, i.e. when the capture occurs (recall that all the orientations in the reduced space are measured with respect to the positive y-axis).

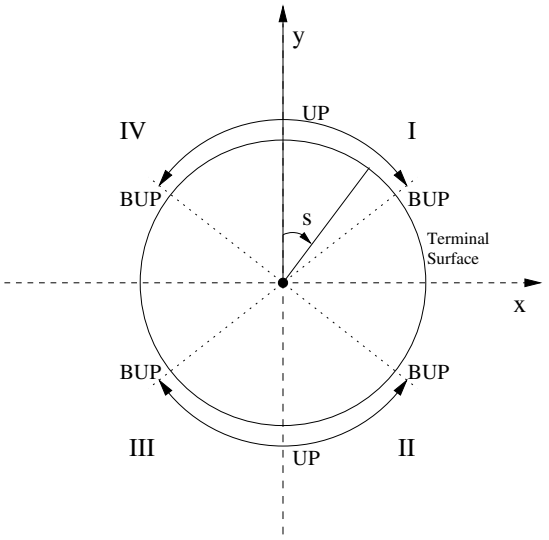

FIGURE 6.3: Representation of the terminal surface, usable part and its boundary in the reduced space.

At the end of the game

$$x = l \sin s,\ y = l \cos s \tag{6.5}$$

Lemma 6.1. *In this game, the usable part has two regions:*

1. *The first region corresponds to capturing the evader when the DDR is moving forward following a straight line in realistic space. This region contains all the points on ζ such that $\cos s > \rho_v$ and its boundary is given by those points where $\cos s = \rho_v$.*

2. *The second region corresponds to capturing the evader when the DDR is moving backward following a straight line in realistic space. This region contains all the points on ζ such that $\cos s < -\rho_v$ and its boundary is given by those points where $\cos s = -\rho_v$.*

Proof. The outward normal $\mathbf{n}$ to ζ is defined by

$$\mathbf{n} = [\sin s \quad \cos s] \tag{6.6}$$

The usable part after substituting Eq. (6.4) and Eq. (6.6) into inequality (5.5) is given by

$$\begin{aligned} \text{UP} = \{s : \min_{u_1,u_2} \max_{v_1,v_2} \{ & \sin s \left[\left(\frac{u_2 - u_1}{2b} \right) y + v_1 \sin v_2 \right] \\ & + \cos s \left[- \left(\frac{u_2 - u_1}{2b} \right) x - \left(\frac{u_1 + u_2}{2} \right) + v_1 \cos v_2 \right] \} < 0 \} \end{aligned} \tag{6.7}$$

Substituting Eq. (6.5) into inequality (6.7) and after straightforward algebraic manipulation, we find that

$$\text{UP} = \left\{ s : \min_{u_1,u_2} \max_{v_1,v_2} \left[v_1 \cos(v_2 - s) - \left(\frac{u_1 + u_2}{2} \right) \cos s \right] < 0 \right\} \tag{6.8}$$

As the evader is the maximizer player it wants the term $v_1 \cos(v_2 - s)$ be positive, and with the largest value possible. Therefore, $v_1 = V_e^{\max}$ and $v_2 = s$, i.e., the evader is moving at maximum speed with an angle s with respect to the pursuer's heading. Substituting these values into Eq. (6.8) we have

$$\text{UP} = \left\{ s : \min_{u_1,u_2} \left[V_e^{\max} - \left(\frac{u_1 + u_2}{2} \right) \cos s \right] < 0 \right\} \tag{6.9}$$

In inequality (6.9) we have two cases, (1) $\cos s > 0$ or (2) $\cos s < 0$. In order to make inequality (6.9) minimal, u_1 and u_2 must be equal and saturated (that is equal to $|V_p^{\max}|$). Hence the pursuer moves in straight line. If $\cos s > 0$ then $\left(\frac{u_1+u_2}{2}\right) = V_p^{\max} > 0$, the DDR is moving forward and if $\cos s < 0$ then $\left(\frac{u_1+u_2}{2}\right) = -V_p^{\max} < 0$, the DDR is moving backward. Note that this pair of controls corresponds to the best action that the DDR can apply against the evader in the min max context of the game, and therefore they give the set of configurations where the DDR captures the evader against any opposition of this player. Note that the same controls u_1 and u_2 are used in both the reduced and realistic spaces. From inequality (6.9) and considering the two cases described above, it is straightforward to find that the region where the DDR is moving forward contains all the points such that $\cos s > \rho_v$ and the region where the DDR is moving backward contains all the points such that $\cos s < -\rho_v$.

□

6.3.3 Hamiltonian

In order to compute the optimal trajectories for both players, we need to construct the Hamiltonian of the system. For problems of *minimum time* [40], as in this game, $L(\mathbf{x}(t), u(t), v(t)) = 1$ and $G(t_f, \mathbf{x}(t_f)) = 0$. $\nabla V = [V_x \ V_y]^T$ where V_x and V_y represent the partial derivatives $\frac{\partial V}{\partial x}$ and $\frac{\partial V}{\partial y}$. Substituting the last expressions and the equations of motion in (6.4) into Eq. (5.13), we obtain

$$\begin{aligned} H(\mathbf{x}, \nabla V, u_1, u_2, v_1, v_2) &= V_x \left(\frac{u_2 - u_1}{2b}\right) y + V_x v_1 \sin v_2 \\ - V_y \left(\frac{u_2 - u_1}{2b}\right) x - V_y \left(\frac{u_1 + u_2}{2}\right) &+ V_y v_1 \cos v_2 + 1 \end{aligned} \tag{6.10}$$

Lemma 6.2. *The Hamiltonian of our system is separable in the controls of the pursuer and the evader, i.e., we can write it in the form* $f_1(\mathbf{x}, \nabla V, u) + f_2(\mathbf{x}, \nabla V, v)$.

Proof. In our case, Eq. (6.10) can be rewritten in the form

$$\begin{aligned} H(\mathbf{x}, \nabla V, u_1, u_2, v_1, v_2) &= \frac{u_1}{2}\left(\frac{-yV_x}{b} + \frac{xV_y}{b} - V_y\right) \\ + \frac{u_2}{2}\left(\frac{yV_x}{b} - \frac{xV_y}{b} - V_y\right) &+ v_1(V_x \sin v_2 + V_y \cos v_2) + 1 \end{aligned} \tag{6.11}$$

Thus the Hamiltonian of our game is separable in the controls u_1, u_2, v_1 and v_2. □

6.3.4 Optimal controls

Lemma 6.3. *The time-optimal controls for the DDR that satisfy the Isaacs' equation (5.6) in the reduced space are given by*

$$\begin{aligned} u_1^* &= -sgn\left(\frac{-yV_x}{b} + \frac{xV_y}{b} - V_y\right) V_p^{\max} \\ u_2^* &= -sgn\left(\frac{yV_x}{b} - \frac{xV_y}{b} - V_y\right) V_p^{\max} \end{aligned} \tag{6.12}$$

We have that both controls are always saturated. If they have the same sign the DDR will move in straight line at maximum translational speed in the realistic space and if they have opposite signs the DDR will rotate in place at maximum rotational speed in the realistic space. The controls of the evader in the reduced space are given by

$$v_1^* = V_e^{\max}, \ \sin v_2^* = \frac{V_x}{\rho}, \ \cos v_2^* = \frac{V_y}{\rho} \tag{6.13}$$

where $\rho = \sqrt{V_x^2 + V_y^2}$. *The evader will also move at maximal speed.*

Proof. By Lemma 6.2 we know that the Hamiltonian of our game is separable in two parts, one in terms of the pursuer's controls and other in terms of the evader's controls. Consider the pursuer first. As the DDR is the minimizer player it wants the Hamiltonian term

$$\frac{u_1}{2}\left(\frac{-yV_x}{b}+\frac{xV_y}{b}-V_y\right)+\frac{u_2}{2}\left(\frac{yV_x}{b}-\frac{xV_y}{b}-V_y\right) \tag{6.14}$$

to be minimal. Let $A=\frac{-yV_x}{b}+\frac{xV_y}{b}-V_y$ and $B=\frac{yV_x}{b}-\frac{xV_y}{b}-V_y$. There are four cases:

In all cases u_1 and u_2 must be saturated to minimize Eq. (6.14) and they correspond (in absolute values) to the maximal rotational speed of the wheels $V_p^{\max}$ (with a suitable choice of units and assuming an unit radius r of the pursuer's wheels [90], the rotational speeds are equivalent to the translational speeds).

1. If $A<0$ and $B<0$ then to minimize Eq. (6.14), $u_1=u_2=V_p^{\max}$, and the pursuer moves forward in a straight line.
2. If $A>0$ and $B>0$ then to minimize Eq. (6.14) $u_1=u_2=-V_p^{\max}$, and the pursuer moves backward in a straight line.
3. If $A>0$ and $B<0$ then to minimize Eq. (6.14) $u_1=-V_p^{\max}$ and $u_2=V_p^{\max}$, and the pursuer rotates in place counterclockwise.
4. If $A<0$ and $B>0$ then to minimize Eq. (6.14) $u_1=V_p^{\max}$ and $u_2=-V_p^{\max}$, and the pursuer rotates in place clockwise.

The DDR switches controls when A or B change signs. When the DDR switches controls A or B are instantaneously zero. One can show (refer to Section C.1 in Appendix C) that if either A or B becomes zero, the corresponding time derivatives $\dot{A}$ or $\dot{B}$ will be different from zero, so that A or B are zero only at the switching instant.

Analogously, since the evader is the maximizer player it wants the term

$$v_1(V_x\sin v_2+V_y\cos v_2) \tag{6.15}$$

to be maximal. The quantity in round parenthesis is the dot product of the vectors $[V_x\ V_y]$ and $[\sin v_2\ \cos v_2]$, and it is maximal when $[\sin v_2\ \cos v_2]$ lies along $[V_x\ V_y]$ (both vectors are parallel and have the same direction). To maximize Eq. (6.15), $v_1=V_e^{\max}$ and $[V_x\ V_y]\parallel[\sin v_2\ \cos v_2]$, from which Eq. (6.13) follows. □

In Lemmas 6.7 and 6.13, we will present the actual evader trajectories.

6.3.5 Adjoint equation

The adjoint equation (5.11) is a differential equation for the gradient of the value function $V(\mathbf{x})$ along the optimal trajectories in terms of the optimal controls. It is given by

$$\frac{d}{dt}\nabla V[\mathbf{x}(t)] = -\frac{\partial}{\partial x}H(\mathbf{x}, \nabla V, u_1^*, u_2^*, v_1^*, v_2^*) \tag{6.16}$$

where the components of $\nabla V(\mathbf{x})$ are called adjoint variables. If t_f is the termination time of the game, we define the retro-time as

$$\tau = t_f - t \tag{6.17}$$

The adjoint equation in retro-time form is

$$\frac{d}{d\tau}\nabla V[\mathbf{x}(\tau)] = \frac{\partial}{\partial x}H(\mathbf{x}, \nabla V, u_1^*, u_2^*, v_1^*, v_2^*) \tag{6.18}$$

Lemma 6.4. *The expressions in retro-time of the adjoint equation of our system are*

$$\frac{d}{d\tau}V_x = -\left(\frac{u_2^* - u_1^*}{2b}\right)V_y, \quad \frac{d}{d\tau}V_y = \left(\frac{u_2^* - u_1^*}{2b}\right)V_x \tag{6.19}$$

Proof. Substituting Eq. (6.11) into Eq. (6.18) (u_1^*, u_2^*, v_1^* and v_2^* denote the optimal controls of both players) it is straightforward to obtain the expressions above. □

Remark 6.5. From Eq. (6.19), notice that the adjoint equation can take four different expressions depending on the values of u_1^* and u_2^*. Therefore, it is necessary to know when and for how long a particular expression is valid during the game, which corresponds to find the switches of the controls associated to the DDR.

In what follows we will show that the players' optimal motion primitives in the realistic space correspond, for the evader, to straight lines (see Lemmas 6.7 and 6.13), and for the pursuer to rotations in place and straight lines, Lemma 6.11. We will also provide the system trajectories in the reduced space (see Theorems 6.9 and 6.14).

6.3.6 Integrating the adjoint equation starting at the usable part

We need to establish the initial conditions of the system, in this case, the values of V_x and V_y on the UP of ζ. From Eq. (6.5) we have that

$$\frac{dx}{ds} = l\cos s, \quad \frac{dy}{ds} = -l\sin s \tag{6.20}$$

Since $V(\mathbf{x}) = 0$ on the UP of ζ it follows that

$$V_s = \frac{dV}{ds} = \frac{\partial V}{\partial x}\frac{dx}{ds} + \frac{\partial V}{\partial y}\frac{dy}{ds} = 0 \tag{6.21}$$

Substituting Eq. (6.20) into Eq. (6.21)

$$V_x \cos s = V_y \sin s \tag{6.22}$$

From Eq. (6.22) we have that on the UP

$$V_x = \lambda \sin s, \;\; V_y = \lambda \cos s \tag{6.23}$$

where λ is a constant value.

Lemma 6.6. *The solution of the adjoint equation (6.19) starting at the usable part is*

$$V_x = \lambda \sin s, \;\; V_y = \lambda \cos s \tag{6.24}$$

Proof. From Lemma 6.1, we know that at the end of game the pursuer follows a translation (straight line). Therefore Eq. (6.19) takes the form

$$\frac{d}{d\tau}V_x = 0, \;\; \frac{d}{d\tau}V_y = 0 \tag{6.25}$$

We can directly verify that Eq. (6.24) satisfies Eq. (6.25). This solution for the adjoint equation will be valid at the UP and as long as the DDR controls do not change, which corresponds to a DDR motion following a straight line in the realistic space. We need to compute a new integration of the adjoint equations when one of the control's expressions in Eq. (6.12) changes sign i.e., the DDR starts rotating in place in the realistic space. In Lemma 6.11, we compute the retro-time when the DDR switches controls. □

Lemma 6.7. *At the end of the game, if the pursuer follows its optimal strategy (i.e. moves in a straight line in the realistic space) the corresponding optimal strategy for the evader is also a straight line in the realistic space, and therefore, the system moves in a straight line in the reduced space.*

Proof. From Eq. (6.24), we know that V_x and V_y have constant values. Substituting those values into the evader's controls in Eq. (6.13), we find that $\nu = v_2^* = s$, the evader's motion direction in the reduced space, is also constant, thus the system follows a straight line in the reduced space at the end of the game.

From Lemma 6.1, we know that the DDR is moving in straight line in the realistic space at the end of the game. Therefore its motion direction θ_p is constant. From the third

equation in the coordinate transformation, Eq. (6.2), and as ν and θ_p are constant, it is straightforward to see that ψ_e, the evader's motion direction in the realistic space, will be constant. □

Remark 6.8. From Lemma 6.3, the controls of the players *are independent*, it would be misleading to conclude that Lemma 6.7 implies that the evader's controls depend on the pursuer's controls. But in order to show a graphical representation of the trajectories in the realistic space it is necessary to know the controls of the DDR to compute the transformation between the reduced and realistic spaces.

6.3.7 Integrating the motion equations starting at the usable part

Theorem 6.9. *The retro-time trajectories of the system in the reduced space leading directly to the end of the game are*

$$\begin{aligned} x(\tau) &= -\tau V_e^{\max} \sin s + l \sin s \\ y(\tau) &= \tau(-V_e^{\max} \cos s \pm V_p^{\max}) + l \cos s \end{aligned} \tag{6.26}$$

the sign + is taken if the pursuer moves forward in the realistic space when it captures the evader and the sign − if it moves backward.

Proof. From Eq. (6.4), the retro-time version of the equations of motion in the reduced space is

$$\begin{aligned} \frac{d}{d\tau}x &= -\left(\frac{u_2 - u_1}{2b}\right) y - v_1 \sin v_2 \\ \frac{d}{d\tau}y &= \left(\frac{u_2 - u_1}{2b}\right) x + \left(\frac{u_1 + u_2}{2}\right) - v_1 \cos v_2 \end{aligned} \tag{6.27}$$

Substituting Eq. (6.24) into the controls expressions in Eq. (6.12) and Eq. (6.13), and the resulting expressions into Eq. (6.27) we obtain

$$\frac{d}{d\tau}x = -V_e^{\max} \sin s, \quad \frac{d}{d\tau}y = -V_e^{\max} \cos s + V_p^{\max} \tag{6.28}$$

when the pursuer is translating forward, and

$$\frac{d}{d\tau}x = -V_e^{\max} \sin s, \quad \frac{d}{d\tau}y = -V_e^{\max} \cos s - V_p^{\max} \tag{6.29}$$

when the pursuer is translating backward. Integrating Eq. (6.28) and Eq. (6.29) with the initial conditions $x = l \sin s$ and $y = l \cos s$ leads to the expressions in Eq. (6.26) for the trajectories. □

Remark 6.10. The trajectories in Eq. (6.26) are referred as the *primary solution* [20].

6.3.8 Transition surface

The solutions in Eq. (6.24), and Eq. (6.26) are valid as long as the DDR does not switch controls. The place where a control variable abruptly changes in value, is known as a *transition surface*. In our problem, after a retro-time interval the DDR switches controls and it starts rotating in place in the realistic space.

Lemma 6.11. *The DDR switches controls and it starts a rotation in place in the realistic space, at* $\tau_s = |\frac{b\cos s}{V_p^{\max}\sin s}|$. *If* $s \in [0,\pi]$, u_2^* *switches first, otherwise,* u_1^* *does.*

Proof. We can compute the time τ_s when the DDR switches controls, substituting Eq. (6.24) and Eq. (6.26) into Eq. (6.12), and verifying which one of the resulting expressions is the first in changing signs. Doing that we find that for $s \in [0, \frac{\pi}{2}]$, u_2^* switches first at

$$\tau_s = \frac{b\cos s}{V_p^{\max}\sin s} = \frac{b}{V_p^{\max}}\tan s \tag{6.30}$$

The other cases can be proved using an analogous reasoning. □

When the game reaches τ_s, we need to start a new integration of the retro-time version of the adjoint equation (6.19) and the equations of motion (6.27). This integration takes as initial conditions the values of V_x, V_y, x, and y at τ_s. We will denote those values as $V_{x_{\tau_s}}$, $V_{y_{\tau_s}}$, x_{τ_s} and y_{τ_s}. The equations in Lemmas 6.12 and 6.13, and Theorem 6.14 were constructed after the DDR switches controls and it starts rotating in place in the realistic space.

Lemma 6.12. *The solution of the adjoint equation (6.19) starting at* τ_s *is*

$$\begin{aligned} V_x &= \lambda \sin\left[s - \left(\frac{u_2^* - u_1^*}{2b}\right)(\tau - \tau_s)\right] \\ V_y &= \lambda \cos\left[s - \left(\frac{u_2^* - u_1^*}{2b}\right)(\tau - \tau_s)\right] \end{aligned} \tag{6.31}$$

for $\tau \geq \tau_s$.

Proof. Computing the retro-time derivative of Eq. (6.19), we obtain two ordinary linear differential equations of second order with constant coefficients

$$\frac{d^2}{d\tau^2}V_x = -\left(\frac{u_2^* - u_1^*}{2b}\right)^2 V_x, \quad \frac{d^2}{d\tau^2}V_y = -\left(\frac{u_2^* - u_1^*}{2b}\right)^2 V_y \tag{6.32}$$

The solutions of this kind of differential equations are

$$\begin{aligned} V_x &= C\cos\left[\left(\frac{u_2^*-u_1^*}{2b}\right)(\tau-\tau_s)\right] + D\sin\left[\left(\frac{u_2^*-u_1^*}{2b}\right)(\tau-\tau_s)\right] \\ V_y &= E\cos\left[\left(\frac{u_2^*-u_1^*}{2b}\right)(\tau-\tau_s)\right] + F\sin\left[\left(\frac{u_2^*-u_1^*}{2b}\right)(\tau-\tau_s)\right] \end{aligned} \tag{6.33}$$

Recall that the integration takes place from τ_s for that reason we have written $(\tau-\tau_s)$. We need to find the values of C, D, E and F. We have that at $\tau=\tau_s$

$$V_x = C = \lambda\sin s \tag{6.34}$$

Computing the retro-time derivative of the expression for V_x, we get

$$\begin{aligned} \frac{d}{d\tau}V_x = &-C\left(\frac{u_2^*-u_1^*}{2b}\right)\sin\left[\left(\frac{u_2^*-u_1^*}{2b}\right)(\tau-\tau_s)\right] \\ &+D\left(\frac{u_2^*-u_1^*}{2b}\right)\cos\left[\left(\frac{u_2^*-u_1^*}{2b}\right)(\tau-\tau_s)\right] \end{aligned} \tag{6.35}$$

We have that at $\tau=\tau_s$

$$\frac{d}{d\tau}V_x = D\left(\frac{u_2^*-u_1^*}{2b}\right) \tag{6.36}$$

From Eq. (6.19), we have that $D=-V_y$ then

$$D = -\lambda\cos s \tag{6.37}$$

Substituting Eq. (6.34) and Eq. (6.37) into Eq. (6.33), we have that

$$\begin{aligned} V_x = &\lambda\sin s\cos\left[\left(\frac{u_2^*-u_1^*}{2b}\right)(\tau-\tau_s)\right] \\ &-\lambda\cos s\sin\left[\left(\frac{u_2^*-u_1^*}{2b}\right)(\tau-\tau_s)\right] \end{aligned} \tag{6.38}$$

Rewriting the last expression, we obtain

$$V_x = \lambda\sin\left[s-\left(\frac{u_2^*-u_1^*}{2b}\right)(\tau-\tau_s)\right] \tag{6.39}$$

The expression for V_y can be computed using an analogous reasoning. □

Lemma 6.13. *For $\tau>\tau_s$, the optimal controls correspond to the evader following a straight line in the realistic space and the DDR rotating in place.*

Proof. Substituting Eq. (6.31) into Eq. (6.13) we have that,

$$\begin{aligned} \sin v_2^* &= \sin\left[s - \left(\frac{u_2^* - u_1^*}{2b}\right)(\tau - \tau_s)\right] \\ \cos v_2^* &= \cos\left[s - \left(\frac{u_2^* - u_1^*}{2b}\right)(\tau - \tau_s)\right] \end{aligned} \tag{6.40}$$

therefore

$$\nu' = v_2^* = s - \left(\frac{u_2^* - u_1^*}{2b}\right)(\tau - \tau_s) \tag{6.41}$$

As the DDR is rotating in place, its motion direction is given by

$$\theta_p' = \theta_p^s - \left(\frac{u_2^* - u_1^*}{2b}\right)(\tau - \tau_s) \tag{6.42}$$

where θ_p^s is the initial motion direction of the DDR in the realistic space. Substituting Eq. (6.41) and Eq. (6.42) into the third expression in Eq. (6.2), we obtain that $\psi_e = \theta_p^s - s$, the evader's motion direction in realistic space. Note that it is a constant value, thus the evader is following a straight line in realistic space. □

Note again that from Lemma 6.3, the controls of the players *are independent*. But in order to show a graphical representation of the trajectories in the realistic space it is needed to know the controls of the DDR.

6.3.9 Integrating the motion equations starting at the TS

Theorem 6.14. *The retro-time trajectories of the system starting at τ_s are*

$$\begin{aligned} x(\tau) =& -y_{\tau_s}\sin\left[\left(\frac{u_2^* - u_1^*}{2b}\right)(\tau - \tau_s)\right] + x_{\tau_s}\cos\left[\left(\frac{u_2^* - u_1^*}{2b}\right)(\tau - \tau_s)\right] \\ & - (\tau - \tau_s)V_e^{\max}\sin\left[s - \left(\frac{u_2^* - u_1^*}{2b}\right)(\tau - \tau_s)\right] \\ y(\tau) =& x_{\tau_s}\sin\left[\left(\frac{u_2^* - u_1^*}{2b}\right)(\tau - \tau_s)\right] + y_{\tau_s}\cos\left[\left(\frac{u_2^* - u_1^*}{2b}\right)(\tau - \tau_s)\right] \\ & - (\tau - \tau_s)V_e^{\max}\cos\left[s - \left(\frac{u_2^* - u_1^*}{2b}\right)(\tau - \tau_s)\right] \end{aligned} \tag{6.43}$$

Proof. Substituting Eq. (6.31) into Eq. (6.13), and the resulting expressions into Eq. (6.27) we obtain

$$\begin{aligned}\frac{d}{d\tau}x &= -\left(\frac{u_2^* - u_1^*}{2b}\right) y - V_e^{\max} \sin\left[s - \left(\frac{u_2^* - u_1^*}{2b}\right)(\tau - \tau_s)\right] \\ \frac{d}{d\tau}y &= \left(\frac{u_2^* - u_1^*}{2b}\right) x - V_e^{\max} \cos\left[s - \left(\frac{u_2^* - u_1^*}{2b}\right)(\tau - \tau_s)\right]\end{aligned} \tag{6.44}$$

Computing the retro-time derivative of Eq. (6.44) and solving the resulting expressions with the initial conditions x_{τ_s} and y_{τ_s} using an analogous reasoning to the one applied in the proof of Lemma 6.12, we obtain the solution in Eq. (6.43). □

6.4 Decision problem

In this section, we find the conditions that make capture possible for the DDR or escape for the evader. These conditions are based on the description of the decision problem, the barrier and its construction in Section 5.3 of Chapter 5. Figure 6.3 shown a representation of the terminal surface, the usable part (UP) and its boundary (BUP) in the reduced space. The system exhibits some symmetries with respect to the x and y-axis in this representation. An analysis for the trajectories in the first quadrant will be provided. This analysis can be extended to the remaining quadrants using an analogous reasoning.

6.4.1 Solving the decision problem

We present two useful properties appearing in some trajectories reaching the UP.

Lemma 6.15. *The retro-time trajectories starting at the UP in the first quadrant (see Fig. 6.3) reach the y-axis before the system switches controls if $l/V_e^{\max} \leq \tau_s$.*

Proof. When the retro-time trajectories reach the y-axis we have that $x = 0$. From Eq. (6.26)

$$-\tau V_e^{\max} \sin s + l \sin s = 0 \tag{6.45}$$

By straightforward algebraic manipulation, we find that $\tau = l/V_e^{\max}$. This is the retro-time it takes to reach the y-axis if the system is following Eq. (6.26), and it will be denoted as $\tau_c = l/V_e^{\max}$. We know that the DDR switches controls at $\tau = \tau_s$. After that, the system starts following Eq. (6.43). If $\tau_c \leq \tau_s$ the system will reach the y-axis before switching controls. □

Lemma 6.16. *The trajectories in Eq. (6.26) that reach the y-axis in the first quadrant, reach it at* $y = l/\rho_v$.

Proof. From Lemma 6.15, we have that $\tau_c = l/V_e^{\max}$ is the retro-time it takes to reach the y-axis when the system is following Eq. (6.26). Substituting τ_c into Eq. (6.26) we have that

$$y = \frac{l}{V_e^{\max}}(-V_e^{\max}\cos s + V_p^{\max}) + l\cos s \tag{6.46}$$

After straightforward algebraic manipulation, we find that $y = l/\rho_v$. This value will be denoted as y_c. □

Lemma 6.17. *The barrier consists of a straight line segment, and it intersects the y-axis in the first quadrant if* $\rho_v \geq |\tan S|/\rho_d$ *where* $S = \cos^{-1}(\rho_v)$ *is the angle at the BUP (see Fig. 6.3).*

Proof. In our game, the barrier is constructed by substituting the value S that satisfies $\cos S = \rho_v$ into Eq. (6.26). The expression in Eq. (6.26) is valid as long as the DDR does not switch controls. After a retro-time interval τ_s the DDR should switch controls and start rotating in place in the realistic space. Then the system should follow the trajectory described by Eq. (6.43) in the reduced space. Figure 6.4 shows both trajectories. The trajectory given by Eq. (6.43) intersects the initial segment of the barrier and it comes back to the UP in the reduced space. According to [20], the barrier is not crossed by any trajectory followed by the system during optimal play, in particular, it cannot cross itself. Therefore the portion of the trajectory given by Eq. (6.43), (the arc in Fig. 6.4) must be discarded. The barrier reaches the terminal surface with $S = \cos^{-1}(\rho_v)$, and it consists only of a straight line in the reduced space given by Eq. (6.26) that ends when $\tau = \tau_s$. From Lemma 6.15, it is straightforward to verify that the barrier will reach the y-axis if $\tau_c \leq \tau_s$. Substituting the values of τ_c and τ_s in the last inequality, we find that it can be expressed as $\frac{V_e^{\max}}{V_p^{\max}} \geq \frac{l|\tan S|}{b}$, which can be rewritten as $\rho_v \geq |\tan S|/\rho_d$. □

Remark 6.18. Note that if the system follows the trajectory composed by the arc from point 1 to point 2 (see Fig. 6.4), and the straight line from point 2 to point 3, the DDR loses the game. The distance between both players equals l over the target set, however, the pursuer will not be able to get closer from the evader than this value and capture cannot be attained (since in the reduced space, the system is pointing tangentially to the terminal surface and it cannot be crossed). In contrast, if the system follows the straight line motion from point 1 to point 4, the system reaches the usable part and it can be crossed. The distance between the players can be reduced by the pursuer and it wins. Hence, the arc given by Eq. (6.43) must be discarded. Indeed, it can be proved

that traveling the arc from point 1 to point 2, and the straight line trajectory from point 2 to point 3 takes more time than traveling the straight line from point 1 to point 4.

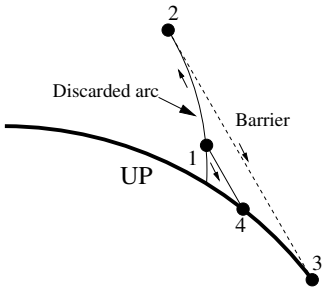

FIGURE 6.4: The system is following the barrier from point 1 to point 3. The two elements of the barrier are, the dashed line which is given by Eq. (6.26), and the solid arc given by Eq. (6.43). The solid straight line represents the optimal trajectory to reach the UP at point 4 from point 1. From points over the solid arc the DDR can attain capture and the system follows a straight line in the reduced space. Therefore this arc must be discarded.

Theorem 6.19. *If $\rho_v < |\tan S|/\rho_d$ the DDR can capture the evader from any initial configuration in the playing space. Otherwise the barrier separates the playing space into two regions:*

1. *One between the UP and the barrier.*
2. *Another above the barrier.*

The DDR can only force the capture in the configurations between the UP and the barrier, in which case, the DDR follows a straight line in the realistic space when it captures the evader.

Proof. It follows from the definition of the barrier and Lemma 6.17. Note that the segment of the barrier corresponding to a rotation in place of the DDR in the realistic space has been discarded and all the trajectories between the barrier and the UP are straight lines reaching the y-axis (refer to Lemma 6.16 and see Fig. 6.5). □

Remark 6.20. For the rest of this work, we assume that the barrier does not intersect the y-axis and therefore capture in all the playing space can be attained by the DDR. In Section 6.8, we make an exception including simulations where the barrier separates the playing space into two regions and showing the strategy followed by the evader to avoid capture.

6.5 Singular surfaces

The singular surfaces and their construction in the context of our game will be described in the next paragraphs giving a solution of the game for the complete playing space.

6.5.1 Identification and construction of the singular surfaces

In this section, we devote our attention to the construction of the singular surfaces appearing on our game.

Lemma 6.21. *The retro-time trajectories reaching the y-axis in the first quadrant have an orientation* $s \in [0, \tan^{-1}(\rho_v \rho_d)]$ *at the UP (see Fig. 6.3).*

Proof. From Lemma 6.15, the retro-time trajectories that reach the y-axis are those where $\tau_c \leq \tau_s$. The last one that can reach it will have $\tau_c = \tau_s$. Substituting the corresponding values

$$\frac{l}{V_e^{\max}} = \frac{b \cos s}{V_p^{\max} \sin s} \tag{6.47}$$

From the last expression we find that

$$\tan s = \rho_v \rho_d \tag{6.48}$$

The trajectory given by $s = 0$ coincides with the y-axis. Therefore, the trajectories reaching the y-axis will have an angle $s \in [0, \tan^{-1}(\rho_v \rho_d)]$ at the UP. □

Lemma 6.22. *The straight lines trajectories that have an orientation* $s \in (\tan^{-1}(\rho_v \rho_d), \cos^{-1}(\rho_v)]$ *in the UP of the first quadrant terminate when the DDR switches controls.*

Proof. From Lemma 6.21 we know that the last trajectory reaching the y-axis has an orientation $s_c = \tan^{-1}(\rho_v \rho_d)$. If $s > s_c$ the DDR switches controls before reaching the y-axis and the system starts following the trajectories given by Eq. (6.43). The value $s = \cos^{-1}(\rho_v)$ corresponds to the barrier and it consists of a straight line in the reduced space. Thus the straight line trajectories reaching the UP at $s \in (\tan^{-1}(\rho_v \rho_d), \cos^{-1}(\rho_v)]$ terminate when a switch of the DDR controls occurs. □

6.5.1.1 Transition surface (TS)

Lemma 6.23. *The points* $\mathbf{x}$ *in the reduced space where* $\tau = \tau_s$ *constitute a TS in the first quadrant. At the TS in the first quadrant, the expression* $yV_x - xV_y - bV_y = 0$ *is satisfied. This surface is bounded by the barrier and the y-axis.*

Proof. From the Lemma 6.22, we know that the trajectories ending at $s \in (\tan^{-1}(\rho_v \rho_d), \cos^{-1}(\rho_v))$ have a switch when $\tau = \tau_s$. The points $\mathbf{x}$ where this happens constitute the transition surface (TS). For the first quadrant, in those points u_2 changes sign. Note that $s = \tan^{-1}(\rho_v \rho_d)$ generates a straight line trajectory of the system in the reduced space reaching the y-axis just before switching controls. If $s = \cos^{-1}(\rho_v)$, the trajectory corresponds to the barrier, which is a straight line in the reduced space ending also just before switching controls. Thus the y-axis and the barrier bound the TS. □

Remark 6.24. The TS indicates the points in the reduced space where the DDR switches controls, and it is not a trajectory followed by the system.

6.5.1.2 Universal surface (US)

Lemma 6.25. *The positive y-axis contains a US where the pursuer captures the evader with its heading directly aligned to the evader.*

Proof. In a universal surface (US), optimal play demands that the system be brought to the surface and remains on it. Hence a necessary condition for a US, is that in this surface there are no switches and the controls of the players remain constant. We find that in our game, this occurs when the system is moving along the positive y-axis in the reduced space.

The game ends with $s = 0$, i.e., the evader's relative position aligned with the pursuer's heading. From Lemma 6.6, we know that at the end of the game,

$$V_x = \lambda \sin s, \quad V_y = \lambda \cos s \tag{6.49}$$

where λ is a constant value. As $s = 0$, in this case

$$V_x = 0, \quad V_y = \lambda \tag{6.50}$$

Substituting those values into the pursuer's controls Eq. (6.12), we find that the expressions inside the switching functions

$$-y\frac{V_x}{b} + x\frac{V_y}{b} - V_y = -\lambda \tag{6.51}$$

and

$$y\frac{V_x}{b} - x\frac{V_y}{b} - V_y = -\lambda \tag{6.52}$$

are constant. Therefore, the DDR will never switch controls when the system is moving in straight line over the positive y-axis in the reduced space and it will remain on it.

Substituting Eq. (6.50) into the evader's controls Eq. (6.13), we find that the motion direction of the evader is given by

$$\sin v_2^* = 0, \quad \cos v_2^* = 1 \tag{6.53}$$

The evader is moving following a straight line in the realistic space while the system is moving over the positive y-axis in the reduced space and it will remain on it. From Lemma 6.21, we know that a portion of the y-axis is also a trajectory reaching the UP, this trajectory ends at the intersection point y_c. This point is considered as the starting point of the US. □

Remark 6.26. The tributary trajectories entering the US are generated by a different combination of the player's optimal controls to the ones used over the surface [20].

Lemma 6.27. *The tributary trajectories over the US associated to the first quadrant correspond to a rotation in place of the DDR and straight line for the evader in the realistic space.*

Proof. In our game, the tributary trajectories entering the US are generated by a different combination of the optimal controls for the DDR (see Lemmas 6.7 and 6.13). Over the US associated to the first quadrant in the reduced space, we have that the DDR always captures the evader moving forward, therefore the tributary trajectories will correspond to a rotation in place of the DDR, in the realistic space. For the first quadrant, we have that $u_1^* = V_p^{\max}$ and $u_2^* = -V_p^{\max}$ (the DDR rotates clockwise to align its heading with the evader's motion direction in the realistic space). Taking these controls, the trajectories in the reduced space can be computed using an analogous reasoning to the one applied in Theorem 6.14. In fact, they satisfy Eq. (6.43) taking $u_1^* = V_p^{\max}$, $u_2^* = -V_p^{\max}$ and $\tau_s = d/V_e^{\max}$, where $d \geq y_c$ is the distance to the UP along the y-axis. □

6.6 Partition of the space

In this section, we initially present a partition of the first quadrant into three regions, and later, we describe a partition of the four quadrants. All the points in each region can be reached by a particular combination of the motion strategies of the players. This partition will contain some singular surfaces. *The complete set of trajectories for each region is sufficient to cover the space.*

6.6.1 Construction of the partition

We construct each one of the regions in quadrant I and we verify that the space is covered by them. The complete construction is shown in Fig. 6.5.

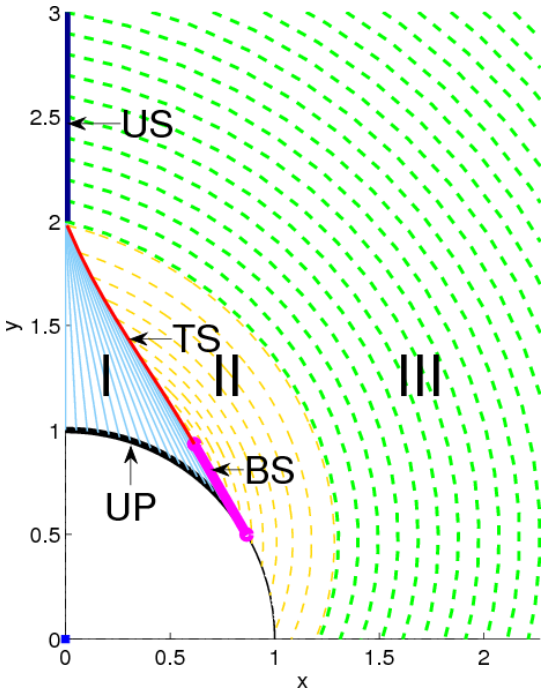

FIGURE 6.5: Partition of the first quadrant in the reduced space. The barrier (in magenta) is labelled as BS, the transition surface (in red) as TS, and the universal surface (in navy blue) as US. The solid lines (in light blue) are trajectories in region I, the dashed lines (in light yellow) are trajectories in region II and the bold dashed lines (in green) are trajectories in Region III.

6.6.1.1 Region I

We denote as *region I* (shown in Fig. 6.5) the set of points that can reach the UP with a single straight line trajectory in the reduced space, which corresponds to a straight line motion of both the DDR and the evader, in the realistic space. From Lemmas 6.17, 6.21, 6.22 and 6.23, we have that the straight line trajectories ending at the UP in the first quadrant are bounded by the y-axis, the barrier (labelled as BS) and the TS. The trajectories in region I can be classified into two types: the ones attain the y-axis at y_c and the ones reaching the transition surface TS. Both types of trajectories in this region are given by Eq. (6.26). Examples of trajectories in this region (solid lines) are shown in Fig. 6.5.

6.6.1.2 Region II

We denote as *region II* (shown in Fig. 6.5) the set of points that attain the TS by following a trajectory given by Eq. (6.43) in the reduced space, which corresponds to a rotation in place for DDR and straight line trajectory for the evader, both in the realistic space. From Lemmas 6.22, 6.23, 6.25 and 6.27, the trajectories in Region II are bounded by the BS, the TS, the x-axis and the trajectory reaching the starting point of the US (in green in Fig. 6.5). Each point inside region II moves according to Eq. (6.43), it hits the TS at some particular point and to attain the UP it must follow the trajectory in region I reaching the same point in the TS. Some trajectories (dashed lines) in region II are shown in Fig. 6.5.

6.6.1.3 Region III

We denote as *region III* (shown in Fig. 6.5) the set of points that attain the US following one of its tributary trajectories given by Eq. (6.43) in the reduced space corresponding to a rotation in place for the DDR and a straight line trajectory for the evader, both in the realistic space. From Lemmas 6.23, 6.25 and 6.27, the trajectories in region III are bounded by the US over the y-axis, the point over the TS touching the y-axis and the trajectory given by Eq. (6.43) reaching that point. Some trajectories in Region III (bold dashed lines) are shown in Fig. 6.5.

Region III in the reduced space corresponds to configurations in the realistic space where the DDR rotates in place until *it aligns its heading* with the segment joining the DDR's position and the evader's position. Then the DDR moves following a straight line towards the evader until the capture condition is achieved. In this case, the evader has the option to change its motion direction at the point over the y-axis in the reduced space where the time-optimal trajectories in region I intersect and it can follow one of them. At this point, the time-optimal trajectories in region I are equivalent and they require the same amount of time to capture the evader. Region II in the reduced space corresponds to configurations in the realistic space where the DDR initially also rotates in place but *it is not necessary to align completely* the DDR's heading with the segment joining the positions of both players in order to capture the evader. In this case, the time-optimal trajectories for both players are unique. We have a bijection between trajectories in region II and region I.

6.6.2 Graph representation

Figure 6.6(a) shows a graph representation of the partition in the first quadrant. The nodes of the graph represent the regions described above, and the edges indicate the transitions between them. For all points in one region of the partition, a particular selection of the controls for both players is used, i.e., the regions are equivalence classes under a relation given by the controls. Note that the transition between regions is uniquely defined, i.e., from the current node in the graph, the system can only reach one node and therefore only a particular selection of the controls for both players can be made. Figure 6.6(a) shows that from any node in the graph, the system will be able to reach the terminal surface following the transitions given by the edges. Also, this figure shows that the sequence followed by the system and the value function are uniquely determined.

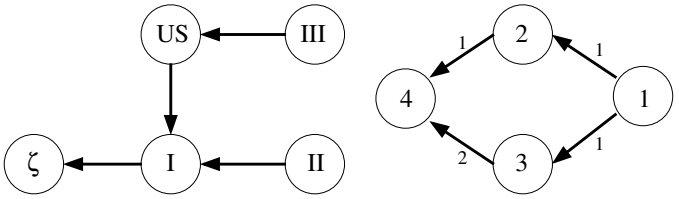

(a) Graph representation of the partition in the first quadrant.

(b) An example where the transitions to reach the goal are not uniquely determined.

FIGURE 6.6: Graph representations

It is well-known in optimal control theory that if the system has two possible locally optimal controls in a particular state, one cannot locally make a selection that guarantees global optimality of the solution. For example, Figure 6.6(b), shows a case, where the transitions between states are not uniquely determined and they have different costs. In this example, from state 1 the system can move to state 2 or 3 with the same cost. From these two states, however, the system moves to state 4 with different costs. It is important to note that from state 1, it is not possible to locally choose the set of transitions that will lead to the minimum cost to reach the state 4, and therefore the PMP, which is a local condition, in general cannot be used by itself to find the globally optimal solution.

Note that this is not the case in the graph representation obtained in this work (see Fig. 6.6(a)). In our case, *the transition between regions is uniquely determine to reach the goal*, so that the PMP and the Isaacs equation provide necessary and sufficient conditions for optimality.

6.6.3 Playing space partition

In Fig. 6.7, we present the partition and the corresponding trajectories for the reduced space. All the regions are defined in an analogous way to the ones in the first quadrant. The bold arrows show the directions in which the different trajectories are travelled in order to reach the terminal surface. In this figure, *the x-axis contains a dispersal surface (DS)*, represented as a bold line, where the rotation-in-place trajectories in retro-time coming from the upper and bottom parts of the UP intersect. Over the DS both players have two choices for their controls. It is important to note that at the DS, the choice of the control of one player *must correspond* to the choice of the control of the other player. If one of the players selects the wrong control, the other player will benefit from that decision. In this problem, the DS corresponds to configurations where the pursuer's heading (orientation of the wheels) is perpendicular to the pursuer's location, and the DDR has the option to rotate either clockwise or counterclowise to catch the evader. If the DDR fails to initially choose the correct sense of rotation against the evader's decision then feedback will be necessary to correct the decision and capture the evader in suboptimal time. To avoid the selection problem, the instantaneous velocity vector of both players should be known, but in general (and in particular for this problem) it is assumed that this information is not available. Therefore, a solution will be to employ an instantaneous mixed strategy (IMS) [20], which means the randomizing of a player's decision in accordance with some probabilistic law until the system is no longer on the DS. The trajectories generated by the correct pair of controls will lead to the same optimal time-to-go. In this problem, the difference will be that at the end the capture will be attained moving forward or backward in straight line in the realistic space.

In the partition, a particular behavior occurs at point y_c (see figure 6.15), where the US meets region I, and the straight line system trajectories reaching the UP with an orientation $s \in [0, \tan^{-1}(\rho_v \rho_d)]$ reaching the y-axis. At this unique point, the system has the option to follow any of the straight line trajectories reaching the y-axis, which will lead to the same optimal capture time but the system will have a different position at the UP. In the realistic space, at the point y_c the evader has the option to select among different motion directions, but all of them correspond to the same optimal capture time.

In Figure 6.8, a graph representation of the playing space is shown. The nodes of the graph represent the regions in the four quadrants of the playing space, and the edges indicate how the state moves from one region to another in order to reach the terminal surface. This representation shows that the capture condition can be attained from any region in the playing space when the barriers do not intersect.

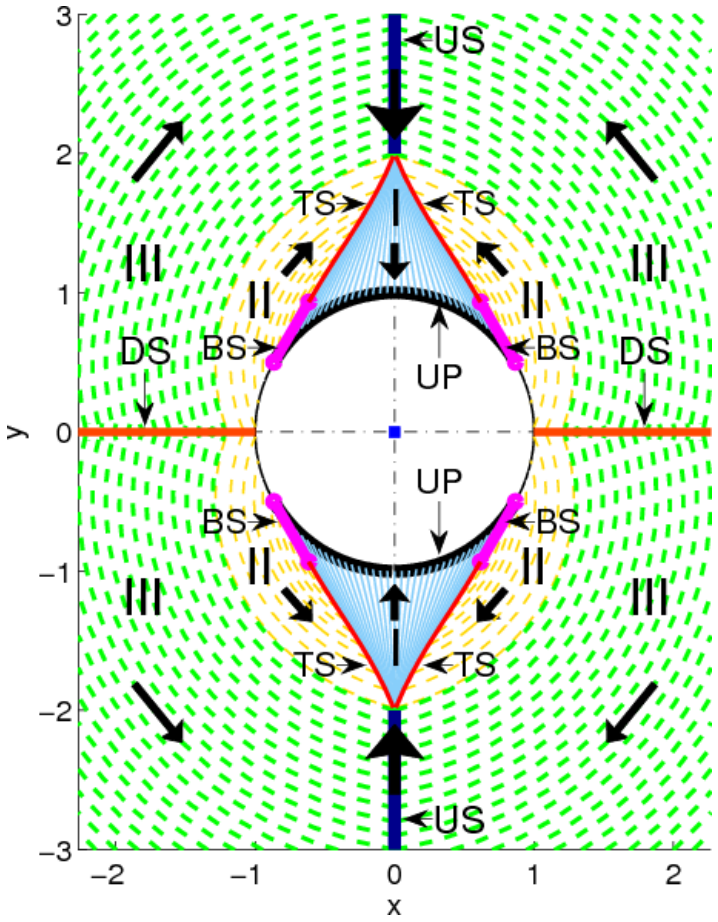

FIGURE 6.7: Partition of the entire reduced space and the corresponding trajectories.

6.7 Computing a feedback-based motion strategies for the DDR

For a given state (x, y) of the system, we describe a method to identify the region of the reduced space partition where it belongs. Using this information we obtain the corresponding time-optimal motion primitive used by the DDR. The main idea behind the approach is to obtain a polar representation of the singular surfaces and the regions defined by them.

6.7.1 Overview of the method

In Fig. 6.9, we have a graphical representation of the regions integrating the partition of the first quadrant. The idea behind the algorithm is comparing the distance from the origin of the reduced space to a given state (x, y) with the distance from origin to the singular surfaces defining the regions in the reduced space. As we can see in Fig. 6.9, all states farther to the origin than the tributary trajectory (green dashed line) belong to

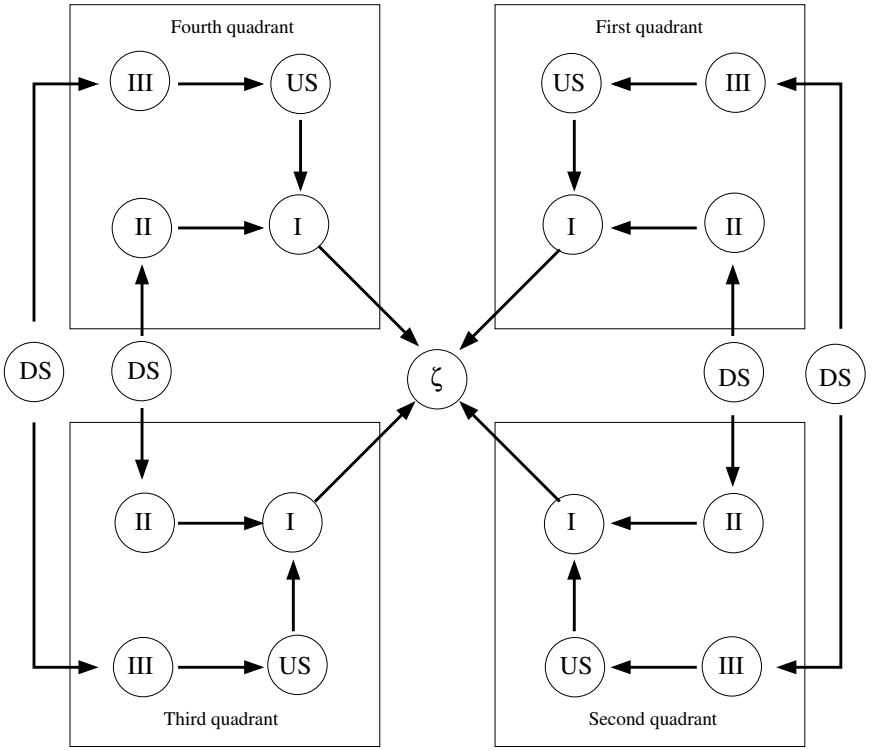

FIGURE 6.8: The nodes of the graph represent the regions in the playing space and the edges show how the state moves from one region to another in order to reach the terminal surface.

Region III. The states in Region II are closer to the origin than the tributary trajectory but farther to the origin that the transition surface (red curve) and the barrier (magenta straight line). Finally, all the states closer to the origin than the transition surface and the barrier but farther to origin that the terminal surface (black arc) correspond to Region I.

To find the region containing a particular state, we compare the distance to the boundaries of these regions, in our case, the distance to the singular surfaces. We propose a top-down approach in the sense that first we verify if the state belongs to Region III (farthest region), if this is not the case, we check if the state belongs to Region II (intermediate region). In other case, we verify if the state belongs to Region I (closest region).

In Fig. 6.9, we observe that Region III is bounded by the first tributary trajectory reaching the universal surface. To identify if a state (x, y) belongs to Region III, we compute its distance from the origin and orientation (r, ϕ), recalling that the orientations are measured with respect to the positive y-axis.

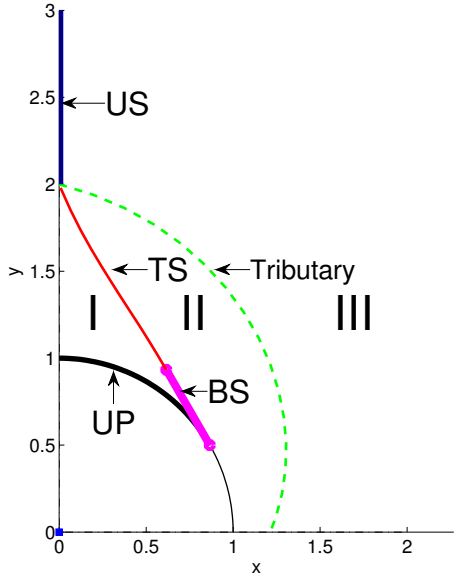

FIGURE 6.9: Partition of the first quadrant and its singular surfaces

$$\begin{aligned} r &= \sqrt{x^2 + y^2} \\ \phi &= \tan^{-1} \frac{x}{y} \end{aligned} \tag{6.54}$$

Next, we compute the distance from the origin to the state over the tributary trajectory having the same orientation ϕ. If the distance from the origin to the state over the tributary trajectory is smaller than the distance from the origin to the state (x, y), then (x, y) belongs to Region III. In Section 6.7.2, we find a representation in polar coordinates of the tributary trajectory bounding Region III. Using that representation, we can easily compute the distance from the origin to the state over the tributary trajectory having a given orientation ϕ.

To find if a configuration belongs to Region II, we have to compare the distance from the origin to the state (x, y) with the distance from the origin to the transition surface, the barrier or the terminal surface. In Fig. 6.9, we observe that for some values of ϕ the comparison is done with the transition surface, for others with the barrier and in some cases with the terminal surface. In Section 6.7.3, we find the orientations defining each one of these three cases. In Section 6.7.3, we also find representations in polar coordinates of the transition surface and the barrier that allow to know if the distance from the origin to the state (x, y) is smaller or not than the distance from the origin to those surfaces.

Finally, if the state does not belong to Region III and II, and the distance from the origin to the state (x, y) is larger than the capture distance l, we have that the state (x, y) belongs to Region I.

6.7.2 Region III

In this section, we find a representation in polar coordinates of the tributary trajectory bounding Region III. For a given state (x, y) with orientation $\phi \in [0, \pi/2]$, we can compute the distance from the origin to the state over the tributary trajectory having the same orientation ϕ.

From Eq. (6.43), and recalling that $x_0 = 0$ and $s = 0$ for the states starting at y-axis, we have that the tributary paths from the universal surface are given by the following expressions

$$x = -y_0 \sin\left[\left(\frac{u_2^* - u_1^*}{2b}\right)\tau\right] - \tau V_e \sin\left[-\left(\frac{u_2^* - u_1^*}{2b}\right)\right] \tag{6.55}$$

$$y = y_0 \cos\left[\left(\frac{u_2^* - u_1^*}{2b}\right)\tau\right] - \tau V_e \cos\left[-\left(\frac{u_2^* - u_1^*}{2b}\right)\right] \tag{6.56}$$

From Lemma 6.25, we know that for tributary trajectories in first quadrant $u_1^* = V_p^{\max}$ and $u_2^* = -V_p^{\max}$. Recalling that $\sin(-x) = -\sin(x)$ and $\cos(-x) = \cos(x)$, Eqs. (6.55) and (6.56) can be rewritten as

$$x = -(y_0 - \tau V_e) \sin\left[\left(\frac{-V_p^{\max}}{b}\right)\tau\right] \tag{6.57}$$

$$y = (y_0 - \tau V_e) \cos\left[\left(\frac{-V_p^{\max}}{b}\right)\tau\right] \tag{6.58}$$

From Eqs. (6.57) and (6.58) we have that

$$\tau = \frac{1}{V_e}\left(\frac{x}{\sin\left[\left(\frac{-V_p^{\max}}{b}\right)\tau\right]} + y_0\right) \tag{6.59}$$

$$\tau = \frac{1}{V_e}\left(\frac{-y}{\cos\left[\left(\frac{-V_p^{\max}}{b}\right)\tau\right]} + y_0\right) \tag{6.60}$$

Equating Eqs. (6.59) and (6.60)

$$-\frac{x}{y} = \frac{\sin\left[\left(\frac{-V_p^{\max}}{b}\right)\tau\right]}{\cos\left[\left(\frac{-V_p^{\max}}{b}\right)\tau\right]} \tag{6.61}$$

The equation above can be rewritten as

$$-\frac{x}{y} = \tan\left[\left(\frac{-V_p^{\max}}{b}\right)\tau\right] \tag{6.62}$$

Therefore

$$\tau = -\frac{\arctan\left(\frac{x}{y}\right)}{\left(\frac{-V_p^{\max}}{b}\right)} \tag{6.63}$$

In polar coordinates, the position of the evader with respect to the DDR is given by (r, ϕ) where

$$r = \sqrt{x^2 + y^2} = y_0 - \tau V_e \tag{6.64}$$

$$\tan\phi = \frac{x}{y} \tag{6.65}$$

Eq. (6.64) is obtained by straightforward manipulation of Eqs. (6.57) and (6.58). Note that in Eq. (6.65), ϕ is measured with respect to the y-axis. Substituting Eq. (6.65) into Eq. (6.63) we obtain that

$$\tau = \frac{-\phi}{\left(\frac{-V_p^{\max}}{b}\right)} \tag{6.66}$$

Substituting Eq. (6.66) into we obtain

$$r_{III} = y_0 + \frac{V_e\phi}{\left(\frac{-V_p^{\max}}{b}\right)} \tag{6.67}$$

The equation above allows to know the distance from the origin of the reduced space to the tributary trajectory starting at y_0 in the y-axis. We know from Lemma 6.25 that the universal surface and its tributaries in the first quadrant start at $y_0 = y_c = l/\rho_v$ where $\rho_v = \frac{V_e}{V_p}$. All the trajectories starting at $y_0 \geq y_c$ belong to Region III. Therefore using Eq. (6.67) it is possible to determine if a state (x, y) is in Region III by comparing its distance from the origin.

6.7.3 Region II

In Fig. 6.9, we can observe that Region II is bounded by the transition surface, the barrier and the terminal surface. As in Section 6.7.2, we identify if a state belongs to Region II using its distance from the origin and orientation (r, ϕ). From Fig. 6.9, if $\phi \in [0, \pi/2]$ we have three possible choices. For the first case, we need to compare against the transition surface, in the second one, we need to compare against the barrier, and in the third case, we compare against the terminal surface. In the following paragraphs, we compute the set of orientations defining the three cases described above.

In Figure 6.9, we can observe that the transition surface starts at the end of the barrier. Once we find the point where the barrier ends it is straightforward to find the orientation of this point. This will be the upper bound orientation that has to be compared with the transition surface. In an analogous way, using the start point of the barrier, we can find the upper bound orientation that has to be compared with the barrier. The remaining states have to be compared with the terminal surface.

From Lemma 6.17, we know that the barrier ends at $\tau = (b\cos S)/(V_p \sin S)$, where $S = \cos^{-1}(V_e/V_p)$. The trajectory of the barrier in the first quadrant is given by

$$\begin{aligned} x &= -\tau V_e \sin S + l \sin S \\ y &= -\tau V_e \cos S + V_p \tau + l \cos S \end{aligned} \tag{6.68}$$

We have that the final state of the barrier is given by

$$\begin{aligned} x &= -\frac{bV_e \cos S}{V_p} + l \sin S \\ y &= -\frac{bV_e \cos^2 S}{V_p \sin S} + \frac{b \cos S}{\sin S} + l \cos S \end{aligned} \tag{6.69}$$

The orientation ϕ_{TS} of this state is given by $\phi_{TS} = \tan^{-1} \frac{x}{y}$. Computing the orientation of the state where the barrier starts is straightforward. In that case, $\phi_B = \phi = \cos^{-1}(V_e/V_p)$.

Therefore, if $\phi \in [0, \phi_{TS})$, we have to compare the distance from the origin to the state (x, y) with the distance from the origin to the state over the transition surface having the same orientation ϕ. If $\phi \in [\phi_{TS}, \cos^{-1}(V_e/V_p)]$, we have to compare the distance from the origin to the state (x, y) with the distance from the origin to the state over barrier having an orientation ϕ. If $\phi \in (\cos^{-1}(V_e/V_p), \pi/2]$, we need to verify against the terminal surface.

In the next paragraphs, we find a polar representation of the transition surface. From Lemma 6.11, we know that for the first quadrant, u_2 switches first, therefore along the transition surface

$$yV_x - xV_y - bV_y = 0 \tag{6.70}$$

In Lemma 6.6, we find that $V_x = \lambda \sin s$ and $V_y = \lambda \cos s$. Therefore Eq. (6.70) takes the form

$$y\lambda \sin s - x\lambda \cos s - b\lambda \cos s = 0 \tag{6.71}$$

Doing some algebraic manipulation of Eq. (6.71), we find that

$$\tan s = \frac{x + b}{y} \tag{6.72}$$

From Lemma 6.22, we know that retro-time straight line trajectories that have an initial orientation $s \in (\tan^{-1}(\rho_v\rho_d), cos^{-1}(\rho_v)]$ in the UP, reach the TS. Thus, the x-coordinates along the TS are given by

$$x = \frac{-bV_e \cos s}{V_p} + l \sin s \tag{6.73}$$

Recalling that $\sin(\arctan(x)) = \frac{x}{\sqrt{1+x^2}}$ and $\cos(\arctan(x)) = \frac{1}{\sqrt{1+x^2}}$, and substituting Eq. (6.72) into Eq. (6.73), we have that

$$x = \frac{-b\frac{V_e}{V_p} + l\left(\frac{x+b}{y}\right)}{\sqrt{1+\left(\frac{x+b}{y}\right)^2}} \tag{6.74}$$

Doing some algebraic manipulation of the expression above, and recalling that $x = r\sin\phi$ and $y = r\cos\phi$, we find that

$$\begin{aligned} &r^4\sin^2\phi\cos^2\phi + r^4\sin^4\phi + 2br^3\sin^3\phi + b^2r^2\sin^2\phi - \frac{V_e^2}{V_p^2}b^2r^2\cos^2\phi \\ &+ 2\frac{V_e}{V_p}blr^2\sin\phi\cos\phi + 2\frac{V_e}{V_p}b^2lr\cos\phi - l^2r^2\sin^2\phi - 2bl^2r\sin\phi - l^2b^2 = 0 \end{aligned} \tag{6.75}$$

To identify if a state (r, ϕ) belongs to Region II, we evaluate the expression above. If the left term is greater than zero then the state is above the transition surface and it belongs to Region II. If this is not the case, the state belongs to Region I.

It is possible to find a polar representation of the barrier. Using this representation, we can compare the distance from the origin to a given state (x, y) and the distance from the origin to the barrier, as we did for Region III, in order to identify if the state belongs to Region II.

We know that the barrier in the first quadrant is given by

$$x = -\tau V_e \sin S + l \sin S \tag{6.76}$$

$$y = -\tau V_e \cos S + \tau V_p + l \cos S \tag{6.77}$$

where $S = \cos^{-1}(V_e/V_p)$ From Eq. (6.76), we have that

$$\tau = \frac{l\sin S - x}{V_e \sin S} \tag{6.78}$$

and from Eq. (6.77), we have that

$$\tau = \frac{l\sin S - y}{V_e \sin S - V_p} \tag{6.79}$$

Equating Eq. (6.78) and Eq. (6.79), we obtain

$$-V_p l \sin S + x V_p = -V_e y \sin S + V_e x \cos S \tag{6.80}$$

Substituting $x = r \sin\phi$ and $y = r \cos\phi$ in the equation above, and applying some trigonometric identities, we have that

$$r_B = \frac{V_p l \sin S}{V_p \sin\phi - V_e \sin(\phi - S)} \tag{6.81}$$

6.7.4 Algorithm description

In Algorithm 1, we describe a procedure to determine the region of the state space partition, in the first quadrant, where the evader's relative position is located. This algorithm is based on the equations developed above. This method can be used in an analogous way in the remaining quadrants of the reduced space.

Data: relative position of the evader (x_e, y_e)
Data: capture distance l
Data: distance r_{III} to the critical curve bounding region III
Data: orientation ϕ_{III} bounding the transition surface
Data: distance r_B to the barrier
Result: region of the partition
Compute polar coordinate representation (r_e, ϕ_e) of the relative position of the evader;
if $r_e > r_{III}$ **then**
  return evader is in region III;
end
if $\phi \in [0, \phi_{TS})$ *and left expression in Eq. 6.75* > 0 **then**
  return evader is in region II;
end
if $\phi \in [\phi_{TS}, cos^{-1}(\frac{V_e}{V_p})]$ *and* $r_e > r_B$ **then**
  return evader is in region II;
end
if $\phi \in (cos^{-1}(\frac{V_e}{V_p}), \frac{\pi}{2}]$ *and* $r_e > l$ **then**
  return evader is in region II;
end
if $r_e > l$ **then**
  return evader is in region I;
end

Algorithm 1: Find the region of the state space partition in the first quadrant where the evader's relative position is located.

6.8 Simulations

In this section, we present some simulation results of our pursuit-evasion game. We use m/sec as units for velocities, meters for distance and seconds for time. First we show the case described in Lemma 6.17, when the barriers intersect and define regions in the reduced space where the evader can indefinitely escape or is captured in finite time (refer to Fig. 6.11). The capture condition is only possible for the configurations inside the closed region defined by the barriers (shown in magenta) and the usable part (bold arc in black). Those configurations are the only ones that can reach the terminal surface; the barriers prevent the remaining configurations from reaching this surface. The circle in Fig. 6.10 represents the terminal surface and the bold arcs correspond to the usable part. The system trajectories inside the closed region end in the y-axis and consist of straight lines in the reduced space (refer to Fig. 6.5), which corresponds to a straight line motion of the DDR and the evader in the realistic space. The parameters of this simulation were $V_p^{\max} = 1$, $V_e^{\max} = 0.787$, $b = 1$ and $l = 1$. Figure 6.10 shows the barrier in the reduced space.

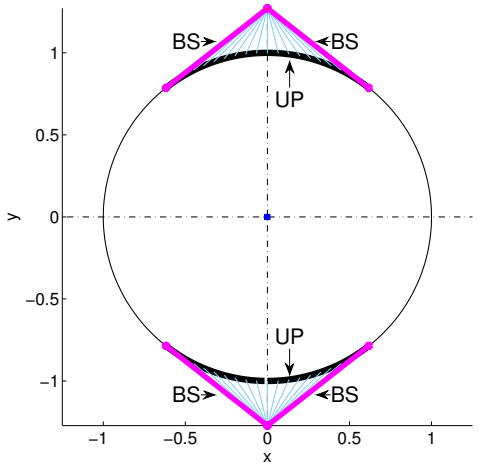

FIGURE 6.10: The barriers intersect creating two regions type I. In the remaining space the DDR cannot attain capture of the evader.

In Fig. 6.11, we also present a trajectory followed by the system in the reduced space when the evader avoids capture. In this case, we assumed that the evader's position is directly aligned with the pursuer's heading, i.e., the evader is in front of the pursuer. The system first moves over the y-axis following the trajectory (T1). When the system hits the barrier it starts following this trajectory (T2) reaching tangentially the terminal surface. Note that the distance between both players equals l over the target set, however, the pursuer will not be able to get closer from the evader than this value and

capture cannot be attained (since in the reduced space, the system is pointing tangentially to the terminal surface). Over the target set, the system will start moving toward the y-axis following the arc trajectory (T3) where the pursuer is aligning is heading with the evader's position. Note that the complete trajectory of the system *is cyclic and the process can be repeated again implying that the evader can always avoid capture.*

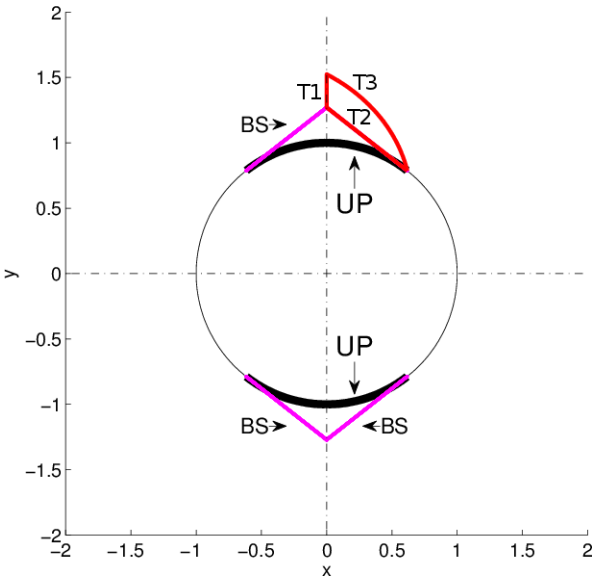

FIGURE 6.11: A trajectory followed by the system in the reduced space when the evader avoids capture.

Figure 6.12 shows the trajectories followed by both players in the realistic space for the case described above. The pursuer's initial position is denoted by P_I and the evader's initial position by E_I. The arrows show the motion direction of the players. The pursuer starts moving directly towards the evader which moves away following a straight line. After a time interval, which corresponds to reaching the barrier in the reduced space, the evader at E_S switches its motion direction but the pursuer at P_S continues moving in the same direction. The circle represents the time instant when the distance between both players, at P_F and E_F, equals l. Note that at this point no matter what the pursuer does (e.g., continue moving in straight line, rotating in place, etc.) the distance between both players increases. If the pursuer starts rotating in place at P_F, which is the optimal strategy, the whole process is repeated, implying that the evader can always avoid capture.

For the rest of the simulations, the parameters were $V_p^{\max} = 1$, $V_e^{\max} = 0.5$, $b = 1$ and $l = 1$. In Fig. 6.13, we show the case when two system trajectories start at the same point over the x-axis (DS), at this point the evader has a relative orientation of $\frac{\pi}{2}$ with respect to the pursuer's heading. The DDR has two possible optimal controls to capture the evader: rotate clockwise or counterclockwise, both leading to the same

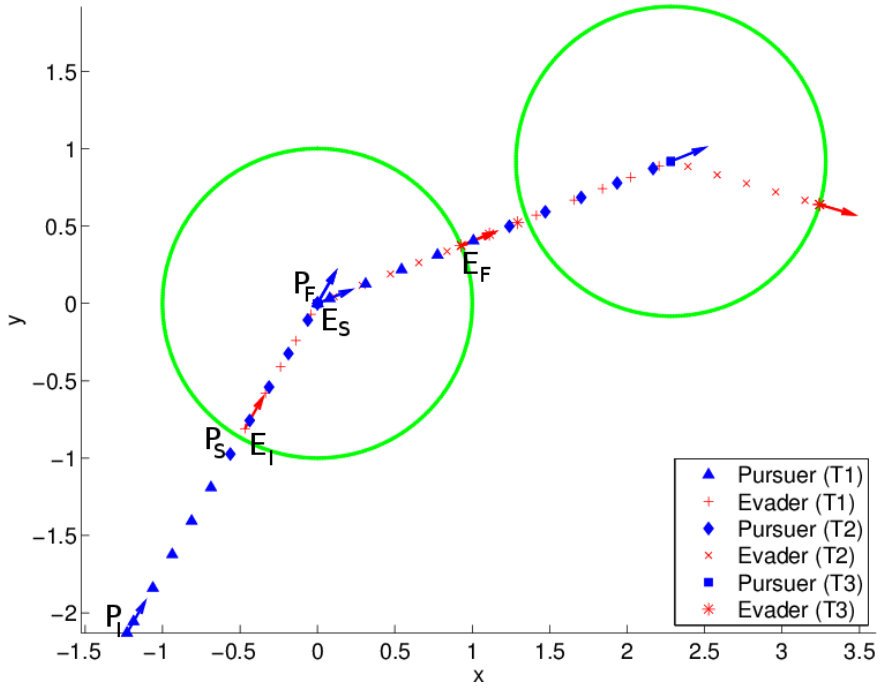

FIGURE 6.12: The trajectories followed by both players in the realistic space when the evader avoids capture. We show the corresponding trajectories in the realistic space when the system is following the trajectories T1, T2 and T3 in the reduced space representation. The arrows show the motion direction of the players. The blue triangles (pursuer) and red plus signs (evader) correspond to T1. The blue diamonds (pursuer) and red crosses (evader) correspond to T2. Finally, the blue squares (pursuer) and red asterisks (evader) correspond to T3.

optimal time-to-go. If the DDR rotates clockwise the trajectory ends in the upper UP and if it rotates counterclockwise the trajectory ends in the bottom UP. Note that these trajectories pass over regions II and I in order to reach the UP.

Figure 6.14 shows in the realistic space the trajectories of the evader and the pursuer. These trajectories correspond in the reduced space to the trajectory ending at the upper UP (shown in Fig. 6.13). In Fig. 6.14, P_I and E_I are the initial positions of the pursuer and the evader, and P_F and E_F the positions where capture is attained.

In Fig. 6.15, we present another system trajectory starting over the x-axis in the reduced space. The system follows a tributary path in region III until reaches the US. Then it moves over the US towards the point y_c. Once at y_c, it follows a trajectory in region I. In Fig. 6.16, we show the representation in the realistic space. The pursuer aligns its heading to the motion direction of the evader and then it moves directly towards the evader.

In Fig. 6.17, we present trajectories in the realistic space, when the evader is not following its optimal strategy. P_I and E_I are the initial positions of the pursuer and the evader in the realistic space. In this case, both players initially follow their optimal

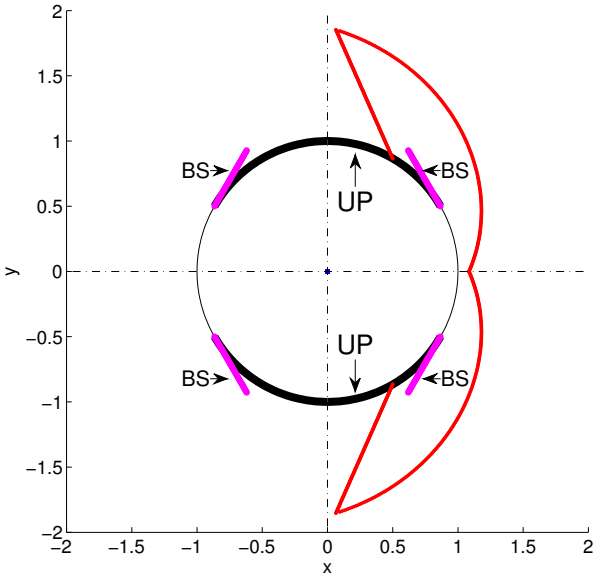

FIGURE 6.13: System trajectories in the reduced space. One ending in the upper UP and the other in the bottom UP. This trajectories pass over regions II and I in order to reach the UP.

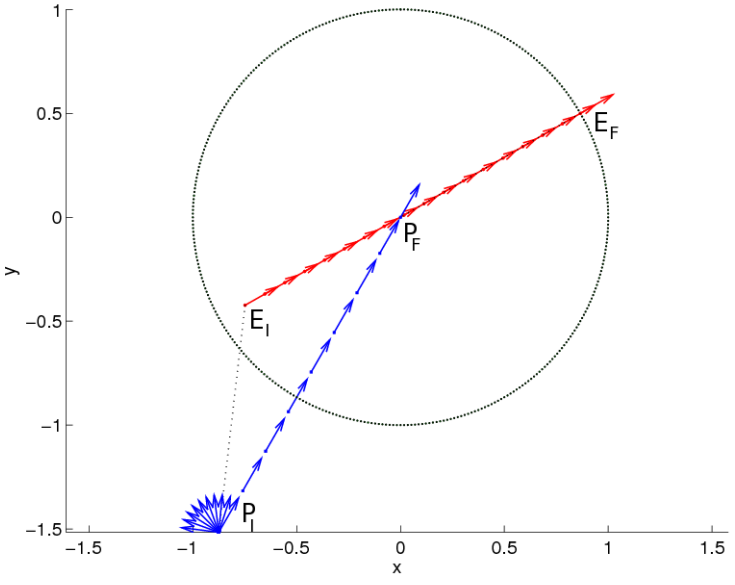

FIGURE 6.14: The DDR captures the evader with a rotation in-place and a forward motion in the realistic space.

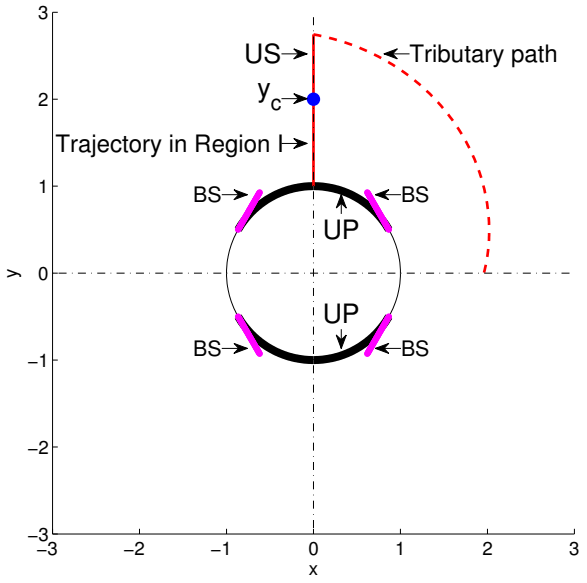

FIGURE 6.15: Trajectory in the reduced space following the US. The trajectory pass over region III, the US and region I in order to reach the UP.

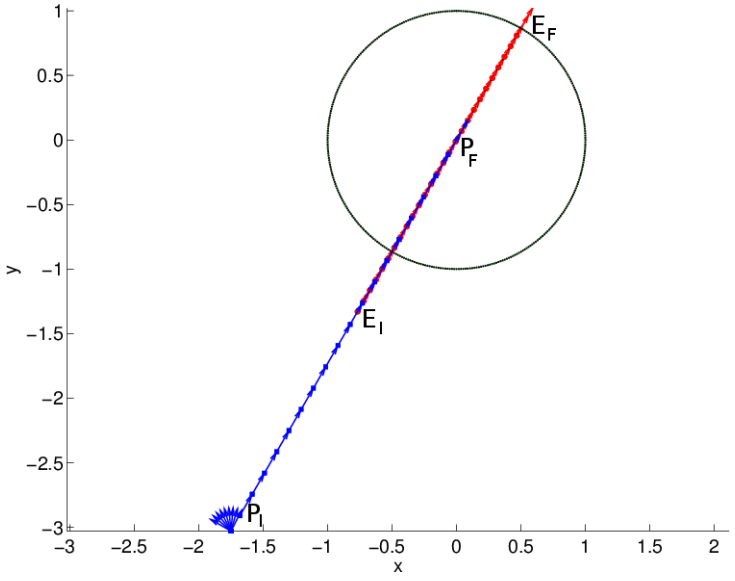

FIGURE 6.16: The DDR captures the evader with a forward motion in the realistic space.

strategies, a rotation in place for the DDR and a straight line for the evader, which corresponds to the arc starting at the x-axis in the reduced space. After a time interval, the DDR switches controls and it starts moving following a straight line in the realistic space. The evader at E_S, stops moving in the optimal direction and it starts moving perpendicular to the motion direction of the pursuer. The capture occurs when the DDR is at P_F and the evader is at E_F. The time-optimal trajectories for the same configuration and assuming the same maximal velocities of the players correspond to the ones in Fig. 6.13 (the one ending in the upper UP) for the reduced space and Fig. 6.14 for the realistic space. The DDR requires a $t = 3.71sec.$ for capturing the evader when both players are following its time-optimal strategies while it requires $t = 2.91sec.$ when the evader is following the strategy described above. The evader is captured in less time when it is not following its optimal strategy.

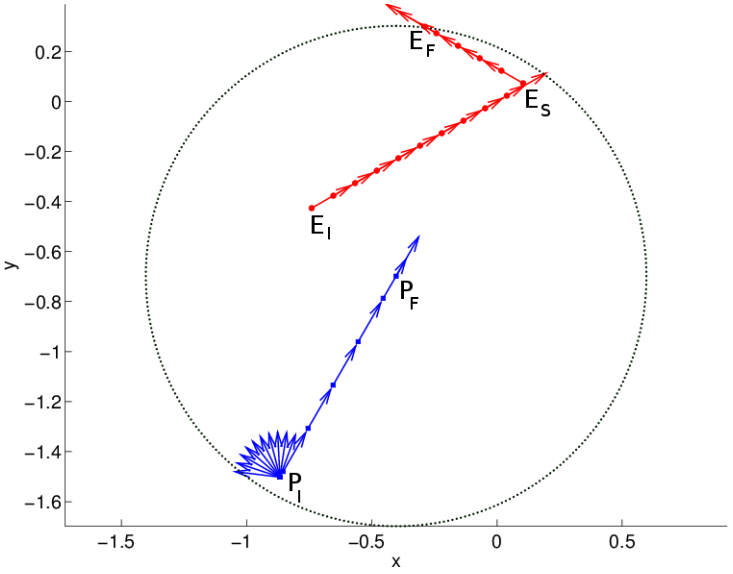

FIGURE 6.17: The DDR captures the evader which is not following its optimal strategy. After a time interval, the evader changes its motion direction and it starts moving perpendicular to the DDR.

6.9 Comparison between our problem's solution and the Homicidal Chauffeur problem solution

This section has as its goal to present three main differences between our contributions and the solution presented in [20] and [21] for the Homicidal Chauffeur problem.

(1) In contrast to the solution proposed for the Homicidal Chauffeur problem, for our problem, we propose a graph representation of the reduced state space partition which exhibits properties that guarantee global optimality (refer to Subsection 6.6.2).

(2) We present a concrete example of a trajectory followed by the evader when it wins, i.e., it avoids capture indefinitely (refer to Section 6.8).

(3) We show that the model for a simple car cannot be used to represent a DDR. In particular, we show that when the distance between the front and rear axles of the car tends to zero and the car steering angle tends to $\frac{\pi}{2}$, both implying that the turning radius tends to zero, then the car-like model approaches to an omnidirectional system and not a DDR.

Consider the kinematic model for a simple car in [92] shown in Fig. 6.18.

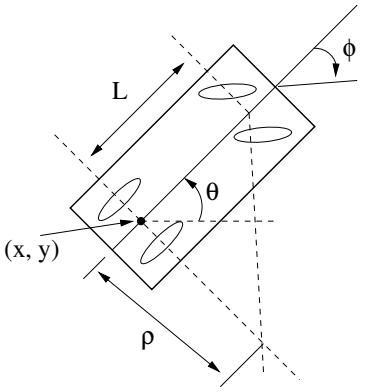

FIGURE 6.18: Model for a car-like.

(x, y, θ) is the configuration of the system, with the origin at the center of rear axle, and the x-axis pointing along the main axis of the car. Let v denote the translation velocity of the car, and ϕ denote the steering angle. Recall, that the distance between the front and rear axles is represented as L. If the steering angle is fixed at ϕ, the car travels in a circular motion, in which the radius of the circle is $\rho = L/\tan\phi$. Suppose that the translational velocity v and the steering angle ϕ are directly specified. The transition equation for a simple car is

$$\begin{aligned} \dot{x} &= v\cos\theta \\ \dot{y} &= v\sin\theta \\ \dot{\theta} &= \frac{v}{L}\tan\phi \end{aligned} \tag{6.82}$$

where $v \in [-v^{\max}, v^{\max}]$ and $\phi \in [-\pi/2, \pi/2]$. The last expression can be rewritten as $\dot{\theta} = (v/\rho)u_n$, where $u_n \in [-1, 1]$. This small variation of the transition equation, considering also that $v \in [0, v^{\max}]$, was used in [20], [21] to model the motion of the car in the Homicidal Chauffeur Problem. Assuming $\dot{\theta} = \omega$, in Fig. 6.19 we can observe the set of admissible controls in the $v - \omega$ space. From $\dot{\theta} = (v/\rho)u_n$, we have that as $\rho \to 0$ then $\dot{\theta} \to \infty$. Therefore, we have that as the turning radius ρ approaches zero,

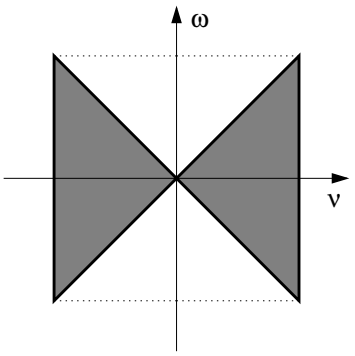

FIGURE 6.19: Control space for a car-like.

the simple car approaches an omnidirectional vehicle, which can instantaneously change its motion direction.

In contrast, the kinematic model for a DDR [90] is given by (see Fig. 6.20):

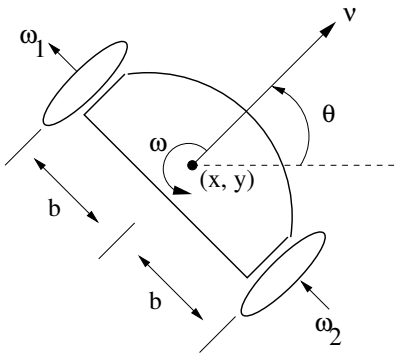

FIGURE 6.20: Model for a DDR.

$$\begin{aligned} \dot{x} &= v\cos\theta \\ \dot{y} &= v\sin\theta \\ \dot{\theta} &= \omega \end{aligned} \tag{6.83}$$

where v is the robot's translational velocity and ω its angular velocity . With a suitable choice of units, we have that

$$v = \frac{\omega_1 + \omega_2}{2}, \quad \omega = \frac{\omega_2 - \omega_1}{2b} \tag{6.84}$$

where ω_1 and ω_2 are the wheel angular velocities. b is the distance between the wheels. For a DDR, assuming $v^{\max} > 0$, we have that

$$|\dot{\theta}| = |\omega| \leq \frac{1}{b}(v^{\max} - |v|) \tag{6.85}$$

The angular velocity is inversely proportional to the translation velocity.

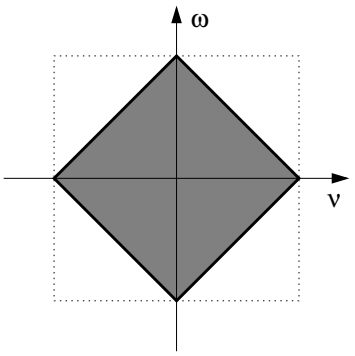

FIGURE 6.21: Control space for a DDR.

Comparing the spaces of admissible controls for both models (see Figs. 6.19 and 6.21) we can see that there are values for v and w that can be valid for one model but not for the other. This leads to different time-optimal motion primitives in nature. It is also important to note a fundamental assumption in the model for a simple car; its four wheels share the same rotational direction and speed, which is not the case for a DDR. Note that for the car-like robot it is possible to set *simultaneously* v and w at their maximal values (saturated values) while for the DDR is not possible to set at the same time v and w at their maximal values. Taking into consideration the arguments given above, we have that it is not possible to model a DDR using the model for a simple car, and therefore, it is also not possible to obtain the solution for a DDR pursuer from the solution for the Homicidal Chauffeur Problem.

6.10 Conclusions and Future Work

In this chapter, we considered the problem of capturing an omnidirectional evader using a nonholonomic robot in an obstacle free environment or, more precisely, the problem of getting closer from the evader than the capture distance l.

Differently to the classical Homicidal Chauffeur problem [20, 21], in which the pursuer is a car-like vehicle, in this work, the pursuer is a Differential Drive Robot (DDR), i.e. the pursuer can rotate in place. The change in the mechanical model of the pursuer has as a distinctive consequence that both the pursuer motion primitives and the motion strategies of the players also change w.r.t. the Homicidal Chauffeur solution. In this chapter, we made the following contributions:

- We presented closed-form representations of the motion primitives and time-optimal strategies for each player.

- In the realistic space, the motion primitives for the pursuer are straight lines and rotations in place and for the evader are straight lines.
- The strategies for the players that we have found are in Nash Equilibrium meaning that any unilateral deviation of each player from these strategies does not provide to such player benefit towards the goal of winning the game.
- We proposed a partition of the playing space into mutually disjoint regions where the strategies of the players are well established. The boundaries of these regions are called *singular surfaces* [20, 21, 40], and they indicate a change in one the player's strategies. The partition is represented as a graph which exhibits properties that guarantee global optimality.
- We also analysed the decision problem of the game and presented the conditions defining the winner of the game.

To the best of our knowledge, this is the first time that the problem of finding time-optimal trajectories for both players, in the game of capturing an omnidirectional evader with a DDR, has been solved. As future work we will include acceleration bounds in the solution of this problem.

Chapter 7

Conclusions and Future Work

In this thesis, we considered the surveillance problem of tracking an omnidirectional evader at constant distance using a DDR in the plane without obstacles. The players have maximum bounded speeds and the DDR is faster than the evader. We assumed that both players have full knowledge of their instantaneous positions and the instantaneous velocity of the evader. We constructed a partition of the configuration space that allows to know at the beginning of the game whether or not the DDR is able to maintain tracking at constant distance. We also found optimal motion strategies for both players, in the sense that they require the minimum capabilities of the players for winning. Some simulation results of this pursuit-evasion game were presented.

We proposed a generalization of the problem described above. We provided a criterion for partitioning the configuration space of the problem into 2 regions, so that in one of them the DDR is able to control the system, in the sense that, by applying a specific strategy (also provided), the DDR can achieve any feasible inter-agent distance, regardless of the actions taken by the other agent. Particular applications of these results include the capture of the OA by the DDR. Simulations that illustrates the trajectories of the system are also included.

Finally, we addressed the problem of capturing an omnidirectional evader with a DDR in minimal time. In this case, the players have only knowledge of their instantaneous positions. We obtained the motion primitives and time-optimal motion strategies for the players that are in Nash Equilibrium. We proposed a partition of the space where the strategies of the players are well established. Using this partition, we found feedback motion policies for the DDR. We also gave the conditions defining the winner of the game.

As future work, we want to extend our results for capturing an omnidirectional evader when one differential drive robot is not able to do it. In this case, we are interested in finding the minimal number of differential drive robots required to guarantee capture and their motion strategies.

Another interesting problem consist of using visual-servo techniques in the implementation of the time-optimal motion strategies found in this thesis. In this case, we assume that a camera is mounted on the robot. Instead of directly using the relative position of the evader, the camera is used to guide the robot. In this case, it is necessary to determine the region of the partition where the evader is located from the images taken by the camera. We want to find a mapping between the singular surfaces appearing in the game and critical events in the images. This information will be used to notify the robot the control it has to apply in order to capture the evader.

Finally, we also want to include acceleration bounds for both players in order to get a more general solution of the problem.

Appendix A

Tracking an Omnidirectional Evader with a Differential Drive Robot

A.1 Determination of u_3

From equation 3.10 we obtain the following two expressions for $\dot{\phi}(t)$

$$\dot{\phi} = \frac{\dot{x}_e - \dot{x}_p}{L \sin \phi} \tag{A.1}$$

$$\dot{\phi} = \frac{\dot{y}_p - \dot{y}_e}{L \cos \phi} \tag{A.2}$$

Substituting equations 3.4 in A.1 and 3.5 in A.2 we obtain

$$\dot{\phi} = \frac{\dot{x}_e - V_p \cos \theta}{L \sin \phi} \tag{A.3}$$

$$\dot{\phi} = \frac{V_p \sin \theta - \dot{y}_e}{L \cos \phi} \tag{A.4}$$

Equating equations A.3 and A.4 and solving for $u_3 = V_p$ we obtain:

$$u_3 = V_p = \frac{\dot{x}_e \cos \phi + \dot{y}_e \sin \phi}{\cos(\theta - \phi)} \tag{A.5}$$

Finally, substituting equations 3.1, 3.2 in A.5, we obtain

$$u_3 = \frac{V_e \cos(\psi - \phi)}{\cos(\theta - \phi)} \tag{A.6}$$

A.2 Determination of $\dot{\phi}$

If the coordinates of the pursuer are x_p, y_p, the following coordinate transformations relate the pursuer's Cartesian coordinates to its polar coordinates relative to the evader:

$$x_p - x_e = L\cos\phi \tag{A.7}$$

$$y_p - y_e = L\sin\phi \tag{A.8}$$

Using equations A.7 and A.8 we obtain an expression for $\tan\phi$, and we differentiate this to obtain an expression for $\dot{\phi}$.

$$\begin{aligned} \frac{d}{dt}\tan\phi &= \frac{d}{dt}\frac{y_p - y_e}{x_p - x_e} \\ \dot{\phi}\sec^2\phi &= \frac{1}{x_p - x_e}\dot{y}_p - \frac{1}{x_p - x_e}\dot{y}_e - \frac{(y_p - y_e)}{(x_p - x_e)^2}\dot{x}_p + \frac{(y_p - y_e)}{(x_p - x_e)^2}\dot{x}_e \end{aligned} \tag{A.9}$$

Making the substitution given by equation A.7 we obtain

$$\begin{aligned} \dot{\phi}\sec^2\phi &= \frac{1}{L\cos\phi}\left(\dot{y}_p - \dot{y}_e - \frac{y_p - y_e}{x_p - x_e}\dot{x}_p + \frac{y_p - y_e}{x_p - x_e}\dot{x}_e\right) \\ \dot{\phi}\sec^2\phi &= \frac{1}{L\cos\phi}\left(\dot{y}_p - \dot{y}_e - (\dot{x}_p - \dot{x}_e)\tan\phi\right) \\ \dot{\phi} &= \frac{1}{L}\left(\dot{y}_p - \dot{y}_e\right)\cos\phi - \frac{1}{L}\left(\dot{x}_p - \dot{x}_e\right)\sin\phi \end{aligned} \tag{A.10}$$

If we now define the pursuer velocity as $\dot{x}_p = V_p\cos\theta$ and $\dot{y}_p = V_p\sin\theta$ we obtain the first form for $\dot{\phi}$

$$\dot{\phi} = \frac{1}{L}V_p\sin(\theta - \phi) - \frac{1}{L}(\dot{y}_e\cos\phi - \dot{x}_e\sin\phi) \tag{A.11}$$

If we parametrize the evader velocity by magnitude and angle, $\dot{x}_e = V_e\cos\psi$ and $\dot{y}_e = V_e\sin\psi$, we obtain

$$\dot{\phi} = \frac{1}{L}V_p\sin(\theta - \phi) - \frac{1}{L}V_e\sin(\psi - \phi) \tag{A.12}$$

Since $u_1 = V_e$, $u_2 = \psi$ and $u_3 = V_p$ equation A.12 can also be expressed as follows:

$$\dot{\phi} = \frac{1}{L}[u_3\sin(\theta - \phi) - u_1\sin(u_2 - \phi)] \tag{A.13}$$

Equation A.13 indicates for every instant of time the rate of rotation of the rod to maintain a constant distance from the evader, and shows that the state variable $\dot{\phi}$ depends on both the evader and pursuer controls.

Now, we can express the state transition model of our system in its first form:

$$\begin{pmatrix} \dot{x}_e \\ \dot{y}_e \\ \dot{\phi} \\ \dot{\theta} \end{pmatrix} = \begin{pmatrix} u_1 \cos u_2 \\ u_1 \sin u_2 \\ \frac{1}{L}[u_3 \sin(\theta - \phi) - u_1 \sin(u_2 - \phi)] \\ u_4 \end{pmatrix} \tag{A.14}$$

Substituting equation A.6 in equation A.12 we can obtain a simplified form for $\dot{\phi}$:

$$\dot{\phi} = \frac{V_e \cos(\psi - \phi)}{L \cos(\theta - \phi)} \sin(\theta - \phi) - \frac{1}{L} V_e \sin(\psi - \phi) \tag{A.15}$$

Setting $v = \theta - \phi$ and $u = \psi - \phi$ we obtain

$$\dot{\phi} = \frac{V_e}{L} \left[\frac{\sin(v)\cos(u) - \cos(v)\sin(u)}{\cos(\theta - \phi)} \right] \tag{A.16}$$

and using the trigonometric identity: $\sin(u - v) = \sin(u)\cos(v) - \cos(u)\sin(v)$ and replacing the values of u and v, we obtain

$$\dot{\phi} = \frac{V_e \sin(\theta - \psi)}{L \cos(\theta - \phi)} \tag{A.17}$$

A.3 Proof of Lemma 3.2

Lemma 3.2. Consider the following functions:

$$\psi_1 = \arctan\left(\frac{\sin\phi - \gamma\cos\theta}{\cos\phi + \gamma\sin\theta}\right) \tag{A.18}$$

$$\psi_2 = \arctan\left(\frac{\sin\phi + \gamma\cos\theta}{\cos\phi - \gamma\sin\theta}\right) \tag{A.19}$$

$$\psi_3 = \arctan\left(\frac{-\sin\phi - \gamma\cos\theta}{-\cos\phi + \gamma\sin\theta}\right) \tag{A.20}$$

$$\psi_4 = \arctan\left(\frac{-\sin\phi + \gamma\cos\theta}{-\cos\phi - \gamma\sin\theta}\right) \tag{A.21}$$

The evader control u_2 that maximizes $g(\phi, \theta, u_2)$ for given values of ϕ and θ is given by

$$u_2 = \begin{cases} \psi_1 \text{ or } \psi_4 = \psi_1 + \pi : & (\theta - \phi) \in [0, \pi] \\ \psi_2 \text{ or } \psi_3 = \psi_2 + \pi : & (\theta - \phi) \in [\pi, 2\pi] \end{cases} \tag{A.22}$$

Proof. Recall that

$$g(\phi, \theta, \psi) = |\cos(\phi - \psi)| + \gamma |\sin(\theta - \psi)| \tag{A.23}$$

	A_i	B_i
$i=1$	$\sin\phi - \gamma\cos\theta$	$\cos\phi + \gamma\sin\theta$
$i=2$	$\sin\phi + \gamma\cos\theta$	$\cos\phi - \gamma\sin\theta$
$i=3$	$-\sin\phi - \gamma\cos\theta$	$-\cos\phi + \gamma\sin\theta$
$i=4$	$-\sin\phi + \gamma\cos\theta$	$-\cos\phi - \gamma\sin\theta$

TABLE A.1: Coefficients A_i and B_i for $g_i(\phi,\theta,\psi)$

in which $0 < \gamma \leq 1$. Since $\max\{|a|+|b|\} = \max\{a+b, a-b, -a+b, -a-b\}$ we have

$$\max_{\psi} g(\phi,\theta,\psi) = \max_{\psi}\{g_1(\phi,\theta,\psi), g_2(\phi,\theta,\psi), g_3(\phi,\theta,\psi), g_4(\phi,\theta,\psi)\} \tag{A.24}$$

in which

$$g_1(\phi,\theta,\psi) = \cos(\phi-\psi) + \gamma\sin(\theta-\psi) \tag{A.25}$$
$$g_2(\phi,\theta,\psi) = \cos(\phi-\psi) - \gamma\sin(\theta-\psi) \tag{A.26}$$
$$g_3(\phi,\theta,\psi) = -\cos(\phi-\psi) + \gamma\sin(\theta-\psi) \tag{A.27}$$
$$g_4(\phi,\theta,\psi) = -\cos(\phi-\psi) - \gamma\sin(\theta-\psi) \tag{A.28}$$

Thus, we proceed by finding the maximizers for each of the g_i. For the case of g_1, using basic trigonometric identities we obtain the following

$$g_1 = \cos(\phi-\psi) + \gamma\sin(\theta-\psi) \tag{A.29}$$
$$= \cos\phi\cos\psi + \sin\phi\sin\psi + \gamma(\sin\theta\cos\psi - \cos\theta\sin\psi) \tag{A.30}$$
$$= \cos\psi(\cos\phi + \gamma\sin\theta) + \sin\psi(\sin\phi - \gamma\cos\theta) \tag{A.31}$$
$$= A_1\sin\psi + B_1\cos\psi \tag{A.32}$$

in which A_1 and B_1 do not depend on ψ and are given by

$$A_1 = \sin\phi - \gamma\cos\theta, \qquad B_1 = \cos\phi + \gamma\sin\theta \tag{A.33}$$

Repeating this process for each of g_2, g_3 and g_4, we obtain the general form

$$g_i = A_i\sin\psi + B_i\cos\psi \tag{A.34}$$

with A_i and B_i given in Table A.1.

This expression for g_i can be rewritten as a sinusoid (see, e.g., [94])

$$g_i(\phi, \theta, \psi) = A_i \sin\psi + B_i \cos\psi = \sqrt{{A_i}^2 + {B_i}^2} \sin\left(\psi + \tan^{-1}\left(\frac{B_i}{A_i}\right)\right) \tag{A.35}$$

Since neither A_i nor B_i depend on ψ, the maximizer satisfies

$$\psi + \tan^{-1}\left(\frac{B_i}{A_i}\right) = \frac{\pi}{2} \tag{A.36}$$

and using the identity $\tan^{-1}(B_i/A_i) = \pi/2 - \tan^{-1}(A_i/B_i)$ we obtain

$$\psi = \tan^{-1}\frac{A_i}{B_i} \tag{A.37}$$

This immediately yields the four values of ψ_i given in the Lemma. To ensure that these values yield a maximum, we examine the second partial derivative of g_i with respect to ψ, which is given by

$$\frac{\partial^2 g_i}{\partial {\psi_i}^2} = -A_i \sin\psi_i \dot{\psi}_i^2 - B_i \cos\psi_i \dot{\psi}_i^2 \tag{A.38}$$

$$\frac{\partial^2 g_i}{\partial {\psi_i}^2} = (-A_i \sin\psi_i - B_i \cos\psi_i)\dot{\psi}_i^2 \tag{A.39}$$

$$\frac{\partial^2 g_i}{\partial {\psi_i}^2} = -(A_i \sin\psi_i + B_i \cos\psi_i)\dot{\psi}_i^2 \tag{A.40}$$

$$\frac{\partial^2 g_i}{\partial {\psi_i}^2} = -g_i \dot{\psi}_i^2 \tag{A.41}$$

Since a maximum of g_i satisfies $\frac{\partial^2 g_i}{\partial {\psi_i}^2} > 0$, equation A.41 implies that $g_i > 0$ must hold. We will show this below.

We note here that a simple relationship holds between ψ_1 and ψ_4, and between ψ_2 and ψ_3. In particular, since

$$\psi_1 = \arctan\left(\frac{A_1}{B_1}\right) \tag{A.42}$$

and

$$\psi_4 = \arctan\left(\frac{-A_1}{-B_1}\right) \tag{A.43}$$

we have $\psi_4 = \psi_1 + \pi$. Likewise, $\psi_3 = \psi_2 + \pi$.

Now, we proceed to evaluate each ψ_i in the corresponding g_i. We will show that if $(\theta - \phi) \in [0, \pi]$ then g is maximized by ψ_1 and ψ_4, and if $(\theta - \phi) \in [\pi, 2\pi]$ then g is maximized by ψ_2 and ψ_3. We begin with the case of g_4.

$$g_4 = \sqrt{{A_4}^2 + {B_4}^2} \sin\left(\psi + \arctan\left(\frac{B_4}{A_4}\right)\right) \tag{A.44}$$

Plugging ψ_4 in g_4, that is $g_4(\psi_4)$, we obtain

$$g_4(\psi_4) = \sqrt{{A_4}^2 + {B_4}^2} \sin\left(\arctan\left(\frac{A_4}{B_4}\right) + \arctan\left(\frac{B_4}{A_4}\right)\right) \tag{A.45}$$

Note that ψ_4 maximizes g_4 at all times, so that the argument of the sine

$$\arctan\left(\frac{A_4}{B_4}\right) + \arctan\left(\frac{B_4}{A_4}\right) = \frac{\pi}{2}. \tag{A.46}$$

since this maximizes the sine, that is:

$$\sin\left(\arctan(\frac{A_4}{B_4}) + \arctan(\frac{B_4}{A_4})\right) = 1 \tag{A.47}$$

Thus

$$g_4(\psi_4) = \sqrt{{A_4}^2 + {B_4}^2} \tag{A.48}$$

Evaluating A_4 and B_4 inside the square root:

$$\begin{aligned} g_4(\psi_4) &= \sqrt{(-\sin\phi + \gamma\cos\theta)^2 + (-\cos\phi - \gamma\sin\theta)^2} \\ &= \sqrt{1 + \gamma^2 + 2\gamma\sin(\theta - \phi)} \end{aligned} \tag{A.49}$$

For g_3 starting from

$$g_3 = \sqrt{{A_3}^2 + {B_3}^2} \sin\left(\psi + \arctan\left(\frac{B_3}{A_3}\right)\right) \tag{A.50}$$

and following a similar procedure that with g_4, we get:

$$g_3(\psi_3) = \sqrt{1 + \gamma^2 - 2\gamma\sin(\theta - \phi)} \tag{A.51}$$

Likewise for g_2 and g_1

$$g_2(\psi_2) = \sqrt{1 + \gamma^2 - 2\gamma\sin(\theta - \phi)} \tag{A.52}$$

$$g_1(\psi_1) = \sqrt{1 + \gamma^2 + 2\gamma\sin(\theta - \phi)} \tag{A.53}$$

To summarizes the forms of g_i evaluated over the respective ψ_i are given by:

$$g_1(\psi_1) = \sqrt{1 + \gamma^2 + 2\gamma\sin(\theta - \phi)} \tag{A.54}$$

$$g_2(\psi_2) = \sqrt{1 + \gamma^2 - 2\gamma\sin(\theta - \phi)} \tag{A.55}$$

$$g_3(\psi_3) = \sqrt{1 + \gamma^2 - 2\gamma\sin(\theta - \phi)} \tag{A.56}$$

$$g_4(\psi_4) = \sqrt{1 + \gamma^2 + 2\gamma\sin(\theta - \phi)} \tag{A.57}$$

If $(\theta - \phi) \in [0, \pi]$ then ψ_1 and ψ_4 maximize g since the $\sin(\theta - \phi) \geq 0$. Likewise, if $(\theta - \phi) \in [\pi, 2\pi]$ then ψ_2 and ψ_3 maximize g since the $\sin(\theta - \phi) \leq 0$.

In the domain $(\theta - \phi) \in [0, \pi]$, g_4 and g_1 are positive (different of zero), since the argument on the square root of equation A.49, that is $1 + \gamma^2 + 2\gamma \sin(\theta - \phi) > 0$.

In the domain $(\theta - \phi) \in [\pi, 2\pi]$, g_3 and g_2 are positive (different of zero), since the argument on the square root of equation A.51, that is $1 + \gamma^2 - 2\gamma \sin(\theta - \phi) > 0$.

□

A.4 Proof of Lemma 3.3

Lemma 3.3. Define the following functions:

$$K(\theta, \phi) = \begin{cases} \psi_4(\theta, \phi), \text{If } (\theta - \phi) \in [0, \pi] \\ \psi_3(\theta, \phi), \text{If } (\theta - \phi) \in [\pi, 2\pi] \end{cases} \tag{A.58}$$

$$u_3^{**}(\theta, \phi) = u_3^{*}(V_p^{max}, K(\theta, \phi), \theta, \phi) \tag{A.59}$$

$$u_4^{**}(\theta, \phi) = s(\theta, \phi) \max |\dot{\theta}| = s(\theta, \phi) \frac{1}{b} (V_p^{max} - |u_3^{**}(\theta, \phi)|) \tag{A.60}$$

with $s(\theta, \phi)$ given by equation 3.30.

If $(\theta - \phi) \in (0, \frac{\pi}{2}) \bigcup (\pi, \frac{3\pi}{2})$ then $g(\phi, \theta, K)$ and $|\dot{\phi}(V_p^{max}, K, \theta, \phi)|$ increase monotonically (w.r.t $(\theta - \phi)$), and $|u_4^{**}(\theta, \phi)| = \max |\dot{\theta}|$ decreases monotonically (w.r.t $(\theta - \phi)$).

Symmetrically, if $(\theta - \phi) \in (\frac{\pi}{2}, \pi) \bigcup (\frac{3\pi}{2}, 2\pi)$then $g(\phi, \theta, K)$ and $|\dot{\phi}(V_p^{max}, K, \theta, \phi)|$ decrease monotonically (w.r.t $(\theta - \phi)$), and $|u_4^{**}(\theta, \phi)| = \max |\dot{\theta}|$ increases monotonically (w.r.t $(\theta - \phi)$).

Proof. This lemma is proved by cases. Since the cases are analogous, we only present in detail the case of ψ_4, and we provide a sketch of the proofs for the other cases. Table 3.1 summarizes the direction of rotation (counterclockwise +1 or clockwise -1) for $\dot{\phi}(V_p^{max}, K, \theta, \phi)$

In all cases, as a first step, we show that $|u_4^{**}(u_3^{**})|$ monotonically increases and that $|\dot{\phi}(V_e^{max}, K, \theta, \phi)|$ monotonically decreases, if $(\theta - \phi) \in (\frac{\pi}{2}, \pi) \bigcup (\frac{3\pi}{2}, 2\pi)$. Symmetrically, $|u_4^{**}(u_3^{**})|$ monotonically decreases and $|\dot{\phi}(V_p^{max}, K, \theta, \phi)|$ monotonically increases, if $(\theta - \phi) \in (0, \frac{\pi}{2}) \bigcup (\pi, \frac{3\pi}{2})$. In a second step, we show that if $(\theta - \phi) \in (0, \frac{\pi}{2}) \bigcup (\pi, \frac{3\pi}{2})$ then $g(\phi, \theta, K)$ monotonically increases.

Analysis for ψ_4:

For ψ_4 there are two cases, which we refer to here as **Case A** and **Case B** for convenience. We now proceed individually with each of these.

Case A: $(\theta - \phi) \in I$ quadrant

Analyzing $\dot{\phi}(V_e^{max}, \psi_4, \theta, \phi)$
First, we obtain the variations of $(\theta - \psi_4)$.

$$\psi_4 = \arctan\left(\frac{-\sin\phi + \gamma\cos\theta}{-\cos\phi - \gamma\sin\theta}\right) \tag{A.61}$$

Subtracting ψ_4 from θ in both sides of the equation.

$$\theta - \psi_4 = \theta - \arctan\left(\frac{-\sin\phi + \gamma\cos\theta}{-\cos\phi - \gamma\sin\theta}\right) \tag{A.62}$$

Expressing θ as $\arctan\left(\frac{\sin\theta}{\cos\theta}\right)$

$$\theta - \psi_4 = \arctan\left(\frac{\sin\theta}{\cos\theta}\right) - \arctan\left(\frac{-\sin\phi + \gamma\cos\theta}{-\cos\phi - \gamma\sin\theta}\right) \tag{A.63}$$

Computing the tangent in both sides of the equation.

$$\tan(\theta - \psi_4) = \tan\left(\arctan\left(\frac{\sin\theta}{\cos\theta}\right) - \arctan\left(\frac{-\sin\phi + \gamma\cos\theta}{-\cos\phi - \gamma\sin\theta}\right)\right) \tag{A.64}$$

Using an equivalence of $\tan(u - v)$

$$\tan(\theta - \psi_4) = \frac{\tan\left(\arctan\left(\frac{\sin\theta}{\cos\theta}\right)\right) - \tan\left(\arctan\left(\frac{-\sin\phi+\gamma\cos\theta}{-\cos\phi-\gamma\sin\theta}\right)\right)}{1 + \tan\left(\arctan\left(\frac{\sin\theta}{\cos\theta}\right)\right)\tan\left(\arctan\left(\frac{-\sin\phi+\gamma\cos\theta}{-\cos\phi-\gamma\sin\theta}\right)\right)} \tag{A.65}$$

This can be further simplified as

$$\begin{aligned}
\tan(\theta - \psi_4) &= \frac{\left(\frac{\sin\theta}{\cos\theta}\right) - \left(\frac{-\sin\phi+\gamma\cos\theta}{-\cos\phi-\gamma\sin\theta}\right)}{1 + \left(\frac{\sin\theta}{\cos\theta}\right)\left(\frac{-\sin\phi+\gamma\cos\theta}{-\cos\phi-\gamma\sin\theta}\right)} && \text{(A.66)}\\
&= \frac{-(\sin\theta\cos\phi - \cos\theta\sin\phi + \gamma)}{-(\sin\theta\sin\phi + \cos\theta\cos\phi)} && \text{(A.67)}\\
&= \frac{-\sin(\theta - \phi) - \gamma}{-\cos(\theta - \phi)} && \text{(A.68)}
\end{aligned}$$

Now we obtain the extremal values of $(\theta - \psi_4)$ for $(\theta - \phi) \in I$ quadrant. If $(\theta - \phi) \in I$ quadrant then the extremal values of $(\theta - \psi_4)$ can be computed as follows:

$$(\theta - \psi_4) = \arctan\left(\frac{-\sin(\theta - \phi) - \gamma}{-\cos(\theta - \phi)}\right) \tag{A.69}$$

Note that the admissible values of the ratio γ satisfy $\gamma \in (0, 1]$. If $(\theta - \phi) = 0$ then $-\sin(\theta - \phi) - \gamma \in [-1, 0)$ and $-\cos(\theta - \phi) = -1$. If $(\theta - \phi) = \frac{\pi}{2}$ then $-\sin(\theta - \phi) - \gamma \in [-2, -1]$ and $-\cos(\theta - \phi) = 0$.

If $(\theta - \phi) = 0$ then according to the value of the ratio γ, the possibles values of $(\theta - \psi_4)$ are within the extremal values:

$$(\theta - \psi_4) = \arctan\left(\frac{0}{-1}\right) \to \pi \tag{A.70}$$

$$(\theta - \psi_4) = \arctan\left(\frac{-1}{-1}\right) = \frac{5\pi}{4} \tag{A.71}$$

If $(\theta - \phi) = \frac{\pi}{2}$ then regardless of the value of the ratio γ, the value of $(\theta - \psi_4)$ is:

$$(\theta - \psi_4) = \arctan\left(\frac{-1}{0}\right) = \frac{3\pi}{2} \tag{A.72}$$

$$(\theta - \psi_4) = \arctan\left(\frac{-2}{0}\right) = \frac{3\pi}{2} \tag{A.73}$$

Thus, if $(\theta - \phi) \in [0, \frac{\pi}{2}]$ then the extremal values of $(\theta - \psi_4) \in (\pi, \frac{3\pi}{2}]$. Note that the admissible values for the ratio $\gamma \in (0, 1]$ can produce a bigger interval, but always within the interval $(\pi, \frac{3\pi}{2}]$, as the ratio γ becomes smaller, the lower limit of the interval approaches π.

It is important to stress that if $(\theta - \phi)$ increases $(\theta - \psi_4)$ also increases and vice-versa, they have the same sense of variation.

Now we show that $|\dot{\phi}(V_e^{max}, \psi_4, \theta, \phi)|$ monotonically increases or decreases. Recall that

$$\dot{\phi}(V_e^{max}, \psi_4, \theta, \phi) = \frac{V_e^{max} \sin(\theta - \psi_4)}{L \cos(\theta - \phi)} \tag{A.74}$$

If $(\theta - \phi) \in I$ quadrant varying from 0 to $\frac{\pi}{2}$ then $(\theta - \psi_4)$ increases within the interval $(\pi, \frac{3\pi}{2}]$, therefore

- $\cos(\theta - \phi) \geq 0$, and its value is decreasing monotonically
- $\sin(\theta - \psi_4) < 0$, and its value is decreasing monotonically
- $|\sin(\theta - \psi_4)| > 0$, and its value is increasing monotonically

Hence, $|\dot{\phi}(V_e^{max}, \psi_4, \theta, \phi)|$ monotonically increases. However, notice that $\dot{\phi}(V_e^{max}, \psi_4, \theta, \phi)$ *is negative*, meaning that it produces a rod clockwise rotation. Symmetrically, if $(\theta - \phi) \in$

I quadrant varying from $\frac{\pi}{2}$ to 0 then $(\theta-\psi_4)$ decreases. Hence, $|\dot{\phi}(V_e^{max},\psi_4,\theta,\phi)|$ monotonically decreases.

Analyzing $u_3^{**}(V_e^{max},\psi_4,\theta,\phi)$ and $|u_4^{**}(|u_3^{**}|)|$

Using a procedure similar to what has been performed above, we obtain

$$(\psi_4-\phi)=\arctan\left(\frac{\gamma\cos(\theta-\phi)}{-1-\gamma\sin(\theta-\phi)}\right) \tag{A.75}$$

Recalling again that $\gamma\in(0,1]$, if $(\theta-\phi)=0$ then $\gamma\cos(\theta-\phi)\in(0,1]$ and $(-1-\gamma\sin(\theta-\phi))=-1$. If $(\theta-\phi)=\frac{\pi}{2}$ then $\gamma\cos(\theta-\phi)=0$ and $(-1-\gamma\sin(\theta-\phi))\in[-2,-1)$.

If $(\theta-\phi)=0$ then according to the value of the ratio γ, the possibles values of $(\psi_4-\phi)$ are within the extremal values:

$$(\psi_4-\phi)=\arctan\left(\frac{1}{-1}\right)=\frac{3\pi}{4} \tag{A.76}$$

$$(\psi_4-\phi)=\arctan\left(\frac{0}{-1}\right)\to\pi \tag{A.77}$$

If $(\theta-\phi)=\frac{\pi}{2}$ then regardless of the value of the ratio γ, the value of $(\psi_4-\phi)$ is:

$$(\psi_4-\phi)=\arctan\left(\frac{0}{-2}\right)=\pi \tag{A.78}$$

$$(\psi_4-\phi)=\arctan\left(\frac{0}{-1}\right)\to\pi \tag{A.79}$$

Thus, if $(\theta-\phi)\in[0,\frac{\pi}{2}]$ then the extremal values of $(\psi_4-\phi)\in[\frac{3\pi}{4},\pi]$. The admissible values for the ratio $\gamma\in(0,1]$ can produce a smaller interval, but always within the interval $[\frac{3\pi}{4},\pi]$, as the ratio γ becomes smaller, the lower limit of the interval approaches π. If $(\theta-\phi)$ increases $(\psi_4-\phi)$ also increases and vice-versa, they have the same sense of variation.

Now we show that $|u_4^{**}(|u_3^{**}(V_e^{max},\psi_4,\theta,\phi)|)|$ monotonically increases or decreases. The term $|u_4^{**}(|u_3^{**}|)|$ can be expressed as follows:

$$|u_4^{**}(|u_3^{**}|)|=\max|\dot{\theta}|=\frac{1}{b}\left(V_p^{max}-|u_3^{**}(V_e^{max},\psi_4,\theta,\phi)|\right) \tag{A.80}$$

We will obtain the variation of $|u_4^{**}|$ using $|u_3^{**}|$. Recall that:

$$u_3^{**}(V_e^{max},\psi_4,\theta,\phi)=\frac{V_e^{max}\cos(\psi_4-\phi)}{\cos(\theta-\phi)} \tag{A.81}$$

If $(\theta - \phi) \in I$ quadrant varying from 0 to $\frac{\pi}{2}$ then $(\psi_4 - \phi)$ increases within the interval $[\frac{3\pi}{4}, \pi]$. Therefore

- $\cos(\theta - \phi) \geq 0$, and its value is decreasing monotonically
- $\cos(\psi_4 - \phi) < 0$, and its value is decreasing monotonically
- $|\cos(\psi_4 - \phi)| > 0$, and its value is increasing monotonically

Hence, $|u_3^{**}(V_e^{max}, \psi_4, \theta, \phi)|$ monotonically increases and consequentially $|u_4^{**}(|u_3^{**}|)|$ monotonically decreases. Notice that, $u_3^{**}(V_e^{max}, \psi_4, \theta, \phi)$ *is negative*, meaning that it produces a pursuer backwards motion.

Symmetrically, if $(\theta - \phi) \in I$ quadrant varying from $\frac{\pi}{2}$ to 0 then $(\psi_4 - \phi)$ decreases. Hence, $|u_3^{**}(V_e^{max}, \psi_4, \theta, \phi)|$ monotonically decreases and $|u_4^{**}(|u_3^{**}|)|$ monotonically increases.

Finally, we show that, $g_4(\psi_4, \theta, \phi)$ monotonically increases or decreases. If $(\theta - \phi) \in I$ quadrant and $(\theta - \phi)$ varies from 0 to $\frac{\pi}{2}$ then $\sin(\theta - \phi) \geq 0$ in equation A.49 (Lemma II), and its value is monotonically increasing. Hence, the value of $g_4(\phi, \theta, \psi_4)$ is monotonically *increasing*. Symmetrically, if $(\theta - \phi)$ varies from $\frac{\pi}{2}$ to 0 then $\sin(\theta - \phi) \geq 0$ in the equation A.49 (Lemma II), and its value is monotonically decreasing. Therefore, the value of $g_4(\phi, \theta, \psi_4)$ is monotonically *decreasing*.

Case B: $(\theta - \phi) \in II$

Analyzing $\dot{\phi}(V_e^{max}, \psi_4, \theta, \phi)$

First, we obtain the extremal values of $(\theta - \psi_4)$ for $(\theta - \phi) \in II$ quadrant.

$$(\theta - \psi_4) = \arctan\left(\frac{-\sin(\theta - \phi) - \gamma}{-\cos(\theta - \phi)}\right) \tag{A.82}$$

If $(\theta - \phi) = \frac{\pi}{2}$ then $-\sin(\theta - \phi) - \gamma \in (-2, -1]$ and $-\cos(\theta - \phi) = 0$. If $(\theta - \phi) = \pi$ then $-\sin(\theta - \phi) - \gamma \in [-1, 0)$ and $-\cos(\theta - \phi) = 1$. If $(\theta - \phi) = \frac{\pi}{2}$ then regardless of the value of the ratio γ, the value of $(\theta - \psi_4)$ is:

$$(\theta - \psi_4) = \arctan\left(\frac{-1}{0}\right) = \frac{3\pi}{2} \tag{A.83}$$

$$(\theta - \psi_4) = \arctan\left(\frac{-2}{0}\right) \rightarrow \frac{3\pi}{2} \tag{A.84}$$

If $(\theta-\phi)=\pi$ then according to the value of the ratio γ, the possibles values of $(\theta-\psi_4)$ are within the extremal values:

$$(\theta-\psi_4)=\arctan\left(\frac{-1}{1}\right)=\frac{7\pi}{4} \tag{A.85}$$

and

$$(\theta-\psi_4)=\arctan\left(\frac{0}{1}\right)\rightarrow 2\pi \tag{A.86}$$

Thus, if $(\theta-\phi)\in[\frac{\pi}{2},\pi]$ then the extremal values of $(\theta-\psi_4)\in[\frac{3\pi}{2},2\pi)$. The admissible values for the ratio $\gamma\in(0,1]$ can produce a bigger interval, but always within the interval $[\frac{3\pi}{2},2\pi)$, as the ratio γ becomes smaller, the upper limit of the interval approaches 2π. If $(\theta-\phi)$ increases $(\theta-\psi_4)$ also increases and vice-versa, they have the same sense of variation.

Now we show that $|\dot{\phi}(V_e^{max},\psi_4,\theta,\phi)|$ monotonically increases or decreases. Recall that

$$\dot{\phi}(V_e^{max},\psi_4,\theta,\phi)=\frac{V_e^{max}\sin(\theta-\psi_4)}{L\cos(\theta-\phi)} \tag{A.87}$$

If $(\theta-\phi)\in II$ quadrant varying from $\frac{\pi}{2}$ to π then $(\theta-\psi_4)$ increases within the interval $[\frac{3\pi}{2},2\pi)$. Therefore

- $\cos(\theta-\phi)\leq 0$, and its value is decreasing monotonically
- $|\cos(\theta-\phi)|\geq 0$, and its value is increasing monotonically
- $\sin(\theta-\psi_4)<0$, and its value is increasing monotonically
- $|\sin(\theta-\psi_4)|>0$, and its value is decreasing monotonically

Hence, $|\dot{\phi}(V_e^{max},\psi_4,\theta,\phi)|$ monotonically decreases, and the value of $\dot{\phi}(V_e^{max},\psi_4,\theta,\phi)$ *is positive*, meaning that it produces a rod counterclockwise rotation.

Symmetrically, if $(\theta-\phi)\in II$ quadrant varying from π to $\frac{\pi}{2}$ then $(\theta-\psi_4)$ decreases. Hence, $|\dot{\phi}(V_e^{max},\psi_4,\theta,\phi)|$ monotonically increases.

Analyzing $u_3^{**}(V_e^{max},\psi_4,\theta,\phi)$ and $|u_4^{**}(|u_3^{**}|)|$

If $(\theta-\phi)\in II$ quadrant then the extremal values of $(\psi_4-\phi)$ can be computed as follows:

$$(\psi_4-\phi)=\arctan\left(\frac{\gamma\cos(\theta-\phi)}{-1-\gamma\sin(\theta-\phi)}\right) \tag{A.88}$$

Since the ratio $\gamma\in(0,1]$, if $(\theta-\phi)=\pi$ then $\gamma\cos(\theta-\phi)\in[-1,0)$ and $(-1-\gamma\sin(\theta-\phi))=-1$. If $(\theta-\phi)=\frac{\pi}{2}$ then $\gamma\cos(\theta-\phi)=0$ and $(-1-\gamma\sin(\theta-\phi))\in[-2,-1)$.

If $(\theta - \phi) = \pi$ then according to the value of the ratio γ, the possibles values of $(\psi_4 - \phi)$ are within the extremal values:

$$(\psi_4 - \phi) = \arctan\left(\frac{0}{-1}\right) \to \pi \tag{A.89}$$

and

$$(\psi_4 - \phi) = \arctan\left(\frac{-1}{-1}\right) = \frac{5\pi}{4} \tag{A.90}$$

If $(\theta - \phi) = \frac{\pi}{2}$ then regardless of the value of the ratio γ, the value of $(\psi_4 - \phi)$ is:

$$(\psi_4 - \phi) = \arctan\left(\frac{0}{-2}\right) = \pi \tag{A.91}$$

$$(\psi_4 - \phi) = \arctan\left(\frac{0}{-1}\right) = \pi \tag{A.92}$$

Thus, if $(\theta - \phi) \in [\frac{\pi}{2}, \pi]$ then the extremal values of $(\psi_4 - \phi) \in [\pi, \frac{5\pi}{4}]$. The admissible values of the ratio $\gamma \in (0, 1]$ can produce a smaller interval but always within the interval $[\pi, \frac{5\pi}{4}]$, as the ratio γ becomes smaller, the upper limit of the interval approaches π.

If $(\theta - \phi)$ increases $(\psi_4 - \phi)$ also increases and vice-versa, they have the same sense of variation.

Now we show that $|u_4^{**}(|u_3^{**}|)|$ monotonically increases or decreases by examining its variation in terms of the value of $|u_3^{**}(V_e^{max}, \psi_4, \theta, \phi)|$. The term $|u_4^{**}(|u_3^{**}|)|$ can be expressed as follows:

$$|u_4^{**}(u_3^{**})| = \max|\dot{\theta}| = \frac{1}{b}\left(V_p^{max} - |u_3^{**}(V_e^{max}, \psi_4, \theta, \phi)|\right) \tag{A.93}$$

Recall that:

$$u_3^{**}(V_e^{max}, \psi_4, \theta, \phi) = \frac{V_e^{max}\cos(\psi_4 - \phi)}{\cos(\theta - \phi)} \tag{A.94}$$

If $(\theta - \phi) \in II$ quadrant varying from $\frac{\pi}{2}$ to π then $(\psi_4 - \phi)$ increases within the interval $(\pi, \frac{5\pi}{4}]$. Therefore

- $\cos(\theta - \phi) \leq 0$, and its value is decreasing monotonically
- $|\cos(\theta - \phi)| \geq 0$, and its value is increasing monotonically
- $\cos(\psi_4 - \phi) < 0$, and its value is increasing monotonically
- $|\cos(\psi_4 - \phi)| > 0$, and its value is decreasing monotonically

Hence, $|u_3^{**}(V_e^{max}, \psi_4, \theta, \phi)|$ monotonically decreases and consequentially $|u_4^{**}(|u_3^{**}|)|$ monotonically increases, and we have $u_3^{**}(V_e^{max}, \psi_4, \theta, \phi)$ is *positive*, meaning that it produces a forward motion.

Symmetrically, if $(\theta - \phi) \in II$ quadrant varying from π to $\frac{\pi}{2}$ then $(\psi_4 - \phi)$ decreases. Hence, $|u_3^{**}(V_e^{max}, \psi_4, \theta, \phi)|$ monotonically increases and $|u_4^{**}(u_3^{**})|$ monotonically decreases.

Finally, we show that $g_4(\phi, \theta, \psi_4)$ monotonically increases or decreases. If $(\theta - \phi) \in II$ quadrant and $(\theta - \phi)$ varies from $\frac{\pi}{2}$ to π then $\sin(\theta - \phi) \geq 0$, and its value is monotonically decreasing. Therefore, the value of $g_4(\phi, \theta, \psi_4)$ is monotonically *decreasing*. Symmetrically, if $(\theta - \phi)$ varies from π to $\frac{\pi}{2}$ then $\sin(\theta - \phi) \geq 0$ in the equation A.49, and its value is monotonically increasing. Therefore, the value of $g_4(\phi, \theta, \psi_4)$ is monotonically *increasing*.

Analysis for ψ_3

$$(\theta - \psi_3) = \arctan\left(\frac{-\sin(\theta - \phi) + \gamma}{-\cos(\theta - \phi)}\right) \tag{A.95}$$

If $(\theta - \phi) \in [\pi, \frac{3\pi}{2}]$ then $(\theta - \psi_3) \in (0, \frac{\pi}{2}]$ and $\dot{\phi}(V_e^{max}, \psi_3, \theta, \phi)$ *is negative*, producing a rod clockwise rotation. If $(\theta - \phi) \in [\frac{3\pi}{2}, 2\pi]$ then $(\theta - \psi_3) \in [\frac{\pi}{2}, \pi)$ and $\dot{\phi}(V_e^{max}, \psi_3, \theta, \phi)$ *is positive*, meaning that it produces a rod counterclockwise rotation.

$$(\psi_3 - \phi) = \arctan\left(\frac{-\gamma\cos(\theta - \phi)}{-1 + \gamma\sin(\theta - \phi)}\right) \tag{A.96}$$

If $(\theta - \phi) \in [\pi, \frac{3\pi}{2}]$ then $(\psi_3 - \phi) \in [\frac{3\pi}{4}, \pi]$ and $u_3^{**}(V_e^{max}, \psi_3, \theta, \phi)$ is *positive*, meaning that it produces a pursuer forward motion. If $(\theta - \phi) \in [\frac{3\pi}{2}, 2\pi]$ then $(\psi_3 - \phi) \in [\pi, \frac{5\pi}{4}]$ and $u_3^{**}(V_e^{max}, \psi_3, \theta, \phi)$ is *negative*, causing the pursuer to move backward.

We show now that $g_3(\psi_3, \theta, \phi)$ monotonically increases or decreases. If $(\theta - \phi) \in III$ quadrant, and $(\theta - \phi)$ varies from π to $\frac{3\pi}{2}$ then $\sin(\theta - \phi) \leq 0$ in equation A.51 (Lemma II), and its value is monotonically decreasing. Consequently, $-\sin(\theta - \phi) \geq 0$ in equation A.51 (Lemma II), and its value is monotonically increasing. Hence, the value of $g_3(\psi_3, \theta, \phi)$ is monotonically *increasing*. Symmetrically, if $(\theta - \phi)$ varies from $\frac{3\pi}{2}$ to π then the value of $g_3(\psi_3, \theta, \phi)$ is monotonically *decreasing*. If $(\theta - \phi) \in IV$ quadrant, and $(\theta - \phi)$ varies from $\frac{3\pi}{2}$ to 2π then $\sin(\theta - \phi) \leq 0$ (in equation A.51, Lemma II), and its value is monotonically increasing. Consequently, $-\sin(\theta - \phi) \geq 0$ (in equation A.51, Lemma II), and its value is monotonically decreasing. Therefore, the value of $g_3(\psi_3, \theta, \phi)$ is monotonically *decreasing*. Symmetrically, if $(\theta - \phi)$ varies from 2π to $\frac{3\pi}{2}$ then the value of $g_3(\psi_3, \theta, \phi)$ is monotonically *increasing*.

Analysis of ψ_2

$$(\theta - \psi_2) = \arctan\left(\frac{\sin(\theta-\phi)-\gamma}{\cos(\theta-\phi)}\right) \tag{A.97}$$

If $(\theta-\phi) \in [\pi, \frac{3\pi}{2}]$ then $(\theta-\psi_2) \in (\pi, \frac{3\pi}{2}]$, and $\dot{\phi}$ is positive, which generates a counterclockwise rotation. If $(\theta-\phi) \in [\frac{3\pi}{2}, 2\pi]$ then $(\theta-\psi_2) \in [\frac{3\pi}{2}, 2\pi)$, and $\dot{\phi}(V_e^{max}, \psi_2, \theta, \phi)$ is negative, which generates a clockwise rotation.

$$(\psi_2 - \phi) = \arctan\left(\frac{\gamma\cos(\theta-\phi)}{1-\gamma\sin(\theta-\phi)}\right) \tag{A.98}$$

If $(\theta-\phi) \in [\pi, \frac{3\pi}{2}]$ then $(\psi_2-\phi) \in [\frac{7\pi}{4}, 2\pi]$, then $u_3^{**}(V_e^{max}, \psi_2, \theta, \phi)$ is negative, which generates a backward pursuer motion. If $(\theta-\phi) \in [\frac{3\pi}{2}, 2\pi]$ then $(\psi_2-\phi) \in [0, \frac{\pi}{4}]$, and $u_3^{**}(V_emax, \psi_2, \theta, \phi)$ is positive, which generates a forward pursuer motion.

Analysis of ψ_1

$$(\theta - \psi_1) = \arctan\left(\frac{\sin(\theta-\phi)+\gamma}{\cos(\theta-\phi)}\right) \tag{A.99}$$

If $(\theta-\phi) \in [0, \frac{\pi}{2}]$ then $(\theta-\psi_1) \in (0, \frac{\pi}{2}]$ and $\dot{\phi}(V_e^{max}, \psi_1, \theta, \phi)$ is positive, which generates a counterclockwise rotation. If $(\theta-\phi) \in [\frac{\pi}{2}, \pi]$ then $(\theta-\psi_1) \in [\frac{\pi}{2}, \pi)$ and $\dot{\phi}(V_e^{max}, \psi_1, \theta, \phi)$ is negative, which generates a clockwise rotation.

$$(\psi_1 - \phi) = \arctan\left(\frac{-\gamma\cos(\theta-\phi)}{1+\gamma\sin(\theta-\phi)}\right) \tag{A.100}$$

If $(\theta-\phi) \in [0, \frac{\pi}{2}]$ then $(\psi_1-\phi) \in [\frac{7\pi}{4}, 2\pi]$ and $u_3^{**}(V_e^{max}, \psi_1, \theta, \phi)$ is positive, which generates a forward pursuer motion. If $(\theta-\phi) \in [\frac{\pi}{2}, \pi]$ then $(\psi_1-\phi) \in [0, \frac{\pi}{4}]$ and $u_3^{**}(V_e^{max}, \psi_1, \theta, \phi)$ is negative, which generates backward pursuer motion.

□

A.5 Proof of Corollary 3.4

Corollary 3.4. If $(\theta-\phi) \in (0, \frac{\pi}{2}) \cup (\pi, \frac{3\pi}{2})$ then the DPDR is clockwise (cw), i.e. $sgn(u_4^{**}) = s(\theta,\phi) = -1$ (as given by Eq. 3.30), and the DEDR is also clockwise (cw), i.e. $sgn(\dot{\phi}(\psi_i)) = -1$. Conversely, if $(\theta-\phi) \in (\frac{\pi}{2}, \pi) \cup (\frac{3\pi}{2}, 2\pi)$ then the DPDR is counterclockwise (ccw) $sgn(u_4^{**}) = s(\theta,\phi) = +1$ (as given by Eq. 3.30), and the DEDR is also counterclockwise (ccw) $sgn(\dot{\phi}(\psi_i)) = +1$. Thus, the following controls must be

applied by the players according to the value of $(\theta - \phi)$, to obtain the required direction of rotation of both u_4^{**} and $\dot{\phi}(V_p^{max}, K, \theta, \phi)$.

The evader control u_2^*, is given in table 3.1.

The sign (direction of rotation) of $u_4^{**} = \max|\dot{\theta}| = \frac{1}{b}(V_p^{max} - |u_3^{**}|)$ is defined by equation 3.30.

Proof. Figure A.1 illustrates the direction of rotation for the pursuer strategy. In that figure the orientation of the pursuer heading θ is measured with respect to the value of ϕ, the rod's orientation. The pursuer rotates its heading either clockwise θ^- or counterclockwise θ^+ based on the direction that requires a smaller rotation to reach a parallel alignment of the robot heading with respect to the rod orientation, that is $(\theta - \phi) = \{0, \pi, 2\pi\}$, without bringing the pursuer heading (pursuer wheels) and the rod closer to perpendicularity (i.e. $(\theta - \phi) = \{\frac{\pi}{2}, \frac{3\pi}{2}\}$.

If $(\theta - \phi)$ is within the first or third quadrant then the pursuer rotates clockwise θ^-, and if $(\theta - \phi)$ is within the second or fourth quadrant then the pursuer rotates counterclockwise θ^+.

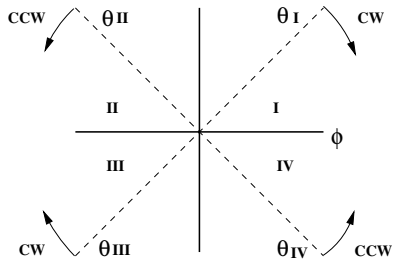

FIGURE A.1: Direction of rotation

Symmetrically, the evader must select a rod's counterclockwise or a clockwise rotation, based on the current state of rod and pursuer wheels orientation. The evader control ψ_i must produce a rod rotation that brings the rod perpendicular to the pursuer wheels (pursuer heading) without bringing the rod and the pursuer heading (pursuer wheels) closer to parallelism (i.e.$(\theta - \phi) = \{0, \pi, 2\pi\}$). Therefore, if $(\theta - \phi)$ is in the first or third quadrant the evader should rotate the rod clockwise (ϕ^-), and if $(\theta - \phi)$ is in the second or fourth quadrant the evader should rotate the rod counterclockwise (ϕ^+). Furthermore, the evader control must maximize g.

By Lemma II, if $(\theta - \phi) \in [0, \pi]$ then g is maximized by ψ_1 and ψ_4, and if $(\theta - \phi) \in [\pi, 2\pi]$ then g is maximized by ψ_2 and ψ_3. Hence, If $(\theta - \phi) \in [0, \pi]$ then the evader must select either ψ_1 or ψ_4, and if $(\theta - \phi) \in [\pi, 2\pi]$ then the evader must select either ψ_2 or ψ_3

Refer to table 3.1. If $(\theta - \phi) \in [0, \frac{\pi}{2}]$ the evader must select ψ_4, since it produces a rod's clockwise rotation, if $(\theta - \phi) \in [\frac{\pi}{2}, \pi]$, the evader must also select ψ_4, since it produces a counterclockwise rotation. Similarly, if $(\theta - \phi) \in [\pi, \frac{3\pi}{2}]$ the evader must select ψ_3, since it produces a rod's clockwise rotation, and if $(\theta - \phi) \in [\frac{3\pi}{2}, 2\pi]$ the evader must also select ψ_3. Hence, ψ_1 and ψ_2 are not used.

□

A.6 Proof of remaining cases of Theorem 3.8

Proof. **Case II** $(\theta - \phi) \in [\frac{\pi}{2}, \pi]$

First, assume that $M(V_e^{max}, V_p^{max}, \theta, \phi) < 0$ at the beginning of the game. This implies that $\max|\dot{\theta}(t_0)| > |\dot{\phi}(t_0)|$ and $V_p^{max}|\cos(\theta - \phi)| > |u_1^*| \cdot g(\phi, \theta, u_2^*)$. By Lemmas II and III $g(\phi, \theta, u_2^*)$ is maximal and varies monotonically by applying the optimal $u_2^* = \psi_4$. By Lemma III $g(\phi, \theta, u_2^*)$ monotonically decreases and $|\cos(\theta - \phi)|$ monotonically increases as $(\theta - \phi)$ varies from $\frac{\pi}{2}$ to π.

If $\max|\dot{\theta}(t_0)| > |\dot{\phi}(t_0)|$ then $(\theta(t_0) - \phi(t_0)) < (\theta(t_0 + \epsilon) - \phi(t_0 + \epsilon))$ for $\epsilon \to 0$. By Lemma III $\max|\dot{\theta}|$ monotonically increases and $|\dot{\phi}|$ monotonically decreases as $(\theta - \phi)$ varies from $\frac{\pi}{2}$ to π. Hence $\forall t > t_0,\ \max|\dot{\theta}(t)| > |\dot{\phi}(t)|$. Therefore $\forall t > t_0, (\theta(t_0) - \phi(t_0)) < (\theta(t) - \phi(t))$, and $(\theta(t) - \phi(t))$ increases monotonically until it reaches π yielding a pursuer winning.

Now assume that $M(V_e^{max}, V_p^{max}, \theta, \phi) > 0$ at the beginning of the game. This implies that $\max|\dot{\theta}(t_0)| < |\dot{\phi}(t_0)|$ and $V_p^{max}|\cos(\theta - \phi)| < |u_1^*| \cdot g(\phi, \theta, u_2^*)$. Then by Lemma III $g(\phi, \theta, u_2^*)$ monotonically increases by applying the optimal $u_2^* = \psi_4$, and $|\cos(\theta - \phi)|$ monotonically decreases as $(\theta - \phi)$ varies from π to $\frac{\pi}{2}$.

If $\max|\dot{\theta}(t_0)| < |\dot{\phi}(t_0)|$ then $(\theta(t_0) - \phi(t_0)) > (\theta(t_0 + \epsilon) - \phi(t_0 + \epsilon))$ for $\epsilon \to 0$. By Lemma III $\max|\dot{\theta}|$ monotonically decreases and $|\dot{\phi}|$ monotonically increases as $(\theta - \phi)$ varies from π to $\frac{\pi}{2}$. Hence $\forall t > t_0,\ \max|\dot{\theta}(t)| < |\dot{\phi}(t)|$. Therefore $(\theta(t_0) - \phi(t_0)) > (\theta(t) - \phi(t))$ and $(\theta(t) - \phi(t))$ decreases monotonically until it reaches $\frac{\pi}{2}$ yielding an evader winning.

Case III $(\theta - \phi) \in [\pi, \frac{3\pi}{2}]$

First, assume that $M(V_e^{max}, V_p^{max}, \theta, \phi) < 0$ at the beginning of the game. This implies that $\max|\dot{\theta}(t_0)| > |\dot{\phi}(t_0)|$ and $V_p^{max}|\cos(\theta - \phi)| > |u_1^*| \cdot g(\phi, \theta, u_2^*)$. By Lemmas II and III $g(\phi, \theta, u_2^*)$ is maximal and varies monotonically by applying the optimal $u_2^* = \psi_3$. By Lemma III $g(\phi, \theta, u_2^*)$ monotonically decreases and $|\cos(\theta - \phi)|$ monotonically increases as $(\theta - \phi)$ varies from $\frac{3\pi}{2}$ to π.

If $\max|\dot{\theta}(t_0)| > |\dot{\phi}(t_0)|$ then $(\theta(t_0)-\phi(t_0)) > (\theta(t_0+\epsilon)-\phi(t_0+\epsilon))$ for $\epsilon \to 0$. By Lemma III $\max|\dot{\theta}|$ monotonically increases and $|\dot{\phi}|$ monotonically decreases as $(\theta-\phi)$ varies from $\frac{3\pi}{2}$ to π. Hence $\forall t > t_0,\ \max|\dot{\theta}(t)| > |\dot{\phi}(t)|$. Therefore $\forall t > t_0, (\theta(t_0)-\phi(t_0)) > (\theta(t)-\phi(t))$, and $(\theta(t)-\phi(t))$ decreases monotonically until it reaches π yielding a pursuer winning.

Now assume that $M(V_e^{max}, V_p^{max}, \theta, \phi) > 0$ at the beginning of the game. This implies that $\max|\dot{\theta}(t_0)| < |\dot{\phi}(t_0)|$ and $V_p^{max}|\cos(\theta-\phi)| < |u_1^*| \cdot g(\phi, \theta, u_2^*)$. Then by Lemma III $g(\phi, \theta, u_2^*)$ monotonically increases by applying the optimal $u_2^* = \psi_3$, and $|\cos(\theta-\phi)|$ monotonically decreases as $(\theta-\phi)$ varies from π to $\frac{3\pi}{2}$.

If $\max|\dot{\theta}(t_0)| < |\dot{\phi}(t_0)|$ then $(\theta(t_0)-\phi(t_0)) < (\theta(t_0+\epsilon)-\phi(t_0+\epsilon))$ for $\epsilon \to 0$. By Lemma III $\max|\dot{\theta}|$ monotonically decreases and $|\dot{\phi}|$ monotonically increases as $(\theta-\phi)$ varies from π to $\frac{3\pi}{2}$. Hence $\forall t > t_0,\ \max|\dot{\theta}(t)| < |\dot{\phi}(t)|$. Therefore $(\theta(t_0)-\phi(t_0)) < (\theta(t)-\phi(t))$ and $(\theta(t)-\phi(t))$ increases monotonically until it reaches $\frac{3\pi}{2}$ yielding an evader winning.

Case IV $(\theta-\phi) \in [\frac{3\pi}{2}, 2\pi]$

First, assume that $M(V_e^{max}, V_p^{max}, \theta, \phi) < 0$ at the beginning of the game. This implies that $\max|\dot{\theta}(t_0)| > |\dot{\phi}(t_0)|$ and $V_p^{max}|\cos(\theta-\phi)| > |u_1^*| \cdot g(\phi, \theta, u_2^*)$. By Lemmas II and III $g(\phi, \theta, u_2^*)$ is maximal and varies monotonically by applying the optimal $u_2^* = \psi_3$. By Lemma III $g(\phi, \theta, u_2^*)$ monotonically decreases and $|\cos(\theta-\phi)|$ monotonically increases as $(\theta-\phi)$ varies from $\frac{3\pi}{2}$ to 2π.

If $\max|\dot{\theta}(t_0)| > |\dot{\phi}(t_0)|$ then $(\theta(t_0)-\phi(t_0)) < (\theta(t_0+\epsilon)-\phi(t_0+\epsilon))$ for $\epsilon \to 0$. By Lemma III $\max|\dot{\theta}|$ monotonically increases and $|\dot{\phi}|$ monotonically decreases as $(\theta-\phi)$ varies from $\frac{3\pi}{2}$ to 2π. Hence $\forall t > t_0,\ \max|\dot{\theta}(t)| > |\dot{\phi}(t)|$. Therefore $\forall t > t_0, (\theta(t_0)-\phi(t_0)) < (\theta(t)-\phi(t))$, and $(\theta(t)-\phi(t))$ increases monotonically until it reaches 2π yielding a pursuer winning.

Now assume that $M(V_e^{max}, V_p^{max}, \theta, \phi) > 0$ at the beginning of the game. This implies that $\max|\dot{\theta}(t_0)| < |\dot{\phi}(t_0)|$ and $V_p^{max}|\cos(\theta-\phi)| < |u_1^*| \cdot g(\phi, \theta, u_2^*)$. Then by Lemma III $g(\phi, \theta, u_2^*)$ monotonically increases by applying the optimal $u_2^* = \psi_3$, and $|\cos(\theta-\phi)|$ monotonically decreases as $(\theta-\phi)$ varies from 2π to $\frac{3\pi}{2}$.

If $\max|\dot{\theta}(t_0)| < |\dot{\phi}(t_0)|$ then $(\theta(t_0)-\phi(t_0)) > (\theta(t_0+\epsilon)-\phi(t_0+\epsilon))$ for $\epsilon \to 0$. By Lemma III $\max|\dot{\theta}|$ monotonically decreases and $|\dot{\phi}|$ monotonically increases as $(\theta-\phi)$ varies from 2π to $\frac{3\pi}{2}$. Hence $\forall t > t_0,\ \max|\dot{\theta}(t)| < |\dot{\phi}(t)|$. Therefore $(\theta(t_0)-\phi(t_0)) > (\theta(t)-\phi(t))$ and $(\theta(t)-\phi(t))$ decreases monotonically until it reaches $\frac{3\pi}{2}$ yielding an evader winning.

□

Appendix B

Appendix B - Surveillance and Capture Strategies for an Omnidirectional Agent and a Differential Drive Robot

B.1 Proof of Lemma 4.1

Lemma 4.1. Let $\delta^*(L)$ be the curve separating the regions where $M(L,\delta) < 0$ and $M(L,\delta) > 0$ (refer to Fig. B.1).

1. There is a critical value $L = L_o^*$ such that $\delta^*(L_o) = 0$.
2. For $L > L_o^*$, $\delta^*(L)$ is a strictly increasing function.
3. If $L \to \infty$ then $\delta^*(L) \to \cos^{-1}\left(\frac{V_e^{\max}}{V_p^{\max}}\right) \leq \frac{\pi}{2}$.
4. For $L < \infty$, $\delta^*(L) < \cos^{-1}\left(\frac{V_e^{\max}}{V_p^{\max}}\right) \leq \frac{\pi}{2}$.

Proof. From (4.7), and recalling that $M(L,\delta^*(L)) = 0$, we have that

$$M(L,\delta^*(L)) = V_e^{\max}\sqrt{1+\frac{2b}{L}\sin(\delta^*(L))+\left(\frac{b}{L}\right)^2} - V_p^{\max}\cos(\delta^*(L)) = 0 \tag{B.1}$$

If $\delta^*(L) = 0$ then

$$M(L,0) = V_e^{\max}\sqrt{1+\left(\frac{b}{L}\right)^2} - V_p^{\max} = 0 \tag{B.2}$$

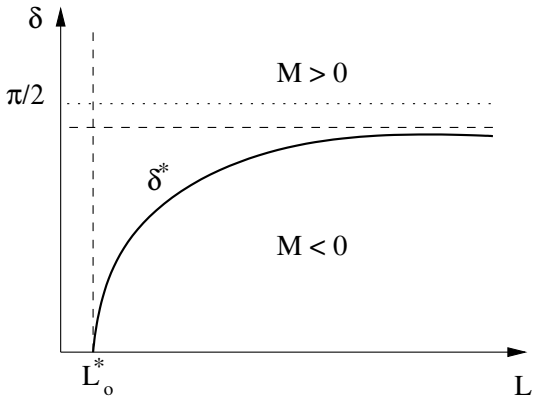

FIGURE B.1: Detail of Fig. 4.1, for $\delta \in [0, \frac{\pi}{2}]$

From the last expression, and by doing some algebra, we obtain the value L_o such that $\delta^*(L_o) = 0$

$$L_o^* = \frac{V_e^{\max} b}{\sqrt{(V_p^{\max} - V_e^{\max})(V_p^{\max} + V_e^{\max})}} \tag{B.3}$$

which may also be written as:

$$L_o^* = \frac{\rho b}{\sqrt{1-\rho^2}} \tag{B.4}$$

where

$$\rho = \frac{V_e^{\max}}{V_p^{\max}} \tag{B.5}$$

This proves the first part of the lemma.

Note that as $\rho \to 1$, $L_o^* \to \infty$, which implies that the OA can always break constant distance surveillance, which implies, as shown below, that the OA can always obtain an arbitrary distance from the DDR. On the other hand, for $\rho \approx 0$, $L_o^* \to 0$. In what follows it will always be assumed that $\rho < 1$.

From (4.7), we observe that in order to keep a constant value of 0 for $M(L, \delta)$, if we increase the value of L, then we have also to increase the value of δ. Therefore, $\delta^*(L)$ is an strictly increasing function with respect to $L > L_o^*$, which proves the second part of the lemma.

If $L \to \infty$ we have that (B.1) takes the form

$$M(L, \delta^*(L)) = V_e^{\max} - V_p^{\max} \cos(\delta_\infty^*) = 0 \tag{B.6}$$

By straight forward manipulation of (B.6), we obtain

$$\delta_\infty^* = \cos^{-1}(\rho) \tag{B.7}$$

Note that $\delta^*_\infty < \frac{\pi}{2}$, and for $\rho \approx 0$, $\delta^*_\infty \to \frac{\pi}{2}$. This proves the last part of the lemma. □

B.2 Proof of Theorem 4.3

Theorem 4.3. Assume that for the initial configuration $M(L_I, \delta_I) < 0$. Given $\epsilon > 0$, define $L^*_B = L^*_o + \epsilon$. Let $(L_I, L_G, L) > L^*_B + \epsilon$, be the initial, the goal and the current distance between the DDR and the OA. The DDR can reach a distance $L \in [L_G - \epsilon, L_G + \epsilon]$ in finite time, using the following strategy:

1. If $\delta(L) > 0$, move at constant L, changing the DDR's heading until it is parallel to the orientation of the rod, i.e., make $\delta(L) = 0$.
2. If $\delta(L) = 0$, move during a time $\widehat{T} = \min(T^*, \frac{|L-L_G|}{2V_p^{\max}})$ directly towards or away from the position of the OA at time t, depending on the sign of $L - L_G$, with a velocity $V = \text{sgn}(L - L_G) \cdot V_p^{\max}$ where

$$T^* = \min\left(\frac{\epsilon}{2V_p^{\max}}, \frac{L^*_B \sin(\delta^*(L^*_B))}{V_e^{\max}}\right) \tag{B.8}$$

Proof. It follows directly from the results in Chapter 3 that if $M(L, \delta) < 0$ the DDR can make $\delta(L) = 0$ in finite time, using the controls u^*_3, u^*_4. For the second part of the strategy, one has to show that if the DDR moves with a velocity $V = \text{sgn}(L - L_G) \cdot V_p^{\max}$ during a time $\widehat{T}$, $|L - L_G|$ will decrease and the system will remain in the region where $M(L, \delta) < 0$. To do this, we consider two cases:

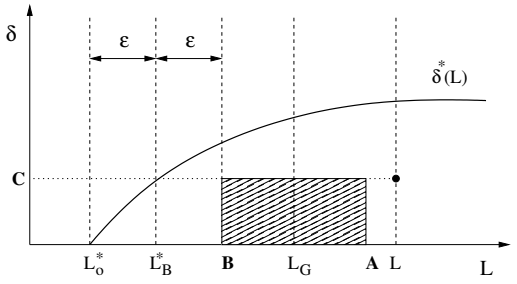

FIGURE B.2: Auxiliary constructions for the case $L_G < L$ (see text)

Case I: $L_G < L$.

In this case, we show that in (L, δ) space, after an incremental motion of duration $\widehat{T}$, the new system configuration (L', δ') falls inside the shaded rectangle of Fig. B.2, with $A = L - (V_p^{\max} - V_e^{\max})\widehat{T}$; $B = L^*_B + \epsilon$ and $C = \delta^*(L^*_B)$, which means that L is decreasing as a function of time, and the system never leaves the region where $M(L, \delta) < 0$.

Since the DDR wants to decrease the inter-player distance, it moves toward the OA during a time $\widehat{T}$. In order to show that $L' < L$, it is enough to consider the worst case for the bound A, namely, when the OA moves directly away from the DDR at maximum speed, in which case, $L' = A < L$. We use an analogous reasoning in order to prove the next cases.

To show that $L' \geq B$, again one considers the worst case for this bound, namely, when the OA moves directly towards the DDR at maximum speed. In this case, from the definitions of $\widehat{T}$ and T^*, one has that

$$L' = L - (V_p^{\max} + V_e^{\max})\widehat{T} > L - 2V_p^{\max}\widehat{T} > L - \epsilon > B \tag{B.9}$$

Finally, for the bound C, the worst case obtains when the OA moves perpendicularly to the rod at maximum speed (see Fig. B.3). In this case, the final angle δ' satisfies:

$$\sin(\delta') \leq \frac{V_e^{\max}T^*}{L'} < \frac{V_e^{\max}T^*}{L_B^*} \leq \sin(\delta^*(L_B^*)) \tag{B.10}$$

where the last inequality follows from (B.8). Since the $\sin(\cdot)$ function is increasing in the interval $[0, \frac{\pi}{2}]$, one gets from Lemma 4.1 that $\delta' < \delta^*(L_B^*) < \delta^*(L')$.

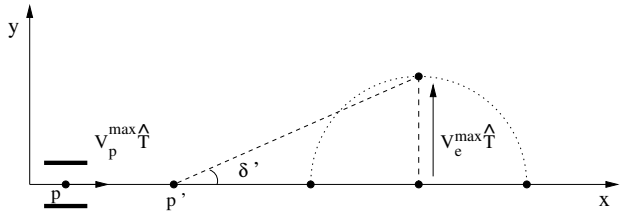

FIGURE B.3: The DDR moves toward the OA, and the OA moves perpendicularly to the rod at maximum speed.

Case II: $L_G > L$.

In this case there are only two bounds to consider for the new configuration (L', δ') (see Fig. B.4): $D = L + (V_p^{\max} - V_e^{\max})\widehat{T}$ and $C = \delta^*(L_B^*)$. The first one obtains when the OA moves directly towards the DDR at maximum speed, in which case, $L' = D > L$, and the second one when the DDR moves perpendicularly to the rod at time t, as in case I, in which case,

$$\sin(\delta') \leq \frac{V_e^{\max}T^*}{L'} < \sin(\delta^*(L_B^*)) < \sin(\delta^*(L')) \tag{B.11}$$

and therefore $\delta' < \delta^*(L')$ as above. This completes the proof. □

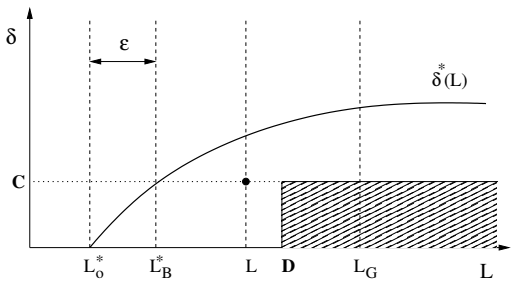

FIGURE B.4: Auxiliary constructions for the case $L_G > L$ (see text)

Note that in both cases, since

$$\widehat{T} \leq \frac{\epsilon}{2V_p^{\max}} < \frac{\epsilon}{2V_e^{\max}} \tag{B.12}$$

the bound on the magnitude of the maximum overshoot (or undershoot) from the target distance is

$$(V_p^{\max} + V_e^{\max})\widehat{T} < 2V_p^{\max}\widehat{T} \leq \epsilon \tag{B.13}$$

Note also that, this overshoot or undershoot is due to the assumption that while one of the players changes the inter-player distance, the motion direction of the other player is unknown. In the worst case a player would move in the opposite direction to the one assumed to establish the bounds.

Appendix C

Appendix C - Time-Optimal Motion Strategies for Capturing an Omnidirectional Evader using a Differential Drive Robot

C.1 A or B are instantaneously zero at the switching instant in Lemma 6.3

From Lemma 6.3, the Hamiltonian depends linearly on the controls of the DDR, and the DDR's controls are restricted to being between an upper and lower bound. To minimize the Hamiltonian, the controls need to be as big or as small as possible, depending on the sign of A and B. When A or B are zero in the Hamiltonian, the Pontryagin's principle fails to yield a solution, because the control associated with the term equal to zero is not defined properly and could take any value. In particular, one can instantaneously assign to that control the optimal value before the zero crossing. If A or B are different from zero during any non-zero time interval then the solution is straightforward and corresponds to a bang-bang control that switches from the largest to the smallest value whenever A or B change sign.

Theorem C.1. *The value of* $A = \frac{-yV_x}{b} + \frac{xV_y}{b} - V_y$ *or* $B = \frac{yV_x}{b} - \frac{xV_x}{b} - V_y$ *inside the switch functions in Eq. (6.12) is instantaneously zero when the DDR switches controls.*

Proof. To prove that in our game, A or B are non-zero during any non-zero time interval, we show that if $B = 0$ then $\mathring{B} \neq 0$, where $\mathring{B} = \frac{dB}{d\tau}$. And if $A = 0$ then $\mathring{A} \neq 0$. Note that we are considering retro-time, which means that the time τ is measured starting from the capture condition. From Lemmas 6.1 and 6.3, if $s \in [0, \frac{\pi}{2}]$, u_1 and u_2 are initially equal to $V_p^{\max}$. From Lemma 6.11, we know that for this case u_2 will switch its value first. This means that B has a zero crossing before A. From Lemma 6.3, we have that

$$B = \frac{yV_x}{b} - \frac{xV_y}{b} - V_y \tag{C.1}$$

From (C.1), we have that

$$\mathring{B} = \frac{y\mathring{V}_x}{b} + \frac{\mathring{y}V_x}{b} - \frac{x\mathring{V}_y}{b} - \frac{\mathring{x}V_y}{b} - \mathring{V}_y \tag{C.2}$$

From Lemma 6.6, when u_1 and u_2 are initially equal to $V_p^{\max}$

$$\begin{aligned} &\mathring{V}_x = 0, \quad \mathring{V}_y = 0 \\ &V_x = \lambda \sin s, \quad V_y = \lambda \cos s \end{aligned} \tag{C.3}$$

where λ is a positive constant value. Substituting (C.3) into (C.2), we obtain

$$\mathring{B} = \mathring{y}\lambda \sin s - \mathring{x}\lambda \cos s \tag{C.4}$$

The corresponding transition equation in retro-time is given by

$$\begin{aligned} \mathring{x} &= -V_e^{\max} \sin s \\ \mathring{y} &= -V_e^{\max} \cos s + V_p^{\max} \end{aligned} \tag{C.5}$$

Substituting (C.5) into (C.4), and assuming that u_1 and u_2 are set equal to $V_p^{\max}$ when $B = 0$, we get that if $B = 0$ then

$$\mathring{B} = \frac{V_p^{\max} \lambda \sin s}{b} \tag{C.6}$$

From the last expression, we observe that $\mathring{B} \neq 0$ for $s \in (0, \frac{\pi}{2}]$. This means that B is only zero instantaneously. The case $s = 0$, corresponds to the singular surface in Lemma 6.25. For that case, we have proved in Lemma 6.25 that both A and B are always constant and different from zero.

The other case, where B has a zero crossing before A, is obtained assuming that $s \in [\frac{\pi}{2}, \pi)$, where u_1 and u_2 are initially equal to $-V_p^{\max}$. The procedure to prove it is analogous to the one described above. If $s \in (\pi, \frac{3\pi}{2}]$ then u_1 and u_2 are initially equal to $-V_p^{\max}$. From Lemma 6.11, we know that for this case u_1 will switch its value first. This means that A will have a zero crossing before B. From Lemma 6.3, we have that

$$A = \frac{-yV_x}{b} + \frac{xV_y}{b} - V_y \tag{C.7}$$

From (C.7), we have that

$$\mathring{A} = -\frac{y\mathring{V}_x}{b} - \frac{\mathring{y}V_x}{b} + \frac{x\mathring{V}_y}{b} + \frac{\mathring{x}V_y}{b} - \mathring{V}_y \tag{C.8}$$

From Lemma 6.6, when u_1 and u_2 are initially equal to $-V_p^{\max}$

$$\begin{aligned} &\mathring{V}_x = 0, \quad \mathring{V}_y = 0 \\ &V_x = \lambda \sin s, \quad V_y = \lambda \cos s \end{aligned} \tag{C.9}$$

where λ is a positive constant value. Substituting (C.9) into (C.8), we obtain

$$\mathring{A} = -\mathring{y}\lambda \sin s + \mathring{x}\lambda \cos s \tag{C.10}$$

The corresponding transition equation in retro-time is given by

$$\begin{aligned} \mathring{x} &= -V_e^{\max} \sin s \\ \mathring{y} &= -V_e^{\max} \cos s - V_p^{\max} \end{aligned} \tag{C.11}$$

Substituting (C.11) into (C.10), and assuming that u_1 and u_2 are set equal to $-V_p^{\max}$ if $A = 0$, we get that if $A = 0$ then

$$\mathring{A} = \frac{V_p^{\max} \lambda \sin s}{b} \tag{C.12}$$

From the last expression, we observe that $\mathring{A} \neq 0$ for $s \in (\pi, \frac{3\pi}{2}]$. This means that A is only zero instantaneously. The case $s = \pi$, corresponds to the singular surface in Lemma 6.25. For that case, we have proved in Lemma 6.25 that both A and B are always constant and different to zero. The other case where A has a zero crossing before

B is obtained assuming that $s \in [\frac{3\pi}{2}, 2\pi)$, where u_1 and u_2 are initially equal to $V_p^{\max}$. The procedure to prove it is analogous to the one described above.

□

Bibliography

[1] A.A. Melikyan. *Generalized Characteristics of First Order PDEs: Applications in Optimal Control and Differential Games*. Birkhauser, 2000.

[2] S. Bhattacharya, R. Murrieta-Cid, and S. Hutchinson. Optimal paths for landmark-based navigation by differential drive vehicles with field-of- view constraints. *IEEE Transactions on Robotics and Automation*, 23(1), February 2007.

[3] S. Bhattacharya and S. Hutchinson. On the existence of nash equilibrium for a two player pursuit-evasion game with visibility constraints. *International Journal on Robotics Research*, 29(7):831–839, 2010.

[4] J. Espinoza, A. Sarmiento, R. Murrieta-Cid, and S. Hutchinson. A motion planning strategy for finding an object with a mobile manipulator in 3-d environments. *Journal Advanced Robotics*, 25(13-14):1627–1650, 2011.

[5] L. Guibas et. al. Visibility-based pursuit-evasion in a polygonal environment. *International Journal of Computational Geometry and Applications*, 1997.

[6] V. Isler, S. Kannan, and S. Khanna. Randomized pursuit-evasion in a polygonal environment. *IEEE Transactions on Robotics*, 5(21):864–875, 2005.

[7] A. Lazanas and J. C. Latombe. Landmark-based robot navigation. *Algorithmica*, 13:472–501, 1995.

[8] E. U. Acar and H. Choset. Exploiting critical points to reduce position error for sensor-based navigation. In *Proc. IEEE Int. Conf. on Robotics and Automation*, 2002.

[9] S. Hutchinson and A. C. Kak. Planning sensing strategies in a robot work cell with multi-sensor capabilities. *IEEE Transactions on Robotics and Automation*, 5(6), 1989.

[10] S. Lacroix, P. Grandjean, and M. Ghallab. Perception planning for a multi-sensory interpretation machine. In *Proc. IEEE Int. Conf. on Robotics and Automation*, 1992.

[11] H. H. Gonzalez-Banos and J.-C. Latombe. Navigation strategies for exploring indoor environments. *International Journal on Robotics Research*, 21(10/11):829–848, October-November 2002.

[12] G. Borghi and V. Caglioti. Minimum uncertainty explorations in the self-localization of mobile robots. *IEEE Transactions on Robotics and Automation*, 14(6), 1998.

[13] G. Oriolo, G. Ulivi, and M. Vendittelli. Real-time map building and navigation for autonomous robots in unknown environments. *Transactions on Systems, Man, and Cybernetics*, 28(3):316–333, 1998.

[14] B. Tovar, L. Mu noz Gomez, R. Murrieta-Cid, M. Alencastre-Miranda, R. Monroy, and S. Hutchinson. Planning exploration strategies for simultaneous localization and mapping. *Journal Robotics and Autonomous Systems*, 54(4):314–331, April 2006.

[15] S. Hert, S. Tiwari, and V. Lumelsky. A terrain-covering algorithm for an auv. *Autonomous Robots*, 3:91–119, 1996.

[16] S.M. LaValle, H.H. González-Ba nos, C. Becker, and J.-C. Latombe. Motion strategies for maintaining visibility of a moving target. In *Proc. IEEE Int. Conf. on Robotics and Automation*, 1997.

[17] H.H. González, C.-Y. Lee, and J.-C. Latombe. Real-time combinatorial tracking of a target moving unpredictably among obstacles. In *Proc. IEEE Int. Conf. on Robotics and Automation*, 2002.

[18] B. Jung and G. Sukhatme. Tracking targets using multiple robots: the effect of environment occlusion. *Journal Autonomous Robots*, 12:191–205, 2002.

[19] T. Bandyopadhyay, Y. Li, M.H. Ang, and D. Hsu. A greedy strategy for tracking a locally predictable target among obstacles. In *Proc. IEEE Int. Conf. on Robotics and Automation*, 2006.

[20] R. Isaacs. *Differential Games: A Mathematical Theory with Applications to Warfare and Pursuit, Control and Optimization.* John Wiley and Sons, Inc., 1965.

[21] A. W. Merz. *The homicidal chauffeur – a differential game.* PhD thesis, Stanford University, 1971.

[22] V. Isler, S. Kannan, and S. Khanna. Locating and capturing an evader in a polygonal environment. In *Sixth International Workshop on the Algorithmic Foundations of Robotics*, 2004.

[23] S. M. LaValle, D. Lin, L. Guibas, J.-C. Latombe, and R. Motwani. Finding an unpredictable target in a workspace with obstacles. In *Proc. IEEE Int. Conf. on Robotics and Automation*, 1997.

[24] S. M. LaValle and J. Hinrichsen. Visibility-based pursuit-evasion: An extension to curved environments. In *Proc. IEEE Int. Conf. on Robotics and Automation*, 1999.

[25] I. Suzuki and M. Yamashita. Searching for a mobile intruder in a polygonal region. *SIAM J. Comput.*, 21(5):863–888, 1992.

[26] R. Vidal, O. Shakernia, H.Jin, D. Hyunchul, and S. Sastry. Probabilistic pursuit-evasion games: Theory, implementation, and experimental evaluation. *IEEE Trans. Robotics and Automation*, 18(5):662–669, 2002.

[27] G. Hollinger, S. Singh, J. Djugash, and A. Kehagias. Efficient multi-robot search for a moving target. *International Journal on Robotics Research*, 28(2):201–219, 2009.

[28] J.P. Laumond, P.E. Jacobs, M. Taix, and R.M. Murray. A motion planner for nonholonomic mobile robots. *IEEE Trans. on Robotics and Automation*, 10(5): 577–593, 1994.

[29] J. Barraquand and P. Ferbach. Motion planning with uncertainty: the information space approach. In *Proc IEEE Int. Conf. on Robotics and Automation*, 1995.

[30] S. LaValle and S. Hutchinson. An objective-based framework for motion planning under sensing and control uncertainties. *Journal of Robotics Research*, 17(1), 1997.

[31] J.-L. Marion, C. Rodriguez, and M. de Rougemont. The evaluation of strategies in motion planning with uncertainty. In *Proc IEEE Int. Conf. on Robotics and Automation*, 1994.

[32] A. Efrat *et al.* Sweeping simple polygons with a chain of guards. In *11th annual ACM-SIAM Symposium on Discrete Algorithms*, 2000.

[33] S. Koenig and Y. Liu. Terrain coverage with ant robots: A simulation study. In *5th International Conference on Autonomous Agents*, 2001.

[34] L. Parker. Algorithms for multi-robot observation of multiple targets. *Journal Autonomous Robots*, 12:231–255, 2002.

[35] B. Yamauchi. Frontier-based exploration using multiple robots. In *Int. Conf. on Autonomous Agents*, 1998.

[36] R. Murrieta-Cid, U. Ruiz, J.L. Marroquin, J.P. Laumond, and S. Hutchinson. Tracking an omnidirectional evader with a differential drive robot. *Special Issue on Search and Pursuit/Evasion - Journal Autonomous Robots*, 31(4):345–366, 2011.

[37] U. Ruiz and R. Murrieta-Cid. A homicidal differential drive robot. In *Proc. IEEE Int. Conf. on Robotics and Automation*, 2012.

[38] U. Ruiz, R. Murrieta-Cid, and J.L. Marroquin. Time-optimal motion strategies for a homicidal differential drive robot. *Submitted to IEEE Transactions on Robotics*, 2012.

[39] O. Hájek. *Pursuit Games*. Academic Press, 1965.

[40] T. Basar and G. Olsder. *Dynamic Noncooperative Game Theory*. Academic Press, 1982.

[41] T.D. Parsons. Pursuit-evasion in a graph. *Theory and Application of Graphs*, pages 426–441, 1976.

[42] L. Guibas, J.C. Latombe, S. LaValle, D. Lin, and R. Motwani. Visibility-based pursuit-evasion in a polygonal environment. In *Algorithms and Data Structures*, volume 1272 of *Lecture Notes in Computer Science*, pages 17–30. Springer Berlin / Heidelberg, 1997.

[43] S. Sachs, S.M. LaValle, and S. Rajko. Visibility-based pursuit-evasion in an unknown planar environment. *The International Journal of Robotics Research*, 23(1): 3–26, 2004.

[44] B. Tovar and S. M. LaValle. Visibility-based pursuit - evasion with bounded speed. *International Journal on Robotics Research*, 27(11-12):1350–1360, 2008.

[45] J. Hespanha, M. Prandini, and S. Sastry. Probabilistic pursuit-evasion games: A one-step nash approach. In *Proc. Conference on Decision and Control*, 2000.

[46] T. H. Chung. On probabilistic search decisions under searcher motion constraints. In *Proc. of 2008 Int'l. Workshop on the Algorithmic Foundations of Robotics*, 2008.

[47] N. Megiddo, M Hakimi, M. Garey, D. Johnson, and C. Papadimitriou. The complexity of searching a graph. *Journal of A CM*, 35(1):18–44, 1998.

[48] F. Makedon and I Sudbough. Minimizing width in linear layouts. In *In 10th ICALPS, Lecture Notes in Computer Science. Springer Verlag*, 1983.

[49] B. Monien and H. Sudborough. Min cut is np-complete for edge weighted graphs. *Journal of the ACM*, 9(1):209–229, 1988.

[50] D. Bienstock and P. Seymour. Monotonicity in graph searching. *Journal of Algorithms*, 12:239–245, 1991.

[51] S. Lapaugh. Recontamination does not help to search a graph. *Journal of the ACM*, 40(2):224–245, 1993.

[52] C. Icking and R. Klein. The two guards problem. *International Journal of Computational Geometry and Applications*, 3(2):257–285, 1992.

[53] L. Tseng, P Hefferman, and D. Lee. Two guards walkability of simple polygons. *International Journal of Computational Geometry and Applications*, 8(1):85–116, 1998.

[54] J.H. Lee, S. Park, and K. Chwa. Searching a polygonal room with a door by a 1-searcher. *International Journal of Computational Geometry and Applications*, 10 (2):201–220, 1998.

[55] D. Craas, L. Suzuki, and M. Yamashita. Searching for a mobile intruder in a corridor - the open edge variant of the polygon search problem. *International Journal of Computational Geometry and Applications*, 5(4):397–412, 1995.

[56] B. Tovar, L. Guilamo, and S LaValle. Gap navigation trees: Minimal representation for visibility-based tasks. In *Proc. Workshop on the Algorithmic Foundations of Robotics*, 2004.

[57] B. Espiau, F. Chaumette, and P. Rives. A new approach to visual servoring in robotics. *IEEE Transactions on Robotics and Automation*, 8(3):313–326, 1992.

[58] S. Hutchinson, G. Hager, and P. Coke. A tutorial on visual servo control. *IEEE Transactions on Robotics and Automation*, 2(3):651–670, 1996.

[59] P. Papanikolopous, P. Khosla, and T. Kanade. Visual tracking of a moving target by a camera mounted on a robot: A combination of control and vision. *IEEE Transactions on Robotics and Automation*, 9(1):14–35, 1993.

[60] C. Becker, H. H. González-Baños, J. Latombe, and C. Tomasi. An intelligent observer. In *ISER*, pages 153–160, 1995.

[61] P. Fabiani and J.-C. Latombe. Tracking a partially predictable object with uncertainty and visibility constraints: a game-theoretic approach. In *IJCAI*, 1999.

[62] R. Murrieta-Cid, H. H. Gonzalez-Ba nos, and B. Tovar. A reactive motion planner to maintain visibility of unpredictable targets. In *Proc. IEEE Int. Conf. on Robotics and Automation*, 2002.

[63] R. Murrieta-Cid, B. Tovar, and Seth Hutchinson. A sampling-based motion planning approach to maintain visibility of unpredictable targets. *Journal Autonomous Robots*, 19(3):285–300, 2005.

[64] R. Murrieta-Cid, A. Sarmiento, and S. Hutchinson. On the existence of a strategy to maintain a moving target within the sensing range of an observer reacting with delay. *In Proc. IEEE/RSJ Int. Conf. On Intelligent Robots and Systems*, pages 1184–1191, 2003.

[65] R. Murrieta-Cid, A. Sarmiento, S. Bhattacharya, and S. Hutchinson. Maintaining visibility of a moving target at a fixed distance: The case of observer bounded speed. In *Proc IEEE Int. Conf. On Robotics and Automation*, 2004.

[66] R. Murrieta-Cid, L. Mu noz, M. Alencastre, A. Sarmiento, S. Kloder, S. Hutchinson, F. Lamiraux, and J.-P. Laumond. Maintaining visibility of a moving holonomic target with a non-holonomic robot. In *Proc. IEEE/RSJ Int. Conf. on Intelligent Robots and Systems*, pages 2028–2034, 2005.

[67] R. Murrieta-Cid, T. Muppirala, A. Sarmiento, S. Bhattacharya, and Seth Hutchinson. Surveillance strategies for a pursuer with finite sensor range. *International Journal on Robotics Research*, 26(3):233–253, March 2007.

[68] A. Efrat, H. H. Gonzalez, S. G. Kobourov, and L. Palaniappan. Optimal motion strategies to track and capture a predictable target. In *Proc IEEE Int. Conf. on Robotics and Automation*, 2003.

[69] T. Bandyopadhyay, M. H. Ang Jr., and D. Hsu. Motion planning for 3-d target tracking among obstacles. In *Int. Symp. on Robotics Research*, 2007.

[70] J. M. O'Kane. On the value of ignorance: Balancing tracking and privacy using a two-bit sensor. In *Proc. International Workshop on the Algorithmic Foundations of Robotics*, 2008.

[71] O. Tekdas, W. Yang, and V. Isler. Robotic routers: Algorithms and implementation. *International Journal on Robotic Research*, 29(1):110–126, 2010.

[72] E. A. Stump. *Control for localization and visibility maintenance of an independent agent using robotic teams.* PhD thesis, University of Pennsylvania, 2009.

[73] J. Lewin and J.V. Breakwell. The surveillance-evasion game of degree. *Journal of Optimization Theory and Applications*, 16(3-4):339–353, 1975.

[74] J. Lewin and G.J. Olsder. Conic surveillance evasion. *Journal of Optimization Theory and Applications*, 27(1):107–125, 1979.

[75] M. Pachter and Y. Yavin. A stochastic homicidal chauffeur pursuit-evasion differential game. *Journal of Optimization Theory and Applications*, 34(3):405–424, 1981.

[76] Y. Yavin. Stochastic two-target pursuit-evasion differential games in the plane. *Journal of Optimization Theory and Applications*, 56(3):325–343, 1988.

[77] V.Y. Glizer. Homicidal chauffeur game with target set in the shape of a circular angular sector: Conditions for existence of a closed barrier. *Journal of Optimization Theory and Applications*, 101(3):581–598, 1999.

[78] S. Bopardikar, F. Bullo, and J. Hespanha. A cooperative homicidal chauffeur game. *Automatica*, 45:1771–1777, 2009.

[79] A.W. Merz. The game of two identical cars. *Journal of Optimization Theory and Applications*, 9(5):324–343, 1972.

[80] A.W. Merz and M. Pachter. Capturability in a two-target "game of two cars". *Journal Guidance and Control*, 4(1):15–21, 1981.

[81] I. Greenfeld. A differential game of surveillance evasion of two identical cars. *Journal of Optimization Theory and Applications*, 52(1):53–79, 1987.

[82] Y. Yavin and R. De Villiers. Game of two cars: Case of variable speed. *Journal of Optimization Theory and Applications*, 60(2):327–339, 1989.

[83] I. Mitchell. Games of two identical vehicles. Technical report, Stanford University, July 2001.

[84] J. Flynn. Lion and man: The boundary constraint. *SIAM Journal of Control*, 11: 397–411, 1973.

[85] J. Flynn. Lion and man: The general case. *SIMA Journal of Control*, 12:581–597, 1974.

[86] J. Lewin. The lion and the man problem revisited. *Journal of Optimization Theory and Applications*, 49(3):411–430, 1986.

[87] J. Sgall. Solution of david gale's lion and man problem. *Theoretical Computer Science*, 259(1-2):663–670, 2001.

[88] N. Karnad and V. Isler. Lion and man game in the presence of a circular obstacle. In *Proc. IEEE Int. Conf. on Intelligent Robots and Systems*, 2009.

[89] J.T. Schwartz and M. Sharir. On the piano movers' problem: I. the case if a two-dimensional rigid polygon body moving amidst polygonal barriers. *Communications on Applied Mathematics*, 36:345–398, 1987.

[90] D.J. Balkcom and M.T. Mason. Time optimal trajectories for bounded velocity differential drive vehicles. *International Journal of Robotics Research*, 21(3):219–232, 2002.

[91] L. S. Pontryagin, V. G. Boltyanskii, R. V. Gamkrelidze, and E. F. Mishchenko. *The Mathematical Theory of Optimal Processes*. JohnWiley, 1962.

[92] S.M. LaValle. *Planning Algorithms*. Cambridge University Press, 2006.

[93] P. Bernhard. Singular surfaces in differential games: An introduction. In *Differential Games and Applications*, pages 1–33, 1977.

[94] I. Bronshtein and K. Semendiaev. *Manual de Matemáticas para Ingenieros y Estudiantes*. Editorial Mir Moscu, 1977.